Nanostructured Plasmonic Sensors

Matthew E. Stewart,[†] Christopher R. Anderton,[†] Lucas B. Thompson,[†] Joana Maria,[‡] Stephen K. Gray,[§] John A. Rogers,[†,‡] and Ralph G. Nuzzo*[,†,‡]

Department of Chemistry, University of Illinois at Urbana–Champaign, Urbana, Illinois 61801, Department of Materials Science and Engineering, University of Illinois at Urbana–Champaign, Urbana, Illinois 61801, and Chemistry Division and Center for Nanoscale Materials, Argonne National Laboratory, Argonne, Illinois 60439

Received June 2, 2007

Contents

1. Introduction

Surface plasmons (SPs) are coherent oscillations of conduction electrons on a metal surface excited by electromagnetic radiation at a metal−dielectric interface. The growing field of research on such light−metal interactions is known as 'plasmonics'.[1−3] This branch of research has attracted much attention due to its potential applications in miniaturized optical devices, sensors, and photonic circuits as well as in medical diagnostics and therapeutics.[4−8] Plasmonics is also a highly active area due, in part, to recent advances in nanofabrication methodologies.[9−12] These methodologies have led to the realization of metal nanostructures composed of nanoparticles (NPs),[13] nanoholes,[14] and other components[15] with precisely controlled shapes, sizes, and/or spacings.[16,17] Such exquisite synthetic control in combination with advances in theory and the emergence of quantitative electromagnetic modeling tools has provided a better understanding of the optical properties of isolated and electromagnetically coupled nanostructures of various sizes and shapes. In addition to control over the geometry and optical properties of nanostructures,[18,19] various strategies for modifying the surfaces of these materials make it possible to effect the selective binding and detection of specific targets for chemical and biological sensing.[20,21]

Detection schemes based on techniques that utilize plasmons experience enhancements that are commensurate with the magnitudes of the associated electric fields. These enhancements lead to new competencies for chemical sensing that are both useful and extraordinarily sensitive—with detection levels in some cases reaching that of single molecules.[22] As the field of plasmonic-based sensing grows, it is understood that the explicit control of nanostructured components will continue to provide techniques with unparalleled sensitivity, improved ease of fabrication, and thus enhanced utility outside of the laboratory.

Two types of surface plasmon resonances (SPRs) are used in surface-based sensing: (i) propagating surface plasmon polaritons (SPPs) and (ii) nonpropagating localized SPRs (LSPRs) (The terms 'propagating' and 'nonpropagating' are used here to describe evanescently confined surface plasmons. It should be kept in mind that a 'nonpropagating' LSPR is intimately coupled to ordinary or nonevanescent propagating light since the LSPR is excited by and scatters such light.). SPPs can be excited on thin metal films using grating or prism couplers.[23] These plasmons propagate tens to hundreds of micrometers along the metal surface with an associated electric field that decays exponentially from the surface (normal to the dielectric−metal interface).[24] Changes in the refractive index above the metal shifts the plasmon resonance condition, which can be detected as intensity, wavelength, or angle shifts in sensing applications.[25] SPR sensors that utilize propagating SPPs are covered in an article by Homola in this issue of *Chemical Reviews*. LSPRs are

* To whom correspondence should be addressed. Phone: 217-244-0809. Fax: 217-244-2278. E-mail: r-nuzzo@uiuc.edu.
[†] Department of Chemistry, University of Illinois at Urbana−Champaign.
[‡] Department of Materials Science and Engineering, University of Illinois at Urbana−Champaign.
[§] Argonne National Laboratory.

10.1021/cr068126n CCC: $71.00
Published on Web 01/30/2008

Matthew Stewart received his B.S. degree in Chemistry from Wittenberg University (Springfield, OH) in 2002, graduating *summa cum laude* with both departmental and university honors. In the summer of 2003 he worked as a flavor chemist at Givaudan, developing yeast blends, conducting accelerated aging experiments, and testing production lots for quality control. He joined Professor Ralph Nuzzo's group at the University of Illinois at Urbana–Champaign in the fall of 2003 to pursue his Ph.D. degree in Analytical Chemistry. His research interests include plasmonics, microfabrication, nanostructured materials, biomolecular–surface interactions, and microanalytical systems.

Lucas B. Thompson was born on March 27, 1981, in Cleveland, OH. Lucas received his B.A. degree from The College of Wooster (Wooster, OH) in 2003. While at Wooster, he computationally modeled the reconstruction of adlayers on metal surfaces under the supervision of Professor Wingfield V. Glassey. In the fall of 2003 he joined Professor Ralph Nuzzo's group at The University of Illinois at Urbana–Champaign to pursue his Ph.D. degree in Materials Chemistry. His research interests include collecting and analyzing cellular release with microfluidic devices, SPR as an analytical tool for selectively sensing biomolecules, and nanoparticle-enhanced polymer and hydrogel sensors.

Christopher Anderton was born in Colorado Springs, CO. He received his Bachelors of Science degree in Chemistry with highest distinction at the University of Colorado, Colorado Springs (UCCS). While at UCCS he worked under Professor David Weiss, researching flavonoid activity in many commercially available teas and green tea supplements. He also completed two NSF Research Experiences for Undergraduates under Professor Donald Dittmer at Syracuse University and under Professor Francisco Zaera at the University of California, Riverside. He is a third year analytical chemistry graduate student at the University of Illinois at Urbana–Champaign under Professor Ralph Nuzzo. His research interests include plasmonics, plasmonic enhancement from nanomanipulations, and microanalytical systems.

Joana Maria was born and raised in Lisbon, Portugal. She graduated with a degree in Engineering Physics from the New University of Lisbon and is currently pursuing her Ph.D. degree in Materials Science and Engineering under the guidance of Professor John A. Rogers at the University of Illinois at Urbana–Champaign. She does research in soft optical lithography and plasmonic sensors.

nonpropagating plasmon excitations that can be resonantly excited on metal NPs and around nanoholes or nanowells in thin metal films. The spectral position and magnitude of the LSPR depends on the size, shape, composition, and local dielectric environment.[26,27] This latter property has been exploited for label-free optical sensing where adsorbate-induced refractive index changes near or on plasmonic nanostructures are used to monitor binding events in real time.[28] Electromagnetic field enhancements also accompany these plasmonic resonances, which are used for performing surface-enhanced spectroscopies. This review focuses mostly, although not exclusively, on LSPRs and their use in chemical[29] and biological[30] sensing and surface-enhanced spectroscopies.[31]

2. Theoretical Considerations: Optical Properties of Metal Nanoparticles and Nanoholes

Gold (Au) and silver (Ag) metal NPs are frequently studied because they can exhibit strong SPRs in the visible wavelength range.[32] At these wavelengths, their optical properties are best described by a complex, wavelength-dependent dielectric constant

$$\epsilon(\lambda) = \epsilon_r(\lambda) + i\epsilon_i(\lambda) \quad (1)$$

where $\epsilon = m^2$ and $m = n + ik$ is the complex refractive index given as a function of the refractive index, n, and the absorption coefficient, k. Noble-metal NPs can support LSPRs[33] when the incident photon frequency is resonant with the collective oscillation of the conduction electrons confined in the volume of the NPs (Figure 1).[34] The simplest type of LSPR is a dipolar LSPR, which can be viewed as following in the limit of the particle's diameter, d, being much smaller than the wavelength of the incident light, λ ($d \ll \lambda$). The

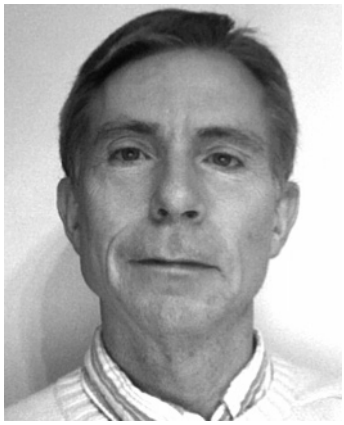

Stephen Gray was born in Sherbrooke, Québec, Canada. He received his B.Sc. (Hons) degree in Chemistry from Ottawa's Carleton University in 1977. Carrying out undergraduate thesis research work with Professor James Wright inspired him to pursue a career in theoretical chemistry. He went on to obtain his Ph.D. degree in Chemistry from the University of California at Berkeley in 1982 with Professor William Miller as his Ph.D. advisor. This was followed by post-doctoral work with Professor Mark Child at Oxford University and Professor Stuart Rice at The University of Chicago. He was an Assistant Professor of Chemistry at Northern Illinois University in DeKalb from 1986 to 1990 before joining the scientific staff at Argonne National Laboratory. His research interests include the quantum dynamics of chemical reactions and electrodynamics of metallic nanostructures.

John A. Rogers is Founder Professor of Engineering at the University of Illinois at Urbana–Champaign with primary appointment in the Department of Materials Science and Engineering, where his research includes materials for large area and unusual format electronics. From 1995 to 1997, he was a Junior Fellow in the Harvard University Society of Fellows. He joined Bell Laboratories as a Member of the Technical Staff in the Condensed Matter Physics Research Department at the end of 1997 and served as Director of this department from the end of 2000 to the end of 2002. He has been on the faculty at Illinois since January 2003. He has published more than ~180 papers and is co-inventor on ~70 patents and patent applications, more than 40 of which are licensed or in active use. His research has been recognized with many awards including most recently the Xerox Distinguished Lectureship (2006), the Dorn Lectureship at Northwestern University (2007), the 2007 Daniel Drucker Eminent Faculty Award, the highest honor from the University of Illinois College of Engineering, and the 2007 Baekeland Award from the American Chemical Society for outstanding achievement by a chemist under the age of 40. Rogers was elected a Fellow of the American Physical Society in 2006. He serves or has recently served on several Editorial Boards, including those for *Applied Physics Letters*, *Journal of Applied Physics*, and *Nano Letters*. He is Associate Editor *of IEEE Transactions on Nanotechnology* and *SPIE Journal of Microlithography, Microfabrication and Microsystems*.

Ralph G. Nuzzo is the William H. and Janet G. Lycan Professor of Chemistry at the University of Illinois at Urbana–Champaign, where he also holds an appointment as a Professor of Materials Science and Engineering. He received his AB degree with High Honors and Highest Distinction in Chemistry from Rutgers College in 1976, where he was also recognized as a Henry Rutgers Scholar, awarded the Merck Prize for undergraduate research, and elected to Phi Beta Kappa. He earned his Ph.D. degree in Organic Chemistry from the Massachusetts Institute of Technology in 1980. He accepted the position of Member of Technical Staff in Materials Research at Bell Laboratories in Murray Hill, NJ, in 1980, where he was named a Distinguished Member of the Staff in Research in 1987—a title held until he left to join the Illinois faculty in 1991. He is a fellow of the American Academy of Arts and Sciences, the World Innovation Foundation, and the American Vacuum Society. In 2006 he was recognized by the Wall Street Journal Innovators Award for Semiconductors and the Adamson Award of the American Chemical Society in 2003 for original discoveries leading to the development of self-assembled monolayers. He currently serves as a Senior Editor of *Langmuir* as well as a member of numerous advisory boards.

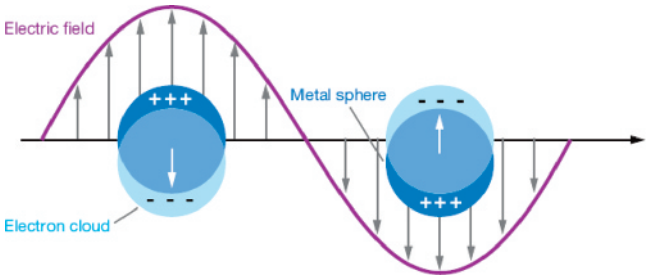

Figure 1. Schematic illustration of a localized surface plasmon of a metal sphere showing the displacement of the electron charge cloud relative to the nuclei. Reprinted with permission from ref 34. Copyright 2007 by Annual Reviews.

conduction electrons inside the particle will all move in phase upon plane-wave excitation. This leads to the buildup of polarization charges on the particle surface that will act as a restoring force, allowing a resonance to occur at a specific frequency known as the particle dipole plasmon frequency.[33,35] A resonantly enhanced field builds up inside the NP, which in the small particle limit is homogeneous throughout its volume, while a dipolar field is produced outside. This results in strong light scattering, the appearance of intense surface plasmon absorption bands, and the enhancement of the near-field in the immediate vicinity of the particle surface. The spectroscopic responses of larger metallic NPs are modified due to the excitation of higher order modes such as quadrupoles and retardation and skin depth effects.[33,35] The bandwidth, peak height, and position of the absorption maximum depend on the particle material, size, and geometry (Figure 2) and the dielectric function of the surrounding environment.[33,36,37]

Classical Mie theory[38] corresponds to the rigorous analytical solution of Maxwell's equations for the optical properties of a spherical particle. It assumes that the particle and the surrounding medium are homogeneous.[33,35] Solutions have

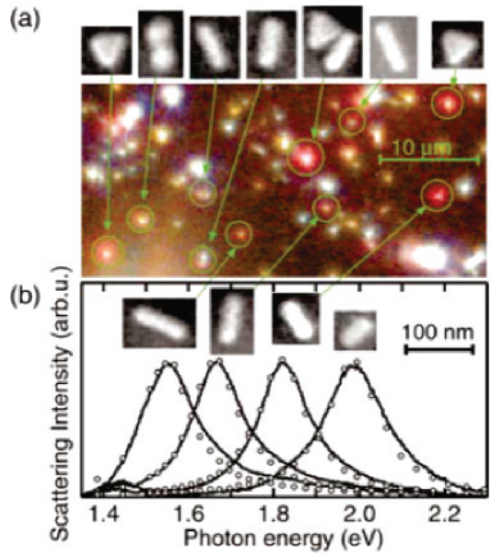

Figure 2. (a) Dark-field microscopy image and corresponding SEM images and (b) light scattering spectra of Au nanocrystals of different shapes. Reprinted with permission from ref 54. Copyright 2003 American Institute of Physics.

subsequently been developed for other particle shapes, including more general spheroidal forms;[32,39−41] such solutions are also often referred to as "Mie Theory". These analyses are greatly simplified when the particles are much smaller than the wavelength of light since only the lowest (dipolar) order of the Mie theory scattering coefficients need to be retained. In the long wavelength, electrostatic dipole regime, the extinction $E(\lambda)$—the sum of absorption and scattering cross sections—of a spheroid metallic NP is given by the following equation[33]

$$E(\lambda) \propto \left[\frac{\epsilon_i}{(\epsilon_r + \chi\epsilon_{med})^2 + \epsilon_i^2}\right] \quad (2)$$

where ϵ_{med} is the dielectric constant of the surrounding medium, λ is the excitation wavelength, χ is a form factor that describes the NP's aspect ratio ($\chi = 2$ for a sphere and increases directly with the aspect ratio of the NP), and ϵ_r and ϵ_i are the real and imaginary parts of the dielectric function of the metallic NP, respectively. For a spherical metal NP with $|\epsilon_r| \gg \epsilon_i$, eq 2 has a maximum when $\epsilon_r(\omega) \approx -2\epsilon_{med}$ and this is the LSPR. The position of this resonance red shifts with an increase in magnitude of the dielectric constant of the medium surrounding the NP due to the buildup of polarization charges on the dielectric side of the interface, which is responsible for the weakening of the total restoring force. For nonspherical metallic NPs, the surface plasmons are unevenly distributed around them, manifesting in a shape dependence of the LSPR absorption spectra.[42] The plasmon resonance of metallic nanorods, for example, splits into two peaks: (i) a strongly red-shifted long axis or longitudinal mode (L = polarization parallel to the long axis) and (ii) a slightly blue-shifted transverse mode (T = polarization perpendicular to the long axis). As the aspect ratio of a nanorod increases, the separation between the two plasmon bands becomes more pronounced (Figure 3).[16,43−51] Triangular metallic NPs exhibit multiple plasmon resonances, a longitudinal (bulk) plasmon mode, and very large field enhancements at their sharp tips.[52,53] Although a generalization of the quasistatic approach to metallic NPs of arbitrary shape has been suggested and demonstrated good results,[54] numerical methods such as the T-matrix method,[55] the discrete dipole approximation,[56,57] or finite-difference time-domain simulations[58,59] usually have to be used to calculate the optical properties (resonant frequencies; local field enhancement at the NP surface; absorption, extinction, and scattering efficiencies) for these more complex cases.

For larger metallic NPs beyond the Rayleigh approximation ($d > 30$ nm), the dipolar resonance red shifts and suffers a substantial broadening. The red shift arises due to a reduction of the depolarization field caused by retardation effects[60] where the conduction electrons do not all move in phase, as is true for smaller NPs, which leads to a reduced depolarization field at the particle center generated by the surrounding polarized matter. Radiative losses[61] also start to contribute significantly to the plasmon damping, eventually dominating it totally for Au and Ag NPs with diameters $d > 100$ nm, and for this reason can impact the analytical sensitivity measurements. The latter effect causes significant broadening of the resonance peak. Scattering processes at the NP's surface are thought to begin to contribute to the total damping for NPs smaller than the free-electron scattering length.[33] The depolarization field and additional damping mechanisms for large and small particles can be seen as lowest order corrections to the quasistatic theory leading to decreases in the total enhancement of the excitation field.

Mie theory only applies to noninteracting NPs well separated in the solid state or present at low concentration in solution. Recent advances in particle synthesis and fabrication techniques, however, have allowed the assembly of ordered arrays of interacting metallic NPs, leading to interesting new optical responses.[3,62−68] The plasmon resonances of interacting particles are split and shifted, depending on the polarization of the incident light, relative to those of noninteracting NPs.[65−67] In such cases, each NP with a diameter much smaller than the wavelength of the exciting light acts as an electric dipole. Two types of electromagnetic interactions prevail in this context, depending on the spacing d between adjacent NPs: (i) near-field coupling and (ii) far-field dipolar interactions.[62] Far-field dipolar interactions with a d^{-1} dependence dominate at NP spacings on the order of the wavelength (λ) of the exciting light,[69] while near-field dipolar interactions with a dependence of d^{-3} dominate for spacings much smaller than λ.[63] These distance dependences have important consequences for sensing based on the LSPR peak shifts caused by changes in the electromagnetic interactions that occur upon aggregation (or dissociation) of NPs, a feature that has been broadly exploited for colorimetric sensing.[70]

LSPRs analogous to metal NP LSPRs can be excited around nanoscale holes in thin metal films. This is not surprising in view of Babinet's principle, which relates the diffraction properties of particles to holes.[71] For example, Prikulis et al.[72] demonstrated remarkable correlations between the light scattering of holes in metal films and light scattering by disk-shaped NPs. Nanoholes tend to exhibit somewhat broader scattering features due to the fact that, in addition to the possibility of exciting LSPRs, the holes can serve as point sources for SPP waves in the thin film.[73,74]

As noted in the Introduction, propagating SPP waves form the basis of the SPR sensors reviewed by Homola in this issue. In the case of periodic hole arrays in thin metal films that are reviewed by us here (section 4.4.3), the periodic analog of SPPs and related diffractive phenomena such as

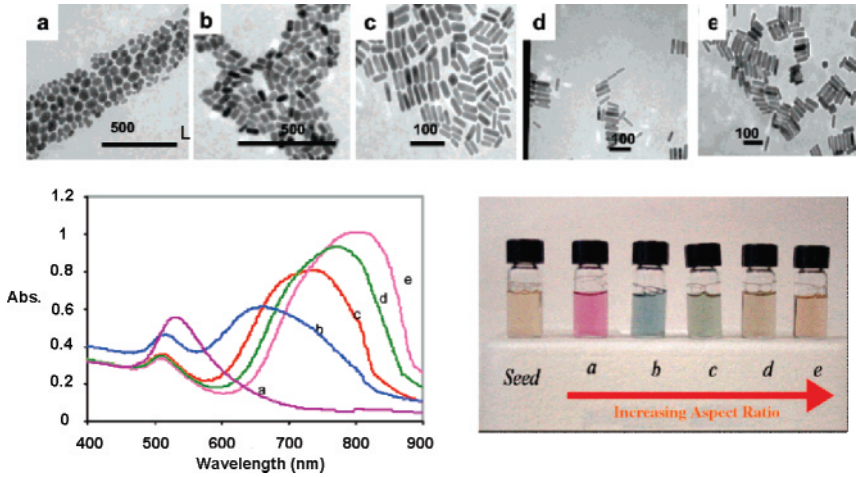

Figure 3. Transmission electron micrographs (top), optical spectra (left), and photographs (right) of aqueous solutions of Au nanorods of various aspect ratios. The seed sample has an aspect ratio of 1. Samples a, b, c, d, and e have aspect ratios of 1.35 ± 0.32, 1.95 ± 0.34, 3.06 ± 0.28, 3.50 ± 0.29, and 4.42 ± 0.23, respectively. Scale bars: 500 nm for a and b, 100 nm for c−e. Reprinted with permission from ref 16. Copyright 2005 American Chemical Society.

Wood's anomalies[75−77] are intimately entangled with LSPRs and so must also be factored into our discussion. We will consider these influences and their consequences for sensing applications in the sections below.

3. Synthesis and Fabrication of Plasmonic Nanostructures

Formation of metal nanostructures has been an active area of research due in part to their growing importance in diverse applications including photonics and optoelectronics,[2,3,6,78−82] electronics,[83−86] chemical and biosensing,[14,87−92] and medical diagnostics and therapies.[93−97] It is now well appreciated that the optical, electronic, and catalytic properties of metal nanostructures can be tuned very broadly by controlling their size, shape, and composition.[25,35,98−101] This has resulted in a wealth of literature on synthetic methodologies for generating isotropic and anisotropic nanostructures with well-controlled sizes and shapes from a variety of materials.[16,17,93,100−104] Nanostructures are typically formed using either so-called top-down or bottom-up approaches.[10] Top-down techniques involve using various forms of conventional lithographic techniques to pattern nanostructures (e.g., onto planar substrates),[65−67,105] whereas bottom-up methods exploit the interactions of atoms, molecules, or more complex mesoscale objects, in conjunction with the controlling influences of process kinetics, to "assemble" nanostructures either on substrates or in solution.[72,106−111] The following sections will describe in more detail the use of these approaches for synthesizing representative metal nanostructures that support propagating and/or localized plasmons and exhibit interesting/useful optical properties.

3.1. Solution-Phase Syntheses

Bottom-up solution-phase synthesis is a versatile approach to forming NPs that allows control over their size,[112−117] shape,[17,101] composition,[98,118−120] and structure (e.g., solid or shell).[95,121,122] This approach generally involves the reduction of metal salts in a solution containing an appropriate stabilizer to control the growth and suppress the aggregation of the NPs.[123,124] The stabilizer—commonly ligands, surfactants, ions, organic acids, or polymers—adsorbs or coordinates to the surface of the NPs and inhibits aggregation by Coulombic repulsion[20,114,125] and/or steric hindrance.[124,126,127] Reduction of the metal salt can be carried out electrochemically,[15,128−132] photochemically,[114,133−136] sonochemically,[137−139] or using chemical reductants such as citrate,[114,117,140] hydrides,[141,142] alcohols,[143,144] hydrogen,[104] hydroxylamine,[145,146] or hydrazine.[147,148] The specific choice of reductant, stabilizer, temperature, and relative concentrations of the reagents can all affect the size and shape of the NPs. Recent work has investigated biosynthetic approaches[149−153] and other environmentally friendly methods of synthesizing NPs.[126,154,155] This topic has been reviewed in a recent issue of *Chemical Reviews*.[156]

Solution-phase synthesis tends to yield *approximately* spherical particles since the lowest surface energy shape is that of a sphere.[4,100] (These particles have facets and should be more correctly called 'quasi-spheres',[4] but will be referred to here as spherical particles for simplicity.) One of the most commonly used procedures for making spherical Au NPs is the citrate reduction of $HAuCl_4$ in an aqueous solution, which was first reported by Turkevitch et al. in 1951.[157] In this protocol the citrate acts as both a reducing agent and an electrostatic stabilizer, and the size of the NPs can be tuned by controlling the citrate to $HAuCl_4$ ratio.[113,158] Citrate can also be employed in the synthesis of Ag particles.[114]

Another broadly adopted solution-phase synthesis that yields highly stable, monodisperse thiol-protected particles with controllable sizes is the Brust−Schiffrin method.[159] This approach uses a biphasic synthesis (an aqueous and organic phase) and tetraoctylammonium bromide as a phase-transfer agent to reduce the $[AuCl_4]^{-1}$ anion with $NaBH_4$ in the presence of alkanethiols to yield thiol-stabilized particles that are one to several nanometers in size.[159] The particle sizes can be controlled between 1.5 and 5.2 nm by adjusting the temperature, reduction rate, and thiol to Au ratio.[13,112,156,160,161] The thiols on these so-called monolayer-protected cluster (MPCs) can be easily switched to introduce functionality,[162,163] such as thiolated oligonucleotides[164] or proteins,[165] through simple place-exchange reactions.[166−169] Other ligands such as amines and phosphines can also be used to stabilize and control the growth of NPs,[170−174] and more recent single-phase adaptations of the Brust method have eliminated the need for phase-transfer agents.[170,175−177]

Well-defined NPs can also be fabricated using seed-mediated growth techniques.[99,102,145,146,178−182] Nanorods are commonly prepared using this approach,[100,102,178,179] although they can also be prepared electrochemically[49,183−185] and photochemically.[133,186] In seed-mediated syntheses, a stable growth solution is prepared containing a metal salt, a mild reducing agent (e.g., ascorbic acid), a surfactant molecule (e.g., cetyl-trimethylammonium bromide, CTAB), and possibly other additives.[45,46,100,179,187] A NP 'seed', the nucleating agent, is added to the solution and the metal salt is reduced directly on the surface of the seed with minimal nucleation occurring in solution.[178] The surfactant acts as an organic micellar template for anisotropic growth. The morphology, aspect ratios, and synthetic yields of the seeding approach are controlled by the composition and concentration of the surfactant, additives, seeds, metal salts, and reducing agent.[45,46,100,179,188−191] Seeding growth can also be used to grow Au and Ag nanorods directly on surfaces,[192−194] where the initial seed concentration affects the resulting nanorod aspect ratios and size distributions.[195]

As noted above, nanorods exhibit two distinct plasmon resonance modes: one associated with electron oscillations parallel to the longitudinal axis and the other with electron oscillations parallel to the transverse axis.[16,43−51] The longitudinal plasmon mode can be tuned by adjusting the aspect ratio of the nanorod, making it a particularly useful structure for applications in photonics and biotechnology.[16,43−51] Au nanoshells are another type of metal nanostructure that have highly tunable plasmon resonances.[95,196] Halas and co-workers formed such core−shell structures by seeded metallization of colloidal silica spheres.[197] The silica particles are functionalized with a monolayer of an amine-terminated silane (aminopropyltriethoxysilane (APTES)), which is subsequently used to bind small colloidal Au particles. After this initial seeding, more Au is deposited by an electroless plating procedure. The thickness of the final Au shell can be controlled by adjusting the initial Au seed coverage and the amount of reductant used in the plating process.[197,198] The plasmon resonance frequency is tuned by adjusting the relative sizes of the core and shell dimensions (Figure 4).[95,196] This synthetic approach has also been used to form a so-called nanorice structure,[199] prolate spheroidal NPs consisting of a hematite core and a Au shell.

The polyol process is a highly versatile synthetic procedure that can be used to form metal and alloy NPs with a variety of shapes, sizes, and optical properties.[17,101,144] This synthesis uses a polyol such as ethylene glycol as both a solvent and reducing agent (at elevated temperatures) for a metal salt precursor. Xia and co-workers used the polyol synthesis to produce a variety of Ag nanostructures with well-defined shapes (including cubes, rods, wires, or spheres) by adjusting the relative amounts of the capping agent (poly(vinyl pyrrolidone)) and the precursor salt ($AgNO_3$) in solution.[17,101,144,200,201] Nanoplates and nanobelts are formed using a different capping agent (such as sodium citrate).[17] Hollow Au or porous Ag/Au alloy nanostructures can also be produced using Ag NPs as a physical template in a well-known galvanic replacement reaction.[121,202] For example, Au nanocages have been generated by simply adding $HAuCl_4$ to a suspension of Ag nanocubes.[203] Adjusting the volume of the $HAuCl_4$ solution added to the Ag nanocube suspension allows formation of a variety of different nanostructures such as hollow Au/Ag alloy nanoboxes and/or Au nanocages. The LSPR of these structures can be tuned from the visible to near-infrared by varying the amount of $HAuCl_4$ solution added to the Ag nanocube suspension.[17,203]

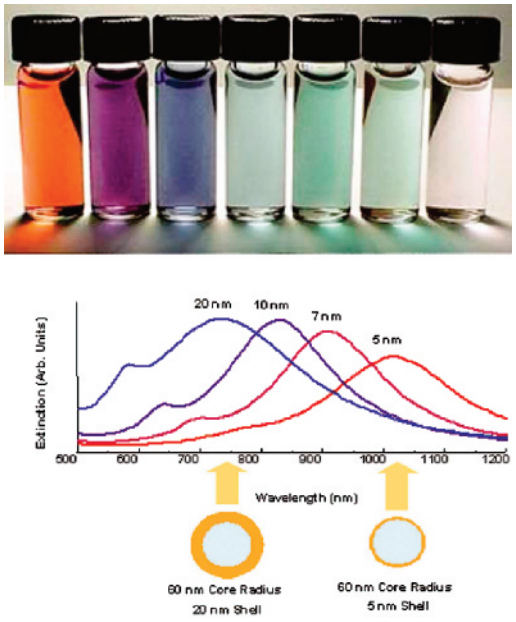

Figure 4. Visual demonstration of the tunability of metal nanoshells (top), and optical spectra of Au shell−silica core nanoshells (the labels indicate the corresponding Au shell thickness). Reprinted with permission from ref 95. www.tcrt.org.

Surfactant aggregates such as micelles, reversed micelles, and microemulsions are also used to make restricted volume nanoreactors for the in-situ synthesis of NPs.[204−209] The interested reader is referred to recent review articles on this synthetic approach[204,205] as well as to a recent *Chemical Review* article for more detailed descriptions of NP syntheses.[13,156,210]

3.2. Top-Down Lithography

The size, shape, and interparticle spacing of surface-bound metallic nanostructures can be exquisitely controlled using scanning beam lithographies, such as electron beam lithography (EBL)[67,105] and focused ion beam (FIB) lithography.[211] This type of control is highly important for making reproducible substrates with tunable optical properties for conducting systematic studies of SERS[212−214] and plasmon-enhanced fluorescence.[215] In EBL a tightly focused beam of electrons is scanned across a thin layer of resist (a radiation-sensitive polymer), which makes it either more or less soluble in an organic developer solution. The patterned resist is then used as a sacrificial mask in subsequent etching or deposition processes to generate nanostructured metallic patterns with well-controlled geometries. EBL can be used to attain sub-20 nm resolution using specialized resists such as hydrogen silsesquioxane (HSQ)[216,217] or NaCl crystals[218] or using more traditional organic resists such as poly(methylmethacrylate) (PMMA) in conjunction with ultrasonically assisted development.[219]

FIB is a related technique that uses a focused beam of ions (typically Ga^+) to perform both additive and subtractive patterning by physical or chemically assisted processes. These include (1) FIB milling,[211,220,221] (2) ion-assisted etching,[222,223] and (3) FIB-induced deposition.[224,225] FIB is capable of forming patterns with ~10 nm resolution using either PMMA[226] or inorganic resists.[227] Various metallic nanostructures such as circular slits,[221] nanoholes,[228,229] slit

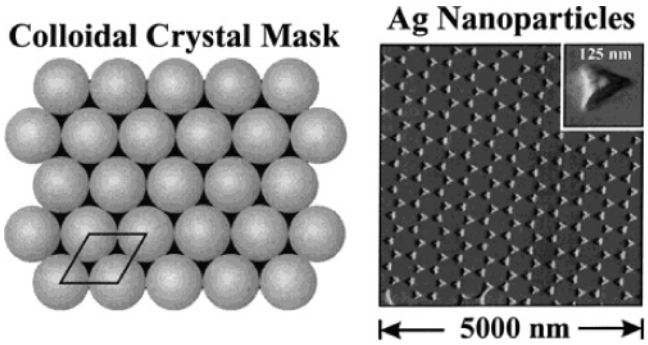

Figure 5. Schematic illustration of hexagonally close pack colloidal crystal mask (left), and a representative AFM image of a triangular NP array (right). Reprinted with permission from ref 109. Copyright 2001 American Chemical Society.

gratings,[230,231] and V-grooves[6,232] have been fabricated by FIB for research in the growing field of plasmonics.

While scanning beam lithographies are capable of precise control over the size, shape, and spacing of metallic nanostructures, more recent research has focused on unconventional lithographic techniques that are capable of patterning large areas in parallel at low cost.

3.3. Unconventional Lithographic Techniques

3.3.1. Nanosphere Lithography

Nanosphere lithography (NSL) is an inexpensive and versatile hybrid bottom-up procedure, popularized by Van Duyne, for fabricating periodic arrays of metallic nanostructures on surfaces.[109,233] This unconventional approach to nanofabrication is a variant of a technique originally named "natural lithography" where monolayers of nanospheres are used as deposition or etch masks.[234,235] NSL extended natural lithography with the development of double-layer colloidal masks, which provide a degree of control over the size and shape of the resulting NPs.[109]

Single-layer NSL begins with the deposition of a single-layer colloidal crystal mask of hexagonally close-packed latex or silica spheres on an appropriate substrate, which yields defect-free domains that are approximately 10−100 μm^2 in size.[109,236,237] The colloidal crystal contains triangular void spaces that are created between three neighboring particles, which make these crystals useful as masks in subsequent deposition or etching processes.[91,109,238] In the case of additive lithography, a metal or other material is deposited through the mask at normal incidence by physical vapor deposition to produce a metallic film over nanosphere (MFON) structure.[31,239,240] This approach has been used to produce Ag FON surfaces that are useful structures for applications based on surface-enhanced Raman spectroscopy (SERS).[240−242] Alternatively, the nanosphere mask can be removed by sonicating in solvent to yield arrays of surface-bound triangular NPs with *P*6*mm* symmetry. These structures can be used for LSPR sensing and SERS (Figure 5).[109,243−246]

Nanostructured films composed of periodic spherical voids can also be formed using self-assembled polystyrene (PS) colloidal crystal masks. These 'nanovoid arrays' support delocalized Bragg and localized Mie plasmons[247,248] and are formed by electrochemical deposition of Au through a single-layer self-assembled colloidal template. The thickness of the metal is controlled by monitoring the current passed through the plating solution and the plating time.[18,249] This allows control over the geometry and thus the spectroscopic/plasmonic properties of the nanostructured films.[18,250] After completing the metal deposition step, the PS spheres are dissolved in tetrahydrofuran to yield a 'nanovoid array' (Figure 6). These structures have been used with some success as substrates for SERS.[249−252]

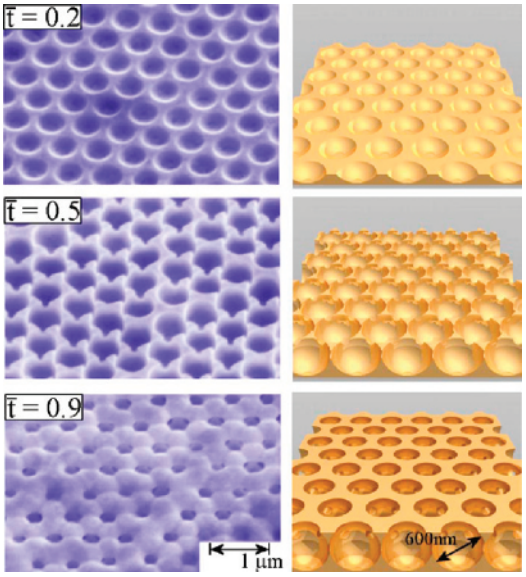

Figure 6. SEM images of nanovoid arrays with void diameters of 600 nm at three normalized thicknesses $t^- = 0.2$, 0.5, and 0.9 (left), and schematic illustrations of the surface at each thickness (right). Reprinted with permission from ref 247. Copyright 2006 The American Physical Society.

Self-assembled colloidal crystals also can be used as an etch mask to form arrays of submicrometer triangular pits in an underlying substrate.[238] Anchored arrays of triangular metal NPs[110] and metal films over nanowells[253] can be formed using this subtractive processing technique. The anchored NPs are formed by depositing metal at normal incidence by physical vapor deposition on the colloidal mask and underlying etched substrate. The spheres are subsequently removed by sonication in an appropriate solvent, leaving behind an array of substrate-embedded triangular NPs.[110] Alternatively, metal deposition can be performed after the spheres are removed from the etched substrate. This results in structured metallic surfaces that support a single, narrow plasmon resonance that exhibits sensitivity to external changes in refractive index.[253]

The attractive features of NSL include its low cost, versatility, and ability to produce well-ordered sub-100 nm array structures. The geometry and shape—and thus the optical properties—of the particles can be tuned by moving the sample during metal deposition,[254] annealing the latex colloidal mask prior to metal deposition,[255] as well as changing the thickness of the deposited metal, size of the colloidal spheres, number of colloidal layers, or angle of the metal deposition.[109,256,257] The size and shape of the NPs can also be changed in a controllable manner using electrochemistry to oxidize the substrate-bound particles.[258] The surface-bound NPs formed by NSL can be released from the substrate into solution by adding surfactant and sonicating to generate both isolated particles and dimers.[111]

3.3.2. Colloidal Lithography

Colloidal lithography[72] is a versatile technique that can be used to form random arrays of nanoholes,[259] nanodisks,[260]

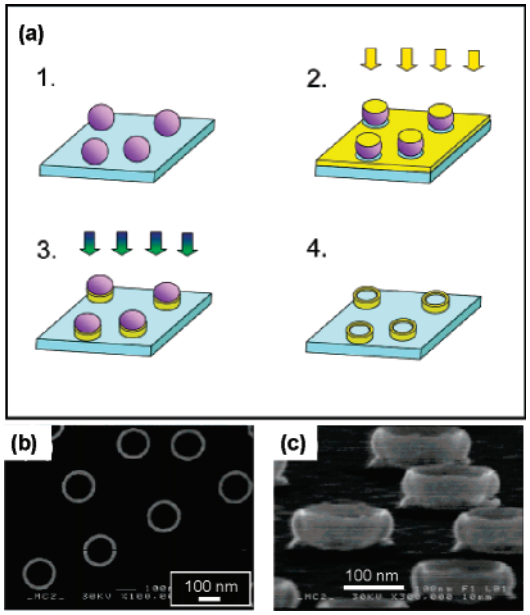

Figure 7. Schematic depiction of nanoring fabrication. (a) (1) Polystyrene colloidal particles are deposited by electrostatic self-assembly onto the substrate in a dispersed layer. (2) A 20−40 nm thick Au film is evaporated onto the particle-coated substrate at normal incidence. (3) Argon-ion beam etching is used to remove the Au film. During the etching, secondary sputtering creates a Au shell around the base of the polystyrene particles. (4) The remainder of the polystyrene particles are removed by UV−ozone treatment, resulting in free-standing Au nanorings on the substrate. SEM images of Au nanorings (150 nm diameter) made using a 40 nm thick sacrificial Au layer at normal incidence (b) and 80° tilt (c). Reprinted with permission from ref 383. Copyright 2007 American Chemical Society.

and nanorings.[108] This unconventional nanofabrication technique involves adsorbing polystyrene (PS) particles onto a substrate via electrostatic self-assembly. The distance between the self-assembled spheres is governed by the particle−particle repulsion, which can be controlled by adjusting the electrolyte concentration of the colloidal solution.[107] The randomly adsorbed particles are then used as a mask for subsequent evaporation and/or etching processes wherein the size of the sphere dictates the size of the resulting nanostructures. The main difference between colloidal lithography and NSL is that the colloidal spheres do not form an hcp monolayer on the substrate in colloidal lithography.

Random nanoholes in Au films can be formed by evaporating metal on top of an assembled colloidal mask followed by lift off of the PS particles by tape stripping or boiling the sample in ethanol.[259] Nanorings are formed on substrates in a similar process with the exception that prior to particle removal an Ar^+-ion beam is used to etch the Au film, during which secondary sputtering creates Au shells around the bottom of the PS particles.[108] The remains of the particles are then removed by an UV−ozone treatment, which leaves free-standing Au rings (Figure 7). Nanodisks can be formed in two ways.[260,261] In one approach, nanodisks are formed by assembling a colloidal mask on top of a Au film followed by etching of the Au and removal of the colloidal mask.[260] In the second approach, a colloidal mask is self-assembled on a PMMA film followed by deposition of a thin Au film. The Au-capped PS particles are then removed by tape stripping, leaving behind holes in the Au film. The exposed PMMA is then etched from the holes, and metal is deposited through the holes onto the substrate.

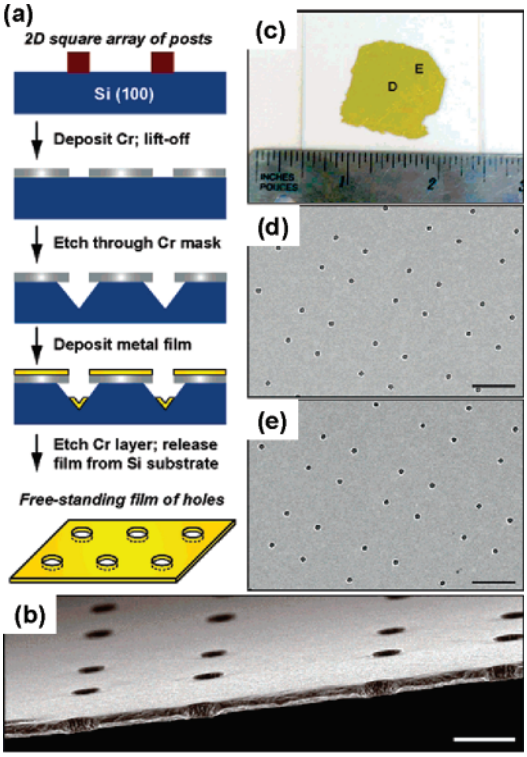

Figure 8. Fabrication and structural characterization of large-area hole arrays. Preparation of free-standing films of subwavelength hole arrays (a). SEM image of a portion of a free-standing 100 nm Au film perforated with 250 nm holes (b). Scale bar: 500 nm. Optical micrograph of a free-standing film placed on a glass substrate (c). SEM images of representative areas of the film illustrating the uniformity of the nanohole array (d and e). The holes are spaced 1.6 × 2.4 μm. Scale bar: 2 μm. Reprinted with permission from ref 270. Copyright 2005 American Chemical Society.

The metal-coated PMMA film is removed by lift off, leaving a random array of metal disks on the substrate.[261]

3.3.3. Soft Lithography

Soft lithography refers to a set of microfabrication techniques that use a structured elastomer as a stamp, conformable photomask, or mold to pattern a material of interest.[262−264] The most commonly used elastomer, Sylgard 184 poly(dimethylsiloxane) (PDMS), has a low modulus, which limits the utility of this elastomer for patterning in the nanometer regime.[265,266] The development of siloxane-based elastomers with larger moduli, such as the so-called hard PDMS (*h*-PDMS)[266−268] and UV-curable PDMS (*hν*-PDMS),[269] has extended the patterning ability of soft lithography to the nanometer regime. Composite stamps consisting of a thin layer of structured *h*-PDMS supported by a thicker planar layer of compliant PDMS are typically used for patterning at the nanoscale due to the mechanical instabilities and difficulty of achieving conformal contact with nonplanar surfaces using *h*-PDMS stamps.

In one embodiment of soft lithography for fabricating plasmonic structures, Odom et al. used high-resolution composite PDMS stamps as conformable phase masks to generate large-area, free-standing 2D nanohole arrays in Au.[270,271] A schematic illustration of the fabrication process is shown in Figure 8. In this process, an array of posts of positive photoresist with diameters of ∼250 nm is patterned first on a Si(100) wafer by phase-shifting photolithography using a conformable composite PDMS photomask.[266,271,272]

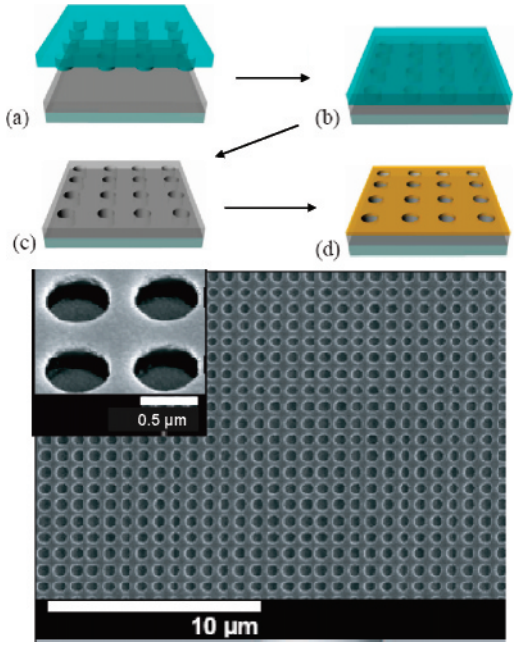

Figure 9. Plasmonic crystal fabrication process: (a) imprint, (b) cure, (c) remove stamp, and (d) Au deposition (top). SEM of a crystal and a high-magnification SEM (inset) that shows the upper and lower levels of Au (bottom). Reprinted with permission from refs 8 (top) and 77 (bottom). Copyright 2005 OSA (top) and Copyright 2006 The National Academy of Sciences of the USA (bottom).

A thin layer of chromium (Cr) is then deposited by electron-beam (e-beam) evaporation followed by removal of the photoresist posts. This yields an array of holes patterned in a thin film of Cr, which acts as an etch mask and as a sacrificial release layer to generate the free-standing nanostructured Au films. The exposed Si is then anisotropically etched using a KOH/isopropyl alcohol (IPA) solution to produce pyramidal-shaped voids directly below the Cr nanoholes. A layer of Au can then be deposited by e-beam evaporation to form a 2D nanohole array Au film on the top surface and pyramidal mesoscale Au particles in the lower pyramidal voids. The top Au nanohole array can be released by selectively etching the Cr film to form a free-standing structure (Figure 8), and the Au pyramids can be released by etching the Si with KOH/IPA. The material and chemical functionality of these nanostructures are easily controlled by depositing other metals or a combination of metals in a layer-by-layer mode using e-beam evaporation.[270] The periodic grating structure of the nanohole array allows the direct coupling of light to SPPs on these films.[270,273] This fabrication protocol has been used to produce pyramidal metallic particles[274] and particle arrays.[275]

Imprint lithography is another unconventional lithographic technique holding broad utility for patterning materials at the nanoscale over large areas.[8,77,276−278] This rapidly emerging technology is used to replicate features on a hard or soft stamp in a thermoplastic or UV-curable polymeric material by embossing or molding (Figure 9). A metal film can be deposited on the resulting polymeric replicas to produce plasmonic structures useful for chemical and biosensing applications.[8,77,279,280] In a recent example, large-area spatially coherent arrays of quasi-3D plasmonic crystals were formed by soft nanoimprint lithography and used for multispectral sensing and imaging of molecular binding events. The arrays were fabricated by embossing a thin UV-curable polyurethane film with a composite *h*-PDMS/PDMS stamp presenting surface relief features in the geometry of a square array of cylindrical posts. The composite PDMS stamp is pressed into the liquid polyurethane film and cured by UV light passed through the stamp. The stamp is then removed, and a thin layer of Au (∼50 nm) is uniformly deposited by e-beam evaporation onto the raised and recessed regions of the structured polyurethane film. This creates a Au film with an array of nanoscale holes (top surface) that is physically separated from a second level of Au disks at the bottom of the wells (Figure 9).

4. Applications of Plasmonic Nanostructures in Sensing and Chemical Imaging

4.1. Colorimetric Sensing Based on Particle−Particle Coupling

Colorimetric detection is perhaps one of the most powerful and simple nanosensing methods available. In an exemplary model of this approach, Mirkin et al.[70] reported an assay using oligonucleotide-functionalized Au NPs that exhibit strong red shifts upon aggregation in the presence of a complementary nucleotide (Figure 10).[281] The color change in this case results from particle−particle plasmonic coupling as well as aggregate scattering[281] and provides a "litmus test" method for determining nucleic acid targets. The optical properties of these assays are due to the aforementioned resonantly exited LSPRs of the NPs. The enhanced electronic fields are confined within a small area around the NPs (typically on the order of the particle radius) and decay approximately exponentially thereafter.[65,66] As the distance between the NPs decreases, near-field coupling begins to dominate, leading to a strong enhancement of the localized electric field within the interparticle spacing producing pronounced red shifts of the LSPR frequency.[65−67] Most reports of colorimetric assays exploit the LSPRs that develop on spherical Au NPs, but the method is also amenable to nonspherical particles[21,282] as well as particles of other noble metals.[283,284] Some benefits to using elongated particles include their inherent higher sensitivity to changes occurring in the local dielectric environment[285] and the capability they afford for multiplexed detection schemes.[286]

Methods exploiting nucleotide interactions have been the most reported of these particle−particle coupling systems. This field of research has advanced rapidly, and biological analyses using oligonucleotide-modified Au NPs have been developed that achieve limits of detection (LOD) for a variety of analytes in the low-picomolar to mid-femtomolar range.[281] Han et al. used oligonucleotide-functionalized Au NPs to determine the relative binding strengths of a variety of duplex and triplex DNA-binding molecules.[287,288] Such data can offer insights into the activity of an array of possible anticancer drugs due to the correlations that can be made between ligand binding strength and biological activity. Kanaras and co-workers[289] demonstrated the use of DNA−Au NP interactions for the determination of the enzymatic cleavage of DNA, in which a recognition site for the restriction endonulease *Eco*RI was designed to monitor the enzymatic cleavage activity, and consequent disassembly of the closely coupled Au NPs, via blue to red color shifts. Peptide nucleic acid (PNA) and aptamer-modified Au NPs have also been used to control assembly rates and aggregate sizes of Au NPs for sensing applications.[87,290−293] The dissolution of aggregated NPs can also be used to monitor binding events.

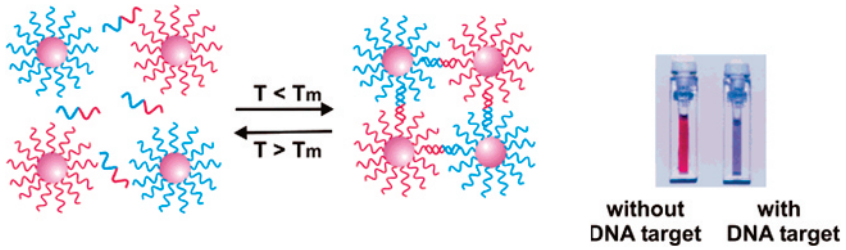

Figure 10. In the presence of complementary target DNA, oligonucleotide-functionalized Au NPs will aggregate (left), resulting in a change in the color of the solution from red to blue (right). Reprinted with permission from ref 281. Copyright 2005 American Chemical Society.

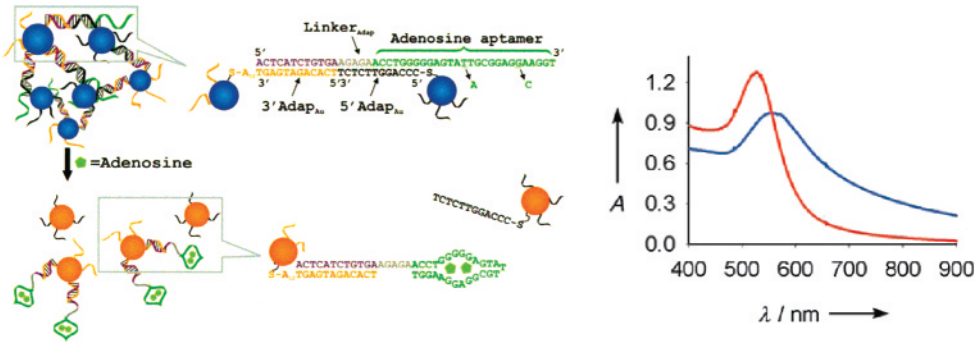

Figure 11. Schematic representation of colorimetric detection of adenosine. Absorbance spectra of the adenosine sensor before (blue) and 10 s after (red) addition of adenosine. Reprinted with permission from ref 87. Copyright 2006 Wiley-VCH Verlag GmbH & Co. KGaA, Weinheim.

In a specific example, Liu and Lu[87] employed aptamer-functionalized Au NP aggregates specific to adenosine and cocaine that become unstable when the target was bound, leading to a color shift from purple to red (Figure 11).[87]

Functionalized Au NPs that do not exploit nucleotide interactions also have been reported that provide a viable route to colorimetric detection.[284,294−303] In a prototypical example, the ubiquitous biotin−avidin system linked to Au NPs was utilized to create a colorimetric assay for kinase inhibitors that could be applied to microplates amenable to parallel screening.[301] Rapid detection of cholera toxin has been demonstrated using lactose-stabilized Au NPs, in which the cholera toxin binds to a lactose derivative inducing NP aggregation, which is detected visually by a red to purple color shift.[299]

In an expansion of the current methods for colorimetric detection, cation-specific functionalized Au NPs have been developed.[88,282,297,304,305] The detection of Pb^{2+} is an area that has received much attention due to its physiological impacts. Demonstrating the use of DNAzymes in Au NP assembly for the detection of Pb^{2+}, Liu and Lu[304] optimized the DNA configuration for NP alignment, the NP size, Pb^{2+}-specific DNAzyme concentration, and salt concentration, leading to a colorimetric detection method for Pb^{2+} that can be performed in the field in less than 10 min. In contrast to the previously mentioned method of sensing lead, Lin et al.[297] used a crown ether specific to Pb^{2+} for colorimetric detection of Pb^{2+} using Au NPs ligated with a mixed monolayer of crown ether thiols and carboxylic acids.[306] Recently, Lee and co-workers[88] demonstrated a detection method for the mercuric ion (Hg^{2+}) analogous to Liu and Lu,[305] which takes advantage of the Hg^{2+} affinity toward T−T mismatches in DNA. Aside from the cation determination methods mentioned here, additional methods have been reported for determining other relevant charged molecules.[296,302,303]

All of these methods employ the plasmonic coupling inherent in aggregated NP systems and demonstrate that detection of desirable biological compounds and other relevant molecules can be accomplished without the use of complex instrumentation. These methods are interesting in that they are sensitive at relevant time scales and that the NPs are easily functionalized to provide chemical and biological selectivity. The optical properties of NPs also have been exploited to enhance the sensitivity of conventional SPR systems as described below.

4.2. Nanoparticle-Enhanced Surface Plasmon Resonance

As mentioned above, SPR spectroscopy is a surface-sensitive technique that can be used to detect refractive index changes that occur within the evanescent field of propagating SPPs excited at metal−dielectric interfaces.[307] A change in refractive index shifts the plasmon resonance condition, which can be detected as intensity, wavelength, or angle shifts to provide quantitative information about the binding event.[307−313] Small refractive index changes caused by the binding of low molecular weight analytes or small quantities of a larger analyte can challenge the sensitivity/detection limits of SPR spectroscopy.[314−319] The sensitivity/detection limits can be improved by coupling the molecular recognition of analyte at the surface of the metal with another event that leads to larger changes in the SPR signal.[314−319] This signal enhancement can be achieved using competitive inhibition or sandwich assays[320−323] and enzymatic amplification.[312,313,324,325] The SPR signal also can be enhanced by labeling the target analyte with dielectric or plasmonic NPs. These labels increase the refractive index at the metal surface and can electromagnetically couple to the flat metal film in the case of plasmonic NPs, leading to larger SPR shifts.[314−319,326]

Figure 12a shows a possible architecture for performing plasmonic NP-enhanced SPR immunoassays.[314] In this approach a surface-immobilized antibody (e.g., anti-human

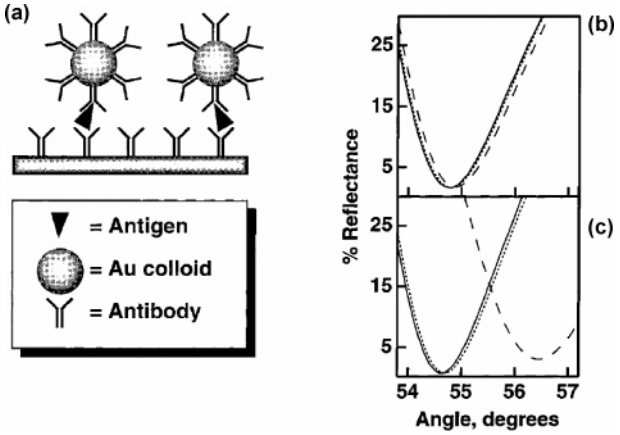

Figure 12. Schematic of plasmonic NP-enhanced SPR immunoassay (a). In situ SPR curves of an evaporated Au film modified with a-h-IgG(γ) (solid line) followed by sequential exposure to a 0.045 mg/mL solution of h-IgG (···) and a 8.5 mg/mL solution of a-h IgG(F_c) (- -) (b). A film modified with a-h-IgG(γ) (solid line) followed by sequential exposure to a 0.045 mg/mL solution of h-IgG (···) and a solution of a-h-IgG(F_c)-10-nm Au colloid conjugate (- -) (c). Reprinted with permission for ref 314. Copyright 1998 American Chemical Society.

immunoglobulin G (a-h-IgG)) is sequentially exposed to antigen (e.g., h-IgG) and a solution of secondary antibody-conjugated Au NPs (e.g., a-h-IgG/Au NPs). The presence of the Au NP leads to an enhancement of the measured SPR shift as shown in Figure 12b and c. Figure 12b shows that the shift of the SPR peak upon binding the secondary antibody alone is small compared to the shift observed when the secondary antibody is conjugated to a Au NP.[314] The particle size, composition, and surface coverage as well as the substrate metal and the distance between the substrate and NP can affect the observed signal enhancement.[314,315,327−329] This approach has been used not only for performing immunoassays[314,330] but also for detecting DNA hybridization,[319,331] protein conformational changes,[332] small molecule binding interactions,[317,318] and single nucleotide polymorphisms.[316] Recently, Fang et al. reported the detection of attomoles of microRNA using NP-enhanced SPR imaging.[333] In addition to flat film SPR, NPs can also be used to enhance the peak shifts obtained from transmission LSPR sensing using Au island films.[334−336] This platform has been used with responsive polymer brushes, surface-immobilized single-stranded DNA, and molecularly imprinted polymers to detect pH changes,[334] DNA hybridization,[336] and cholesterol,[335] respectively.

4.3. Exploiting Rayleigh Scattering for Sensing and Imaging

Biosensing based on the optical scattering properties of plasmonic NPs is regarded as a potentially more powerful, yet remains a less widely exploited, modality of NP sensing than the extinction-based colorimetric assays described above.[337,338] A single 80 nm Au NP, for example, exhibits a light scattering power equivalent to the emission of $\sim 10^6$ fluorescein molecules.[339,340] Unlike molecular fluorophores, however, plasmonic NPs do not undergo photobleaching or blinking. These are enabling distinctions that facilitate long-term single-particle measurements and tracking.[285,341−343] These optical properties have been exploited in a variety of applications where NPs are used for sensing[285,344] and as labels for immunoassays and DNA

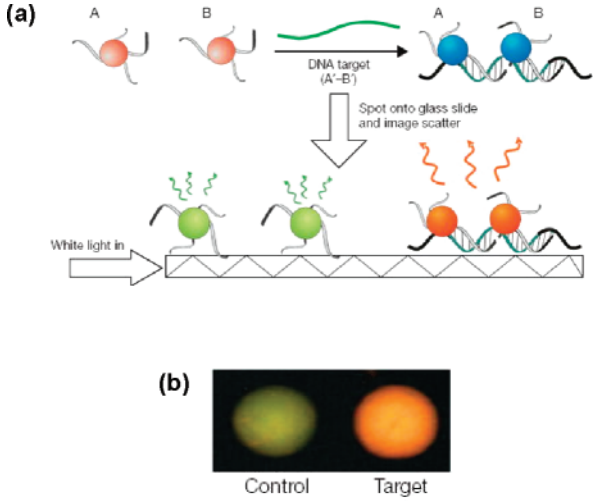

Figure 13. Colorimetric detection of nucleic acids using scattered light (a). Step 1: DNA−Au NP probes (A and B) are hybridized to a DNA target in solution. Step 2: The samples are spotted onto a glass slide, which is illuminated with white light in the plane of the slide. The evanescent induced scatter from the Au NPs is visually observed. Individual 40 to 50 nm diameter Au probes scatter green light, whereas complexed probes scatter yellow to orange light because of a plasmon band red shift (b). Reprinted with permission from ref 352. Copyright 2004 Nature Publishing Group.

microarrays,[345−348] imaging contrast agents,[95,349] and molecular rulers.[341,350,351]

As noted in section 4.1, the changes in extinction (absorption and scattering) that occur due to NP aggregation can be used to detect the presence of a specific target DNA or protein.[70,287,288,301] Monitoring only the changes in the scattering properties of NPs upon target-induced aggregation can also be used to detect target DNA.[344] This method of sensing was demonstrated by immobilizing two different oligonucleotide fragments (A′ and B′, both 15 bases long), separately, on 13 nm Au NPs to create two sets of probe particles that aggregate in the presence of a complementary 30 base long target DNA (AB). Changes in the scattered light intensity upon target-induced aggregation were measured using a commercially available spectrofluorimeter. This approach was used to detect target DNA at picomolar concentrations and allowed the detection of single-nucleotide polymorphisms (SNPs) without the need for temperature control. Even lower concentrations of target DNA were detected by Muller et al.[352] using 50 nm Au particles in conjunction with a light-scattering-based spot test. In this work, a target sequence was added to a solution containing oligonucleotide-modified Au NPs to induce hybridization and aggregation of the probes. An aliquot of the solution was then spotted on a glass slide (a planar waveguide) that was illuminated using a planar fiber optic illuminator (Figure 13a). The evanescently coupled light was scattered from the particles at the surface of the waveguide and imaged with a complementary metal-oxide−semiconductor (CMOS) camera. Au NPs not exposed to target DNA scattered green light (control), whereas Au NPs aggregated in the presence of the target DNA scattered orange light due to particle−particle coupling (Figure 13b). This approach allowed the detection of femtomolar concentrations of target DNA without the need for PCR or signal amplification.[352] The high sensitivity and simple readout make this approach highly promising for use in point-of-care molecular diagnostics.

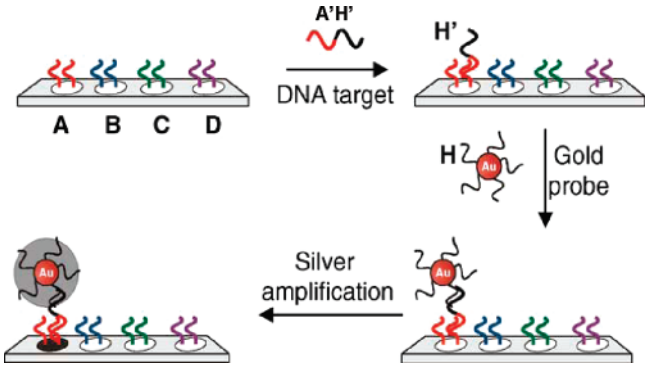

Figure 14. Schematic of DNA hybridization to microarrays and detection using Ag-amplified Au NP probes. Reprinted with permission from ref 346. Copyright Elsevier B.V.

Wavelength-ratiometric plasmon light scattering is another sensing method that measures changes in scattered light to detect target-induced aggregation or dissociation of NPs in solution.[353,354] In this approach, the ratio of the scattered light intensity at two wavelengths is used to quantify a target analyte, such as glucose.[353] Other 'ratiometric' methods of biosensing include measuring the ratio of scattered light intensity[355] or polarization[356] at two different angles as a function of target-induced aggregation or dissociation of plasmonic NPs. The benefits of ratiometric approaches are that the measurements become independent of source and/or detector fluctuations and NP concentration, and in this way improve the analytical stability of protocols relative to single-wavelength measurements.

Fluorescent tagging is the most common method of labeling targets for optical detection; however, the demand for greater sensitivity and simplicity (by removing the need and thus cost and complexity of PCR oligonucleotide target amplification) has led to research on and development of alternative labels, such as plasmonic NPs.[345−348] As an example, the large scattering cross section of plasmonic NPs has also led to their use as alternative labels in microarray-based technologies.[345−348] Microarrays are made by immobilizing biologically relevant moieties, such as DNA or proteins, as discrete spots, typically 10−500 μm in size, on a substrate.[345] These spatially arranged capture agents are then used to bind targets through specific interactions such as hybridization (nucleic acids) or ligand−receptor binding (proteins) to allow multiplexed detection of multiple analytes in a complex solution.

Plasmonic NP labels have been shown to be very promising for improving the sensitivity of microarray-based analyses.[345−348] Muller et al.[347] recently used 15 nm oligonucleotide-modified Au NPs to label captured target DNA on a microarrayed glass slide using a three-component sandwich assay (Figure 14). Once the Au NPs were immobilized, a Ag amplification step was used to increase the target signal by electroless reduction of Ag ions to metal at the surface of the Au NPs.[346] The glass slide was then used as a waveguide, and evanescently coupled light scattered from the NPs was imaged. The Ag-amplified Au NPs provided an approximately 1000-fold increase in sensitivity compared to the Cy3 fluorescent labels commonly used in microarray analyses.[346] This protocol was used to detect femtomolar concentrations of target sequences in human genomic DNA samples without prior PCR amplification.[347] A similar procedure was used to perform multiplexed SNP genotyping in total human genomic DNA without prior complexity reduction or target amplification, which is a major advancement toward point-of-care diagnostic medical applications.[348] It is interesting to note that these light scattering measurements were performed using commercially available systems[357] that can achieve attomolar and zeptomolar sensitivity when used in conjunction with immobilized *trans*-cyclopentane-modified peptide nucleic acid capture strands[358] or bio-bar-code techniques,[359] respectively.

The large scattering cross section[339] and ability to tailor the scattered wavelength of Au NPs,[95] in conjunction with their biocompatibility[198] and the availability of well-characterized surface conjugation chemistries,[360] also makes them attractive candidates for use as contrast agents for imaging applications.[95,349] Such optical measurements provide a promising route to noninvasive, high-resolution diagnostic imaging of tissues and cells with high sensitivity and chemical specificity.[95,350,361] For example, cancer cells can be labeled by conjugating plasmonic NPs to antibodies that target a protein that is overexpressed by cancerous cells. Anti-HER2[93,94] and anti-EGFR[362−364] are commonly used antibodies that target epidermal growth factor receptors (EGFRs),[96,364,365] which are transmembrane glycoproteins that are overexpressed in many types of cancers such as cervical, bladder, breast, lung, and oral cancers.[365] The cells or tissues are incubated with the antibody-conjugated plasmonic NPs, and the labeled cells are then examined using an appropriate form of optical imaging (e.g., dark field microscopy, two-photon luminescence, etc.).[97,362−364] Both spherical Au NPs[362−364] and nanorods[96,97] have been conjugated with antibodies for use in imaging a variety of cancer cells.

Recently, Sokolov et al. used multifunctional Au NPs that incorporated both cytosolic delivery and targeting moieties for real-time intracellular imaging of biomarkers in live cells.[366] The authors used water-soluble 20 nm Au NPs formed by citrate reduction that were functionalized with (i) TAT-HA2 peptides, (ii) anti-actin antibodies, and (iii) 5000 molecular weight PEG-SH (poly(ethylene glycol)-thiol)). The first component serves two purposes: (a) the TAT protein transduction domain induces endocytic uptake of the functionalized Au NPs into the cell, and (b) the HA2 protein destabilizes the endosomal lipid membrane, which causes release of the NPs into the cytosol.[367] The second component allows the NPs to bind to actin, and the third component improves the biocompatibility of the multifunctional particles. NIH3T3 fibroblasts were labeled with these probes and imaged using dark field reflectance microscopy. Actin labeling by these intriguing plasmonic probes was observed as an increase in red scattering due to dipole−dipole coupling between the NPs, and live cell imaging was used to track actin rearrangement.

While the scattering properties of NPs are useful for labeling and optically detecting cancer cells, their large optical absorption cross section can also be exploited for photothermal therapeutic treatments.[93,94,96] The treatment begins with the labeling of cancerous cells with molecular probe-conjugated plasmonic NPs. The labeled cells are then irradiated with light, which is absorbed by the NPs and converted to heat. The local heating causes irreversible damage and kills the cancerous cells. Research has focused on developing nanostructures with absorption peaks in the near-infrared (NIR) due to the transmissivity of blood and tissue at these wavelengths.[198,368] Au nanoshells,[94] nanocages,[93] and nanorods[96] with NIR absorption peaks have all been used to demonstrate this mode of photothermal treat-

ment, although spherical Au NPs with absorption bands in the visible region of the electromagnetic spectrum have also been used.[369]

4.4. Label-Free Optical Detection Based on Changes in Refractive Index

Plasmons are exceptionally sensitive reporters for chemical phenomena that influence the refractive index of the local environment of a probe. SPR spectroscopy[307,370,371] and imaging[24,28,313,333,372,373] are well-known label-free optical detection methods that use this property to monitor surface binding events in real time (as discussed in a separate contribution in this issue). In these techniques, changes in the dielectric environment at the surface of a flat or periodically structured noble-metal film shift the observed SPR resonance, which can be measured using angular interrogation, wavelength interrogation, or intensity measurements. This well-established technique enables determination of kinetic and thermodynamic data for a wide variety of molecular binding events, especially those involving biomolecular targets.[371,374,375] Progress is currently being made to develop nanostructured plasmonic materials for performing similar analyses. Changes in the dielectric environment of nanostructured metals, such as NPs, results in measurable shifts of the LSPR peak position and/or magnitude that can be used to perform label-free chemical or biosensing in real time.[342,343] A variety of noble-metal nanostructures such as NPs in solution[26,286] or immobilized on surfaces,[5,29,376] nanoholes and nanohole arrays,[8,14,77,90,377,378] and nanoisland films[379−381] have been used in this way.

Substrate-bound nanostructures offer several attractive features as platforms for chemical sensing. These include (i) the shape, size, composition, and spacing of the NPs can be readily controlled to provide tunable peak positions and widths[65,77,105,109,256] and (ii) the NPs are free of the capping agents or stabilizers used in solution-phase NP synthesis, making their surfaces readily accessible for functionalization with specific receptors or ligands.[77,92,382,383] In the following discussion we will provide some examples of chemical and biosensing based on refractive index changes near the surface of nanostructured metals in solution and on substrates, where the LSPR is monitored using extinction or scattering spectroscopy. The refractive index sensitivity of each sensing platform will also be given where validated data is available. This sensitivity is commonly defined in terms of the change in an experimentally measurable parameter (typically peak position or magnitude) per 'refractive index unit' (RIU), which corresponds to a change of 1 in the refractive index. These measurements are usually performed by taking spectra of a plasmonic nanostructure in solutions of increasing refractive index while monitoring peak position or intensity changes.

4.4.1. Nanoparticle Dispersions

Au nanostructures are known to exhibit strong plasmonic bands that are dependent on their shape, size, and surrounding media.[26,286,384] Ghosh et al.[26] studied the effects of changing solvents and ligands on the LSPR of Au NPs dispersed in solution. It was found that the surface plasmon absorption maximum of the Au NPs varied between 520 and 550 nm, depending on the refractive index and chemical nature of the surrounding solvent. The authors found that the LSPR peak red shifted linearly with the refractive index of the solvent when using solvents that do not possess active functional groups that could complex with the surface of the Au NPs. A nonlinear relationship between the LSPR peak position and refractive index was found, however, when using solvents with nonbonding electrons capable of complexing to the surface of the Au NPs. Interestingly, these authors found that the LSPR peak position blue shifted ~3 nm for every one carbon atom when the NPs were dispersed in alcohols with varying linear carbon chain lengths.[26] This rather atypical trend reverses in the presence of more strongly coordinating ligands. In such cases, the magnitude of the red shift caused by stabilizing ligands, such as alkyl amines or thiols, increases when the headgroup of the ligand interacts more strongly with the surface of the Au NPs.

In a recent study,[286] a dispersion of gold nanorods (GNRs) with different aspect ratios was used to perform a multiplexed bioanalytical sensing measurement in solution. This work exploited the fact that small changes in the aspect ratio of GNRs lead to drastic changes in their optical properties (the longitudinal plasmon mode red shifts with increasing aspect ratio, as described in section 2). A series of GNRs with aspect ratios (length/width) of 2.1, 4.5, and 6.5—annotated as GNR 1, 2, and 3, respectively—were functionalized with a different recognition molecule (Figure 15a) and dispersed into a single solution.[286] The solution yielded a composite absorption spectrum with three pronounced longitudinal LSPR maxima, each one corresponding to one of the three types of GNR (Figure 15b). The longitudinal peaks, in order of decreasing energy, correspond to GNR 1 > GNR 2 > GNR 3. Targets that were complementary to the different recognition molecules on the GNRs were then added to the solution to initiate binding events that caused a selective red shift of one or more of the longitudinal peaks. For example, when target 1 (complementary to the receptors on GNR 1) was added to the solution, a red shift in the longitudinal peak corresponding to GNR 1 was observed with smaller shifts in the peaks corresponding to GNR 2 and 3 (Figure 15b). When targets 1 and 2 (complementary to the receptors on GNR 1 and 2, respectively) were added to the solution, a shift in the peaks corresponding to GNR 1 and 2 was seen, while only a small shift in the LSPR maximum associated with GNR 3 occurred (Figure 15c). All three peaks red shifted when their corresponding targets were added to the solution (Figure 15d). To our knowledge, this report is the first to take full advantage of the multiplexing potential offered by GNRs and demonstrates the potentially enabling qualities offered by the ability to tailor the optical properties of metallic nanostructures.

4.4.2. Surface-Immobilized Nanoparticles

NPs synthesized in solution can also be immobilized on surfaces for potential 'on-chip' sensing applications and thereby engender more useful multiplexing capabilities.[5,376] Thin Cr or titanium (Ti) films are conventionally applied to substrates such as glass to promote adhesion of Au or Ag to the substrate. These metal layers are known to attenuate and broaden plasmon resonance bands[246,385,386] and lead to markedly adverse effects on conventional SPR and LSPR sensing with noble metals.[385,387] For this reason, it is beneficial to use organic adhesion layers of amine- or mercapto-terminated silanes to immobilize Au or Ag NPs to oxide-bearing substrates such as silica (Figure 16).[5,376,385,388,389] The LSPR of these Ag or Au colloidal monolayers can be measured with a commercially available UV−Vis spectrometer in a simple collinear transmission configuration,[5,376,390] and binding events can be monitored

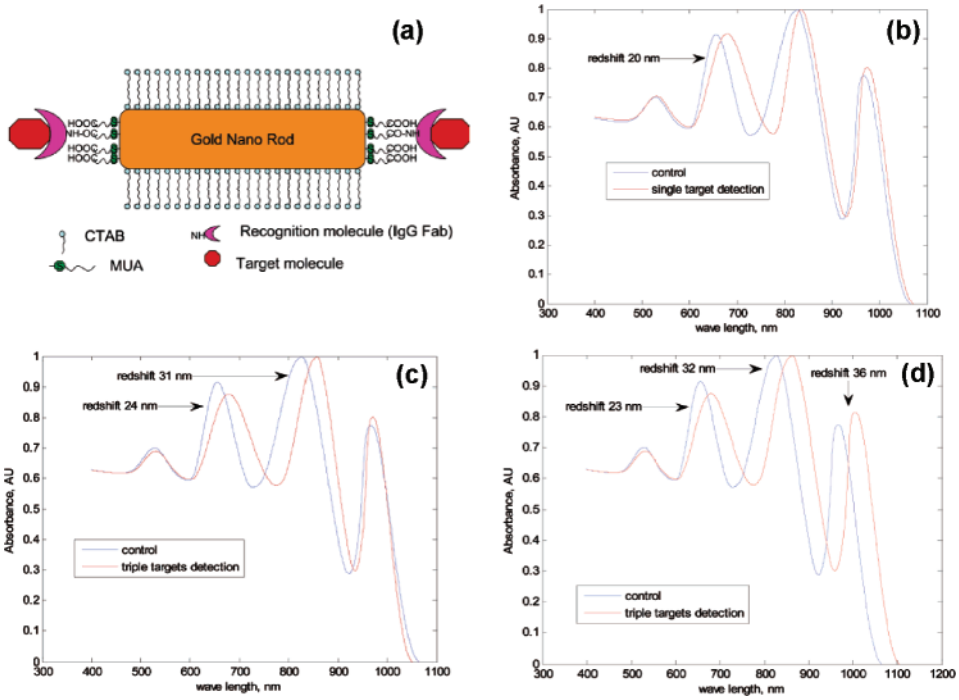

Figure 15. Schematic of a GNR molecular probe (a). Multiplexing detection of various targets using GNR molecular probes: one target (b), two targets (c), and three targets (c). Reprinted with permission from ref 286. Copyright 2007 American Chemical Society.

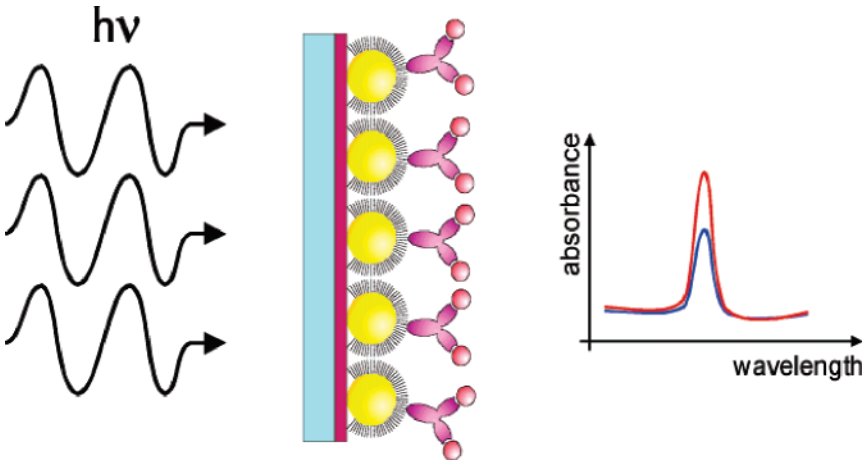

Figure 16. Schematic representation of the applied biosensing principle based on Au or Ag NPs deposited on a quartz substrate. From left to right: light source, quartz substrate, mercaptosilane adhesion layer, Au or Ag NPs, self-assembled monolayer of functional thiols, antibodies and antigens. The resulting absorbance spectra increase upon binding of analytes to the NPs is shown on the right-hand side of the figure. Reprinted with permission from ref 385. Copyright 2003 American Chemical Society.

in real time by integrating the functionalized substrate with a flow cell.[5,376]

Changes in refractive index occurring near the surface of the immobilized NPs (caused, for example, by the adsorption of a protein from a dilute solution) shifts the LSPR peak position and magnitude.[5,376,385,391−393] These devices exhibit peak position sensitivities of ∼167, ∼76, and ∼252 nm/RIU for spherical Ag[391] and Au NPs[5] and Au nanorods[394] respectively, and changes in extinction at an off-peak wavelength of ∼0.4−1.2 and ∼0.8 per RIU for spherical Au NPs[376] and Au nanorods, respectively.[394] This sensitivity can be enhanced using a multireflection attenuated total reflection setup.[389] Surface-immobilized spherical NPs have recently been used to detect the binding of antibodies to BSA and human serum albumin (HSA)[392] and for the selective detection of phosphopeptides on titania-coated Au NPs in complex samples at nanomolar concentrations.[393] The attractive features of this approach to sensing are the relatively easy and low-cost fabrication process and the simple optical setup. This approach has also been used to immobilize NPs on optical fibers,[388,395] which have shown the ability to detect streptavidin (using a model biotin−avidin assay) and staphylococcal enterotoxin B (using a model antibody−antigen immunoassay) at picomolar concentrations.[29,395] Surface-immobilized core shell NPs, such as spherical silica−Au (core−shell, Figure 4) and rice-shaped hematite−Au (core−shell) NPs, have been shown to exhibit bulk refractive index sensitivities of ∼555[396] (dipole resonance) and ∼800 nm/RIU,[199] respectively.

Nanostructures for refractive index sensing have also been formed directly on substrates using NSL,[7,337,382,397] colloidal lithography,[259,383,398,399] soft nanoimprint lithography,[77] or metal thin film evaporation.[379,400,401] Arrays of nanostructures offer the advantage of tunability of the wavelength response.

For example, arrays of triangular Ag NPs formed on substrates by NSL (Figure 5) exhibit an LSPR extinction band that can be tuned from the near-UV to the mid-IR by simply changing the size and shape of the NPs.[257] The peak position λ_{max} is sensitive to the local dielectric environment and red shifts linearly with increasing solvent refractive index with a sensitivity of ~200 nm/RIU.[397] The distance dependence of the LSPR resonance of these triangular NPs has been systematically studied using SAMs,[402] layer-by-layer self-assembly,[403] and atomic layer deposition.[404] These studies provided several important insights into application-relevant parameters including (i) the sensing volume can be systematically tuned by controlling the composition, size, and shape of the NPs, (ii) the sensor response is linear with respect to analyte coverage/quantity when the binding occurs at short distances from the surface of the NPs, and (iii) the sensor response varies in a complex, nonlinear fashion when binding occurs at large distances from the surface of the NPs.[403]

The refractive index sensitivity of triangular Ag NP arrays has been exploited in sensing applications where peak shifts were used to monitor binding events at the surface of the NPs.[7,92,243,382,402,403] The measured peak shifts were used in conjunction with a simple mathematical formalism developed for flat film SPR spectroscopy to quantitatively determine target analyte concentrations.[405] This allowed the quantitative detection of Concanavalin A,[382] streptavidin,[7] and anti-biotin[243] as well as the thermodynamic evaluation of their binding constants. In a recent and notable example, triangular NP arrays were used to detect biomarkers for Alzheimer's disease in both synthetic and human patient samples.[92] In this work, synthetic amyloid-β-derived diffusible ligands (ADDL) were detected at femtomolar concentrations using a sandwich assay.[92] The sensitivity of these types of measurements is enhanced if the molecular resonance of the analyte overlaps with the intrinsic LSPR of the NPs or if the analyte is labeled with a marker that has a resonance that overlaps with the intrinsic LSPR of the NPs.[406,407]

One of the advantages of using plasmonic nanostructures for sensing is their relatively small footprint—one that is more amenable to miniaturization than flat film SPR detection. For example, LSPR sensing has been demonstrated at the single-NP level using spherical (Au[343] and Ag[408]), triangular (Ag),[285,408,409] disk-like (Au),[410] and cubic (Ag) NPs.[342] Scattering-based spectroscopies must be used to characterize the optical properties of single NPs[103,285,343,408−412] since the absorbance of individual NPs is close to the shot noise-governed limit of detection.[285,337] As an example, McFarland et al. have shown that a LSPR peak shift of ~40 nm occurs upon binding of ~100 zeptomoles of 1-hexadecanethiol to a single triangular Ag NP (as measured by resonant Rayleigh scattering spectroscopy). This high sensitivity and small transducer size suggests that single NPs could be useful for the analysis of precious or limited-volume samples.

Rubinstein developed the so-called transmission LSPR (T-LSPR) spectroscopy method.[379] In this protocol one measures the changes that occur in the extinction band of the LSPRs of discontinuous Au or Ag films upon analyte binding, which is monitored in transmission mode using a standard spectrophotometer. Discontinuous and random island films for this plasmonic measurement are prepared by direct evaporation of an ultrathin (≤10 nm nominal thickness) layer of the desired metal onto a transparent substrate like quartz, mica, or polystyrene. Random Au island films, for example, display a SP extinction peak at 550−800 nm—one whose shape, intensity, and position depend on the island morphology, which in turn is determined by the evaporation conditions and postdeposition treatment. Rubinstein and co-workers demonstrated the potential of this method by measuring changes in the position and intensity of the SP extinction band that result from the binding of various molecules to Au islands.[379,400,401,413] A linear relationship was shown to exist between the surface coverage of the adsorbing molecules, ones bound either directly to the Au or through a receptor layer, and the plasmon intensity or wavelength changes.[379,401,413] In an interesting modification of typical RI-based measurement methods, Au island films were modified with a biotinylated monolayer and used to monitor the binding of avidin based on changes in plasmon intensity (rather than the more commonly used wavelength shift) since the binding event caused only a small change in the peak position. T-LSPR spectroscopy was shown to be widely applicable with a sensitivity (under optimized conditions)[380] that is comparable to that of conventional forms of SPR sensing.[379] The instability of T-LSPR sensors, however, is a source of concern. Changes in the optical properties of metal island films due to morphological changes occurring upon immersion in organic solvents and aqueous solutions has been noted to appreciably introduce uncertainties into NP-based sensing measurements. To obtain metal island films with stable and reproducible optical properties, new design schemes for stabilizing the structures of the evaporated film have been devised. The most useful of these reported to date consists of depositing an ultrathin silica layer (1.5 nm thick) on the metal island film by a sol−gel procedure.[381]

Au nanorings formed directly on substrates by colloidal lithography (Figure 7) have recently been used for chemical and real-time biosensing.[383] These plasmonic nanostructures exhibit a bulk refractive index sensitivity of ~880 nm/RIU and show a peak shift of ~5.2 nm per CH_2 unit when SAMs of varying alkanethiol chain lengths were formed on the nanorings by chemisorption. This peak shift per CH_2 unit (short-range refractive index sensitivity) for the Au nanorings is greater than the peak shifts reported for triangular Ag NPs (~3.1 nm per CH_2 unit) and nanoprisms (~4.4 nm per CH_2 unit).[402,409] The greater sensitivity of Ag plasmonic nanostructures compared to Au plasmonic nanostructures suggests that greater sensitivities could be achieved by forming Ag nanorings.[403] Real-time, label-free biosensing was demonstrated using these structures by monitoring the optical changes that occur due to the nonspecific binding of biotin−BSA to the Ag nanorings followed by the specific binding of NeutrAvidin (NA).

4.4.3. Periodic Nanohole Arrays

The enhanced transmission of light through periodic arrays of subwavelength holes in metal films has generated considerable interest since it was first reported by Ebbesen et al. in 1998.[75] Nanohole arrays are typically formed by the serial process of the FIB milling of holes in a thin film of Au supported on a transparent substrate.

While Ebbesen et al. attributed their enhanced transmission to surface plasmons,[75] several authors have pointed out alternatives ranging from waveguide modes to even more novel surface waves.[414−416] In actual fact, and depending on the specific details of the plasmonic structures involved, a

variety of mechanisms can be operative. For this reason, it is necessary to carefully analyze each situation to determine what sorts of resonance and diffractive effects are possible. In most cases involving thin Au films with periodic nanoholes, however, surface plasmons do play a key role.[76,273]

The features in transmission spectra of nanohole arrays are thought to arise from a combination of LSPRs, Bloch wave SPPs (BW-SPPs), and Wood's anomalies.[76] An approximate relation for the allowed wavelengths of BW-SPPs excited by normal incidence illumination on a square array of subwavelength holes in a metal film is given by[76,77,417,418]

$$\lambda = \frac{P}{\sqrt{n_x^2 + n_y^2}} \mathrm{Re} \sqrt{\frac{\epsilon(\lambda)\epsilon_{\mathrm{med}}}{\epsilon(\lambda) + \epsilon_{\mathrm{med}}}} \quad (3)$$

where $\epsilon(\lambda)$ is the wavelength-dependent relative dielectric constant of the metal, ϵ_{med} is the relative dielectric constant of an adjacent medium, P is the nanohole lattice spacing, and n_x and n_y are integer scattering or diffraction orders from the array. Another important equation in analyzing the features of transmission spectra is that for the positions of Wood's anomalies (WAs)[75,76]

$$\lambda = \frac{P\sqrt{\epsilon_{\mathrm{med}}}}{\sqrt{n_x^2 + n_y^2}} \quad (4)$$

which is written here for the case of normal incidence for simplicity. The WAs in this case may be thought of as light moving parallel to the metal surface, i.e., light that is diffracted 90° relative to the normal incident direction. Note that in one classification scheme of WAs this particular WA is often referred to, more precisely, as a Rayleigh anomaly.[419]

Equations 3 and 4 predict a variety of discrete wavelength positions for the BW-SPPs and WAs. Originally a correlation between transmission minima and WAs and transmission maxima and BW-SPPs was noted;[386,417] however, this may not always be the case. At a naïve level, for example, one might associate both the BW−SPP and WA positions with transmission *minima*, not maxima, because they represent wavelengths where incident light is channeled into light moving completely counter to the direction of the transmitted light. Indeed, careful numerical studies made in the absence of experimental imperfections and uncertainties have shown a definite correlation between transmission minima and eqs 3 and 4.[76] It remains a fact, however, that nonradiating BW-SPPs and WAs are an idealization. One can regard the BW-SPPs or WAs as being analogous to zero-order quantum mechanical bound states embedded in a zero-order continuum. In the present case a zero-order continuum state would be light that is predicted to be transmitted by the hole/film structure disregarding the possibility of zero-order bound states. The full problem is described by a coupling of the zero-order bound and continuum states. A Fano resonance line shape (generally an asymmetric line shape with a distinct minimum *and* maximum) can often describe each BW−SPP or WA feature very well.[76,419,420] It often turns out that the same order BW−SPP and WA have wavelengths that are close to one another, which can complicate this picture. Coupled with the fact that the WA features can be narrow and difficult to resolve experimentally, it sometimes follows that only a minimum/maximum resonance feature associated with a particular BW−SPP is seen, along with possibly a dip or kink in the region where the WA would be expected.[76,421] Finally, we note that the features discussed here can occur alongside or be superimposed on generally broader LSPR resonance features. With all these factors taken into account and playing varying roles depending on the specific details of the experiment, it is perhaps not surprising that there has been some confusion in the literature regarding the mechanisms of enhanced transmission.

The involvement of LSPRs, BW-SPPs, and WAs in the optical response of nanohole arrays suggests that the features in the transmission spectra should be sensitive to changes in the local refractive index, making these nanostructures useful for sensing applications. Indeed, the spectral features of 2D Au nanohole arrays have been shown to depend on the external dielectric environment,[14,422,423] which has been used to perform label-free detection of SAM formation on Au followed by subsequent adsorption of bovine serum albumin (BSA).[14] The sensitivity of these structures to changes in the external dielectric environment—measured as peak shift per RIU—is ∼333−400 nm/RIU.[14,377] The advantages of plasmonic nanostructures over flat film SPR systems are their relatively small footprints (i.e., small patterned areas on the order of micrometers[14,377] or single holes[259] or NPs[285,342]) and simple optical setups (i.e., normal incidence transmission or reflection).[14,342,377] These advantages were recently exploited by integrating a microfluidic device with a nanohole array for detecting refractive index changes and surface binding events 'on-chip'.[377]

Plasmonic quasi-3D periodic nanohole arrays have been formed on surfaces using a type of soft nanoimprint lithography (see section 3.3.3 and Figure 9).[8,77] These multilayered structures consist of arrays of nanoscale holes in Au films with a second level of Au disks at the bottom of the embossed wells. The normal incidence transmission spectrum of these structures is complex (Figure 17a, blue spectrum) and shows high transmission despite the fact that no 'line of sight' exists through the sample (i.e., unlike 2D nanohole arrays, the cylindrical holes or perforations are 'capped' with Au disks in a quasi-3D geometry). Rigorous 3D finite-difference time domain (FDTD) simulations were performed to assist in the interpretation of the experimental results (Figure 17a). (See also refs 76 and 424 for related FDTD studies of hole arrays.) The calculated electromagnetic field distributions in and around the metal nanostructures are shown in Figure 17b and c. The two largest features in the spectra (Figure 17a) are labeled B and C. Peak B is associated with excitations of LSPRs on the rims of the nanoholes in the upper Au film near the air/Au interface, while peak C involves overlapping Wood's anomaly and BW-SPPs excitations on the Au disk/polymer side of the device. The intensity associated with peak C also extends vertically up to the hole opening, showing a strong coupling between disk and hole, a feature that is absent in random and ordered 2D nanohole arrays. Quantitative modeling of the experimental spectra required consideration of fine structural details in this region of strong coupling. Good agreement between the experimental and theoretical spectra required the addition of small (20−30 nm), isolated grains of Au on the sidewalls of the nanoholes, just above the edges of the Au disks at the bottom of the nanowells (Figure 17a, red spectrum).

The transmission properties of the quasi-3D nanohole array are sensitive to the nature of the adjacent dielectric medium at the crystal surface (Figure 18a). The bulk refractive index sensitivity of these devices was determined by passing

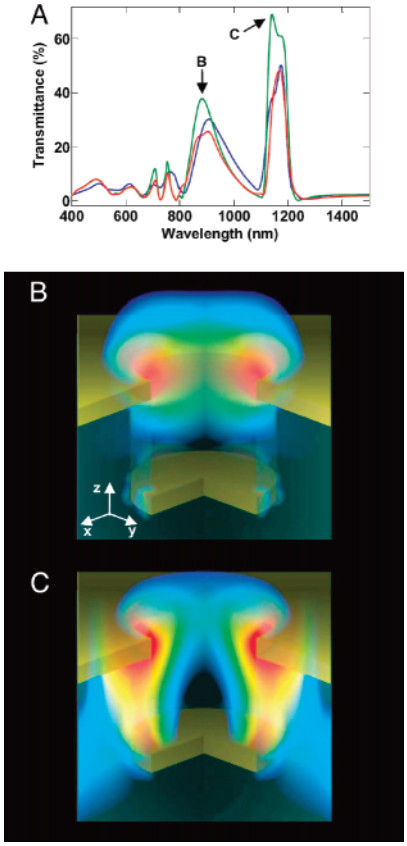

Figure 17. Correlation of transmission spectral features with hole/disk plasmonic excitations. (a) Normal incidence transmission spectrum of a quasi-3D plasmonic crystal (blue), and rigorous electrodynamics modeling of the spectrum for an ideal crystal (green) and one that includes subtle isolated nanoscale grains of Au near the edges of the Au disks (red). (b) Computed electromagnetic field distribution associated with the resonance at 883 nm (labeled B in a). The intensity is concentrated at the edges of the nanoholes in the upper level of the crystal. (c) Field distribution associated with the resonance at 1138 nm (labeled C in a), showing strong coupling between the upper and lower levels of the crystal. Reprinted with permission from ref 77. Copyright 2006 The National Academy of Sciences of the USA.

solutions of increasing concentration (0−7.6 wt %) of polyethylene glycol (PEG) through a fluid flow cell containing a plasmonic crystal. Changes in both peak positions and intensities were observed over a wide spectral range as the refractive index of the PEG solution was increased. The most sensitive peak at ∼1023 nm linearly red shifted with a sensitivity of ∼700−800 nm/RIU and linearly increased in intensity with a sensitivity of ∼2.5−3.5 Abs/RIU as the refractive index of the solution was increased (determined using several devices).[77]

SPR sensing is typically performed by following the response of an individual peak or wavelength to binding events at the surface of the sensor. This method of analysis, however, does not fully capture the sensitivity of the quasi-3D plasmonic sensor since it does not take advantage of all the peak shifts and intensity changes occurring at multiple plasmonic resonances over the spectral range created by the coherent couplings of the LSPRs, BW-SPPs, and Wood's anomaly responses exhibited by this type of system. This wide spectral response was exploited using a type of full, multispectral analysis as described below.

Multispectral analysis of a PEG calibration of a quasi-3D plasmonic crystal is shown in Figure 18a. A series of difference spectra, as referenced to the spectrum at time $t = 0$, illustrate changes in transmission due to both peak shifts and intensity changes throughout the wavelength range as solutions of increasing PEG concentration were injected into the flow cell. As shown in Figure 18b, the transmission can increase or decrease depending on the measurement wavelength. The particular crystal geometry used in this study (hole diameter and periodicity of ∼480 and 780 nm, respectively) exhibited the largest multiwavelength response in the near-infrared region (900−1250 nm) as shown in Figure 18c. The response over all wavelengths, including both positive and negative transmission changes, was calculated using the following equation

$$R = \int |\Delta(\%T(\lambda))\mathrm{d}\lambda \tag{5}$$

This total or integrated response, R, has units of $\Delta\%T\cdot$nm (Figure 18d) and changes linearly with the refractive index of the PEG solution with a sensitivity of ∼22,000 $\Delta\%T\cdot$nm/RIU (inset of Figure 18d). This multispectral analysis also improves the signal-to-noise ratio by a factor of 3−10 times that of a single-wavelength response.[77]

The linear response of the integrated metric was used to perform quantitative sensing and imaging of binding events. The biotin−avidin ligand−receptor conjugate was used to illustrate the utility of these devices for performing quantitative sensing (Figure 19). The device was first exposed to a solution of biotinylated BSA (bBSA), which led to an increase and plateau of the integrated response of the sensor (Figure 19b) upon formation of a bBSA monolayer. This layer rendered the surface of the sensor inert to further nonspecific adsorption, which was demonstrated by the lack of response after rinsing the bBSA monolayer with buffer and exposing it to a solution of nonfunctionalized BSA. Subsequent exposure to avidin, however, led to a response due to a specific binding interaction between the avidin and the initial bBSA monolayer. The surface-immobilized avidin was then used to complete the assay by binding a layer of bBSA to the remaining free biotin binding sites on the avidin layer (inset Figure 19b). This resulted in a response that was smaller than that observed for the initial bBSA adsorption step, an observation that follows the patterns of layer-dependent mass coverage generated in assays of this sort.[77] The integrated response can be converted to an effective protein thickness using a mathematical formalism.[405] Although this model was developed for quantifying binding events measured using flat film SPP-based SPR sensors (i.e., it assumes a uniform plasmon evanescent field), it provides approximate protein coverages that agree with literature values.[425−427]

One notable advantage of soft nanoimprint lithography is the ability to pattern over large areas in parallel with high spatial uniformity and low defect densities, which facilitates large-area imaging for multiplexed microarray-based analyses. The high-quality, large-area patterning capability along with the capacities for quantitative biosensing was combined to perform quantitative imaging. To this end, five lines of nonspecifically adsorbed fibrinogen were patterned on the surface of a plasmonic crystal using a microfluidic device (Figure 20a). Figure 20b shows changes in transmission measured relative to an interchannel region on the crystal that did not come in contact with the protein. The spectral image shows five stripes with the expected geometries, each corresponding to a line of nonspecifically adsorbed fibrino-

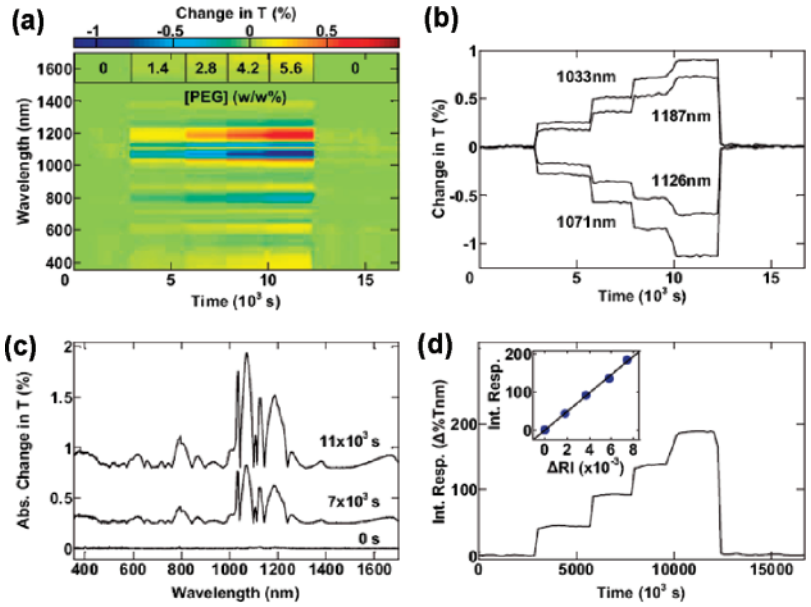

Figure 18. Optical response of a plasmonic crystal to sequential injections of increasing concentrations of aqueous PEG solutions. The color contour plot of the change in transmission (T) as a function of wavelength and time (with the corresponding injection sequence overlaid on the plot) (a), change in T as a function of time during the injection sequence, evaluated at several wavelengths (b), absolute value of the change in T as a function of wavelength evaluated at different times (c), and integrated multispectral plasmonic response as a function of time (d). (Inset) A linear correlation to the change in refractive index. Reprinted with permission from ref 77. Copyright 2006 The National Academy of Sciences of the USA.

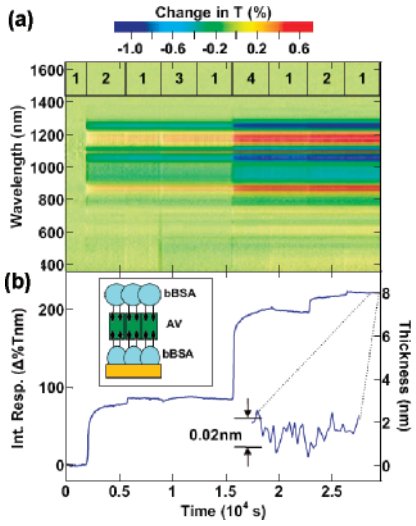

Figure 19. Plasmonic crystal used in a biotin−avidin assay. The color contour plot of the change in T as a function of wavelength and time (a). The overlaid injection sequence corresponds to PBS (1), bBSA (2), BSA (3), and avidin (4). The integrated multispectral plasmonic response and corresponding effective thickness of the biotin−avidin−biotin assay (schematically illustrated in the upper inset) (b). The noise limited refractive index resolution of the crystals corresponds to submonolayer coverages (lower inset). Reprinted with permission from ref 77. Copyright 2006 The National Academy of Sciences of the USA.

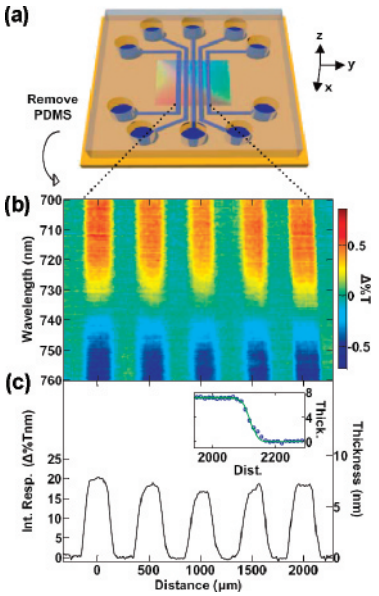

Figure 20. Spatial imaging of fibrinogen nonspecifically adsorbed to the surface of a crystal. A schematic illustrating the use of a multichannel PDMS microfluidic network to pattern the surface of a crystal (shown here with the multicolored appearance that characterizes these crystals) (a), spectroscopic difference image of fibrinogen lines patterned on a crystal (b), and spatially resolved integrated response and corresponding effective thickness illustrating binding events in the geometry of the microfluidic channels (c). (Inset) A measured step edge between a fibrinogen line and bare area of the crystal (blue symbols) and a fitted step edge with a Gaussian width of ∼20 μm. Reprinted with permission from ref 77. Copyright 2006 The National Academy of Sciences of the USA.

gen. Analysis of the step edges (Figure 20c, inset) shows a width of ∼20 μm, which is only slightly larger than the ∼17 μm resolution limit of the imaging optics. The ∼3 μm of additional width in the plasmonic image can be associated with the propagation lengths of plasmons on these structures.[428] The integrated spatial response of the spectral image could be converted to an effective protein thickness of ∼7 nm using the PEG calibration and the mathematical model described above.[77,405] This thickness is consistent with the molecular dimensions of fibrinogen.[429,430] The micrometer-scale imaging resolution and the large area defect-free (and thus uniform response) aspects of the crystals suggest a promising platform for performing parallel diagnostic bioassays. This was further demonstrated by performing quantitative 2D imaging on these quasi-3D devices.[279]

4.4.4. Random Nanohole Arrays

Random nanohole arrays formed by colloidal lithography have been used in enabling ways for the sensing of chemical and biological targets.[90,259,398,399] Randomly arranged holes do not exhibit the long-range higher-order diffractive coupling effects that are observed in the highly ordered, periodic nanohole arrays discussed above.[72,75,90,422] They instead exhibit LSPRs that are concentrated at the edges of the holes with decay lengths on the order of 10−20 nm, which have been used for sensing binding events occurring near or in the holes.[90,259,398,399] The refractive index sensitivity of these random nanohole arrays depends on the metal thickness[398] and the detection modality. As noted above, refractive index sensitivities are often reported as a change in a given measurable parameter per RIU. Sensitivities of ∼100−270 nm/RIU,[72,90,398,399] 0.23−1 Abs/RIU,[398,399] and ∼70 nm/RIU[259] have been reported for measurement of changes in the extinction peak position, extinction peak magnitude, and scattering peak position, respectively. In one notable example of biosensing carried out with such devices, Dahlin et al. used random nanohole arrays to detect membrane-mediated recognition of bioanalytes using surface-immobilized phospholipid bilayers (SPBs). These SPBs were supported on the silica surface within the interior of the nanoholes (Figure 21). This was accomplished by first exposing the nanohole array to bBSA, which preferentially adsorbs to the Au rather than the SiO_2,[431] making it inert to lipid vesicle fusion. The SPBs were then formed on the SiO_2 substrate at the bottom of the nanoholes by performing vesicle adsorption in the presence of Ca^{2+}, which promotes the vesicle fusion process.[432] The top of Figure 21a shows schematically the steps leading to the adsorption of the protein NA within the nanoholes containing the biotin-modified lipids (left). In the absence of biotin-modified lipids the NA binds only to the bBSA on the Au surface, whereas in the presence of biotin-modified lipids the NA binds to both the SPB and the Au surface. The bottom panel of Figure 21 shows the measured changes in extinction as a function of time at ∼725 nm for the two cases, with the signal being more than a factor of 3 greater when NA binds to lipids inside the holes. This demonstrates that the holes are highly sensitive regions for detecting protein-binding events. The top of Figure 21b shows schematics illustrating the binding of cholera toxin to SPBs containing ganglioside G_{M1} glycolipids (left) and hybridization of 15-base single-stranded DNA (ssDNA) to SPBs presenting a complementary strand (right). The bottom of Figure 21b shows the measured changes in extinction as a function of time at ∼725 nm upon binding of the cholera toxin and complementary and noncomplementary ssDNA. These examples demonstrate the potential for using random nanohole arrays as a platform for real-time plasmonic-based label-free sensing. The figure of merit (FOM) for this system appears to be quite good in that analytically discriminable signals could be obtained from zeptomole quantities of protein. Related nanohole arrays also have been used to detect cancer biomarkers where the detected signal (peak shift) was estimated to arise from the binding of picograms of an antigen (a specific tumor biomarker, cancer antigen 19-9) to its corresponding surface-immobilized antibody.[90]

4.5. Surface-Enhanced Spectroscopies

The optical techniques discussed thus far are amenable to chemical functionalizations that engender capacities for molecule-specific sensing, ones that the methods alone lack.

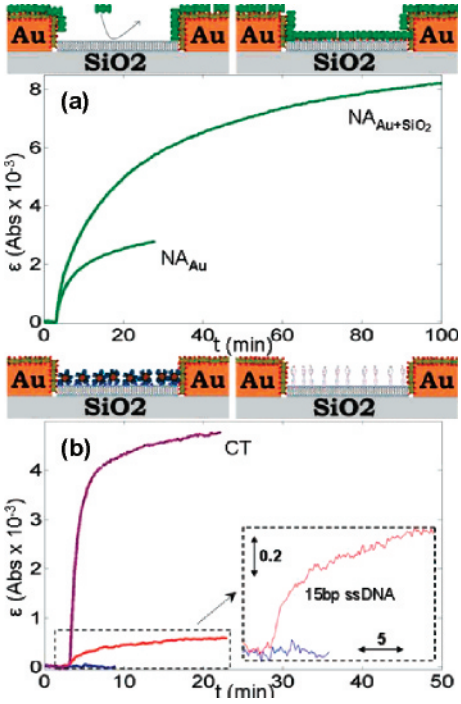

Figure 21. Detection of lipid−membrane-mediated binding events using SPB in random arrays of gold nanohole. (a) Temporal variation in extinction measured at the longer wavelength inflection point (725 nm) of the LSPR peak upon addition of ∼0.3 μM NA. In both cases, Au is modified with biotin−BSA. In one case, biotin-modified SPB patches cover the SiO_2 regions (NA_{Au+SiO_2}), while in the other (top right illustration in a), unmodified SPB patches cover the SiO_2 regions (NA_{Au}) (top left illustration in a). (b) Variation in extinction measured upon addition of ∼0.5μM cholera toxin (CT) to GM1-modified (5 wt %) SPBs (purple curve, illustration of SPB-modified nanohole shown in upper left of b). (Inset) Magnification of changes in extinction versus time upon addition of a 15 base long noncomplementary (0.2 μM, blue) and a fully complementary strand (0.2 μM, red) to SPB patches modified with a DNA construct carrying two cholesterol moieties at its one end and a 15-base-long single strand available for hybridization at the other. Reprinted with permission from ref 399. Copyright 2005 American Chemical Society.

It is useful then to consider cases where other properties besides explicit forms of chemical recognition can be used to discriminate a molecularly specific event. Techniques such as Raman scattering and fluorescence have the capability of providing molecule-specific data, and perhaps most interesting in the context of this review, surface plasmons are able to markedly enhance the sensitivity of these techniques. The utility of Raman spectroscopy, for example, stems from its ability to probe molecular vibrations, but the method suffers from relatively weak signal intensity. In most cases the number of inelastically scattered photons (which directly corresponds with the signal level) is extremely small, corresponding to scattering cross sections of 10^{-30}−10^{-25} cm^2.[22] As a result, even though Raman scattering is a type of spectroscopy that can give very specific molecular information, it lacks the intrinsic sensitivity required of a viable technique for high-throughput detection. Plasmonic architectures provide one general method for enhancing Raman signals to levels that can enable many analytical applications, ones ranging from DNA sequencing to forensics.[337,433,434] The sections below examine several of the more interesting prospects emerging from current research.

4.5.1. Surface-Enhanced Raman Scattering

The first discovery of surface-enhanced Raman scattering (SERS) showed that it was possible for a roughened noble-metal surface to enhance the intensity and sensitivity of Raman spectroscopy.[435,436] Using the SERS effect in a quantitative form is intricately tied to the ability to fabricate nanostructured surfaces with well-defined morphologies. New methods to create nanostructured materials are constantly evolving, and research centered around SERS has followed that trend—work that also has increased the sensitivity to levels required for advanced sensing applications. Signal enhancements of up to 10^{14} over normal Raman scattering have been observed in special cases,[437] a value sufficient to study analytes even at the single-molecule level. The electromagnetic theory of SERS[437−440] suggests that the enhancement effect is a result of the creation of surface plasmons that can transfer energy to the bound molecule through the associated electric field. We direct the interested reader to a number of reviews that have already been published on this subject.[437−440]

The ability to enhance the Raman signal via SERS is fundamentally linked to the precise details of the structured nature of the surface as well as the choice of the metal itself, which includes but is not limited to Ag, Au, and Cu.[438] These metals are used because they have the appropriate values of both the real and imaginary parts of the dielectric constant, which allows surface plasmons to propagate at wavelengths of interest for spectroscopic applications. As the discussions above have revealed, the plasmonic excitations that a system can support depend very sensitively on the metal structure, a factor that in turn drastically affects its overall ability to enhance the Raman scattering cross section.

The advances made in nanomaterial synthesis and NP fabrication have greatly empowered competencies in this latter regard. Such forms of modern SERS substrates span a vast geometrical range encompassing colloids, templated colloidal crystal films, electrochemically roughened electrodes, deposited metal island films, nanohole arrays, and lithographically defined thin films. The ability to use these different structures as SERS substrates allows a variety of experimental setups including solution- and surface array-based sensing.[435,441−446] Solution-based SERS has been shown to provide a viable option for the determination of binding constants and monitoring DNA/RNA mononucleotide recognition.[447] For the latter, detection of mononucleotides at a submicromolar level (3 ppb) was achieved for 2′-deoxyadenosine 5′-monophosphate (dAMP) in the presence of $MgSO_4$, an aggregating agent (Figure 22).[447] The data indicates that it is essential for the analyte to be bound within close proximity to the NPs. Solution-based sensing with NPs has also been applied to the field of cellular biology.[448] In a notable example taken from recent research, it was demonstrated that it is possible to introduce 60 nm Au NPs into a single osteosarcoma cell and use their optical responses to map the distribution of the cellular constituents.[449] It is possible to further enhance the SERS signal of an analyte by altering the physical properties of the NPs.[450−452] For example, using Au octahedrons instead of Au nanospheres allows for a more than 3× greater enhancement in the spectrum of 2-napthalenethiol.[450]

Substrate-bound nanostructures can also be used to enhance Raman signals.[441] Nanosphere lithography, for example, has been used to fabricate two intriguing forms of surface-immobilized structures for SERS: (i) triangular NP arrays (Figure 5) and (ii) metal film over nanosphere (MFON) surfaces (Figure 23). Triangular NP arrays have been shown to be quite sensitive with SERS enhancement factors of $\sim 10^8$.[337] Analytes detected in this way include Alzheimer's precursors,[93] glucose,[433] and Concanavalin

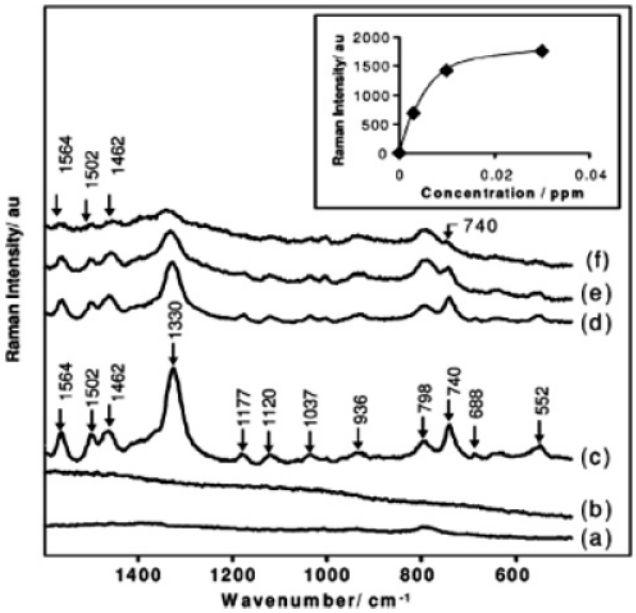

Figure 22. Effect of aggregating agents to the SERS signal of dAMP: 1000 ppm dAMP mixed with Ag colloid (a); mixture after aggregation with 0.1 M $MgCl_2$ (b); 0.1 ppm dAMP mixed with $MgSO_4$-aggregated (0.1 M) Ag colloid (c). Spectra d, e, and f used the same conditions as c except 0.03, 0.01, and 0.003 ppm dAMP. The inset shows the calibration plot of the dAMP (4 s accumulation times). Reprinted with permission for ref 447. Copyright 2006 American Chemical Society.

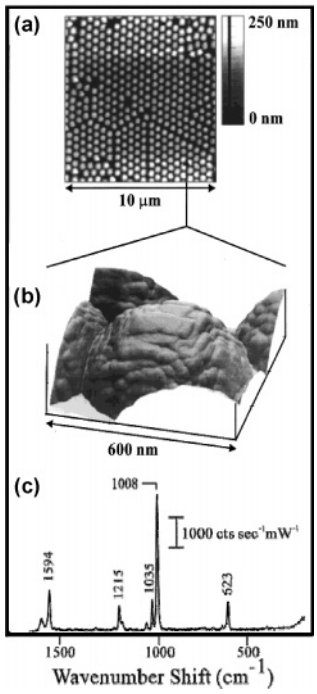

Figure 23. Ambient contact-mode atomic force microscope image of 200 nm Ag over 542 nm diameter polystyrene spheres. Array of spheres (10 μm × 10 μm) and image (600 nm × 600 nm) of one sphere showing substructure roughness (a and b, respectively). AgFON electrode SER spectrum of 50 mM pyridine in 0.1 M KCl at −0.7 V vs Ag/AgCl (c). Reprinted with permission from ref 453. Copyright 2002 American Chemical Society.

A.[382] The highly corrugated MFON surfaces have been used to detect a key component of an analogue to anthrax stimulant at a concentration lower than the infectious dosage.[242,445] The MFON substrates are also useful as electrodes with an improvement in stability and reproducibility over other types of SERS active electrodes.[453] The latter are critical parameters since most SERS active substrates are not particularly stable. It is notable, therefore, that recent work has shown that a sub-1 nm thick alumina film deposited over a MFON surface can extend the stability of the sensor up to seven times, corresponding to a shelf life of at least nine months.[242]

Electrochemistry can be used to roughen an electrode surface for SERS applications, but this method generally yields substrates with irreproducible enhancement factors.[453] An alternative method that can be used to form SERS-active electrode structures is to use a template to create nanowires. As an example, Au nanopillar films can be formed by physical/electrodeposition of Au in an anodized aluminum oxide (AAO) template followed by dissolution of the AAO template.[454] These nanopillar substrates are highly reproducible (to within 20% of the SERS intensity profile) and capable of detecting thionine as a model analyte at concentrations near 10^{-8} M.[454] Nanopillars of Ag can also be fabricated in the form of aligned pillars of controllable length, giving SERS enhancement factors on the order of 10^8.[455] Nanodots,[443] nanohole arrays,[444] and even nanostructured multicore optical fibers[456] have been fabricated for use in SERS applications—work that evidence a broadening research landscape in response to requirements for SERS substrates that are both stable and ultrasensitive.

4.5.1.1. Single-Molecule Surface-Enhanced Raman Scattering. Highly specific single-molecule detection is a challenging goal for chemical sensing.[22,457,458] It is interesting, therefore, to consider how the marked enhancements afforded by SERS compare to this most demanding analytical FOM. Kniepp and co-workers elucidated the fact that single-molecule SERS (SMSERS) detection levels can be achieved both in solution and on surfaces, the latter using patterned metal substrates. Each protocol requires the use of a proximal probe in which incident light is restricted to encompass a probe volume of a few femto- to picoliters. This makes it possible to examine limited volume samples with analyte concentrations as low as $10^{-12}-10^{-14}$ M. Solution-based SMSERS, for example, has been used to detect pseudoisocyanine (PIC) in an aqueous solution at a concentration of 10^{-14} M, corresponding to an enhancement factor on the order of 10^{14}.[22] Ag colloids also have been used to detect yeast cytochrome *c* at near single-molecule levels.[459]

Patterned Ag surfaces have been shown to give enhancements that make it possible to detect single molecules of enkephalin, in this case by monitoring the ring-breathing mode of phenylalanine at 1000 cm^{-1}.[22] The small sample probe volume has other (potentially beneficial) impacts as diffusion brings single molecules into and then out of the probed volume at very low analyte concentrations due to Brownian motion. This leads to a variation in the Raman signal that can be correlated to the number of molecules in the probed volume via models based on Poisson statistics.[434]

4.6. Plasmonics for Detection Beyond the Diffraction Limit

One limitation of SMSERS (or for that matter any optical technique) is that the spatial resolution of the probed area is dictated by the spot size of the incident light. Optical detection methods are constrained by the wave nature of light (which determines the diffraction limit); however, it is particularly interesting that plasmonic nanostructures make it possible to probe systems with a spatial resolution that is well beyond the diffraction limit of light. Two methods that use the enhanced local electric fields associated with plasmons for detection at length scales beyond the diffraction limit are apertureless near-field optical microscopy (a-NSOM) and tip-enhanced Raman spectroscopy (TERS). Both of these methods have enabled the scientific community to optically probe surfaces with resolutions previously only afforded by techniques such as electron microscopy and surface probe microscopy (SPM).

Near field optical microscopy (NSOM), with a typical aperture, is a technique that affords capabilities of sub-100 nm resolution; however, it is important to note that the transmission of light through the fiber tip is typically quite low. One way to improve the resolution and limited transmission is to move to a fully metallized tip that has no aperture (a-NSOM). The apertureless tip is then capable of supporting surface plasmons that lead to enhancement factors of the electric field of 10−1000 times, and the ability to sharpen the tip affords resolution limits on the order of 10 nm.[460] For example, tips coated with 15−25 nm of Ag were used to detect Alexa 532 dye molecules with a resolution of 15 nm.[461] The ability to garner optical images from near-field microscopy is a useful technique for imaging nanostructures with sub-100 nm resolution but lacks the specific chemical information afforded by techniques such as TERS.

The basis of the SERS effect is tied to the nanoscaled structures present on a metal surface, and it is interesting to note that the SERS effect also can be observed using a metallized SPM tip. The surface of the probe tip must be coated with a metal (e.g., Ag, Au, Cu) that exhibits strong SERS enhancements. In this case the Raman scattering is constrained to within a few nanometers of the tip.[462] The enhancement factors realized to date (10^2-10^4) are still moderately low and considerably less than the predicted maximum values (10^{10}).[462]

One particularly interesting aspect of the advances coming from this research is the ability to combine the spatial resolution of SPM with the molecule-specific detection afforded by SERS. An example of this is illustrated by the data shown in Figure 24. In this case the nanoscale roughness, achieved with a 2 nm abrupt step on the surface of a metal-coated sharp TERS tip, can lead to an increase in Raman scattering cross section over a standard proximal probe by over an order of magnitude for benzenethiol adsorbed on Au.[463] The tips of silicon nanowires have also been modified with Au droplets to improve detection limits.[464] The ability to create tips of varying geometrical parameters allows the spatial resolution of the technique to be optimized. These methods also can be used to characterize features of crystalline materials such as GaN with high spatial resolution and enhancement factors as large as 10^4.[465] The ability to break the diffraction limit while gaining chemically specific information constitutes an area of particular opportunity for progress in research, one whose progress will be dictated directly by capabilities to create better tips and to optimize plasmonic excitation and correlated collection optics.[462]

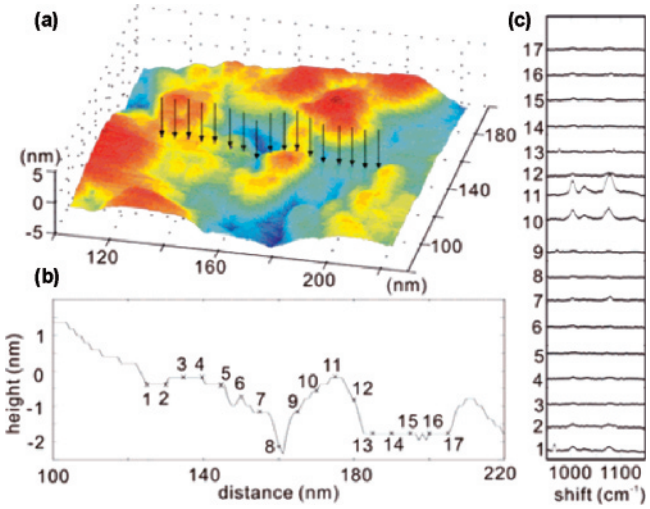

Figure 24. TERS mapping on a rough Au surface. An STM image of the sample is shown in a. TERS data was collected at the positions indicated by the arrows. The cross section of the topography image is shown in b, and the TERS collection sites are labeled with crosses. (c) Corresponding TERS sequence. The numbers denote the sites where the spectra were collected. Reprinted with permission from ref 463. Copyright 2007 American Chemical Society.

4.6.1. Plasmon-Enhanced Fluorescence

Plasmon-enhanced fluorescence (PEF) is a relatively new technique that can be used to increase sensitivity and detection limits. This is a capability that involves integrating the measurement within a device form factor that can exploit the enhanced electrical fields associated with surface plasmons. Fluorescence microscopy and spectroscopy are perhaps the most widely adopted methods used to study complex biomolecular systems.[457,466−468] The use of surface plasmon modes to enhance fluorescence has recently attracted considerable interest as a way to extend the already considerable FOM of this spectroscopic measurement.[215,356,469,470] Fluorophore quenching occurs in close proximity to metallic surfaces (typically < 50 Å);[471] however, at longer distances ranging from 5 to 200 nm an interesting coupling between the fluorophore and the enhanced local field near the metal structure occurs, resulting in both increased absorption cross section and radiative decay rates.[470] The increase of the radiative decay rate is central to a number of other phenomena observed in PEF including increased photostability, enhanced wavelength-tunable emission, and the ability to probe fluorescence resonance energy transfer (FRET) at larger distances than previously possible.[470]

These enhancements have opened new opportunities to improve detection and imaging schemes. A number of different metallic structures such as nanohole arrays, NPs, flat thin films, and deposited nanostructured films have been used for PEF.[215,472−474] Au NPs, for example, have been used to sense mouse IgG at concentrations as low as 7 fM using a sandwich assay format coupled to an optical fiber.[469] Sensing of metal ions such as Cu^{2+} has also been accomplished using fluorophore-labeled Au NPs with a detection limit of 1 μM.[475] This particular sensing scheme has advantages over other methods because it shows increased quantum yields even in the presence of Cu^{2+}, which generally quenches fluorescence. In the same vein, Au NPs have also been used to detect the presence of Hg^{2+} in pond water at concentrations as low as 2.0 ppb.[473] Nanohole arrays can also be used for PEF detection, and such applications are attracting growing attention in research.[468,472,476] In one specific example, Au nanohole arrays exhibited an enhancement of up to 2 times over flat metal films when the fluorophores were beyond the inherent quenching distance.[468] Surface-immobilized Ag NP arrays have also been used as a medium to enhance the fluorescence of common dyes with leading work directed to determine how the geometry of the NP films affects the enhancement factor.[215] It was found that the observed enhancements (of some 10−20 times) were dependent on the width and height of the particles with fluorescein and Cy3 exhibiting a maximum enhancement for particle sizes in the range of 85−95 nm.[215] We believe that the ability to enhance fluorescence through the use of plasmons is an area of research that is not yet mature and will continue to grow in importance and impact as the method is optimized.

5. Concluding Remarks

The rich literature summarized in this review develops a compelling story about both the health of and the prospect for technological impacts following from research in the interdisciplinary field of plasmonics. Whether in the form of refractive-index-based detection schemes for analytes of extremely low concentrations or as optics for chemically sensitive imaging, the reports appearing from many laboratories at this time demonstrate an accelerating pace of underlying progress, one driven by rapidly improving capacities for nanoscale materials synthesis and methods of fabrication. An interesting question to ask at this point is one related to context. Specifically, will the most important impact going forward with respect to chemical analysis come from the development of systems that embed "new physics" (such as those emerging within the vastly interesting topic of metamaterials)[477−480] or from compelling applications of systems that exploit what is currently known? Our hope is that the answer comes from both. There is no doubt that the rapid progress being made in both the fabrication and theory will greatly enhance progress in the field to render the enabling science in a form that begins to become a true form of predictive design for function. Essentially all applications in sensing will benefit from this advent. Still though, what might happen in the context of "new physics" and the opportunities it might engender? An interesting (and nascent) model here is provided by an area only touched on briefly in this review—use of plasmonics as devices for subwavelength "imaging".

It is well appreciated that the spatial resolution in optical microscopy is limited to $\lambda/2$, according to the Rayleigh criterion. This limit is caused by the loss of the evanescent field intensity in the far field, which carries high spatial frequency information. Complex methods can overcome this limit and have been devised in such notable forms as near-field scanning optical microscopy.[460] The complexity of the methods used there carry with them limitations that have tended to limit its widespread use for biological imaging, especially cellular imaging.

Metal nanohole arrays have been shown to inherently give anomalous high transmission of light,[75] and this, in conjunction with "a perfect lens" based on negative index metamaterials,[481] is theorized to make possible subwavelength resolution microscopy down to limits as small as 25 nm. Recent reports have demonstrated[482−485] that a surface plasmon's near-field dimensions are smaller than free-space radiation at the same frequency. Srituravanich et al. examined

this effect by exposing photoresist through a nanohole array, obtaining features with sizes of 90 nm spaced by 170 nm.[485] Fields with dimensions as small as 25 nm were obtained using slightly more complex plasmonic structures.[486] It is therefore most intriguing that wide field optical microscopy with subwavelength resolution, based on the concepts of plasmon-coupled transmission and optical near fields, has been proposed along with methods to implement it.[487−489] More recently, two different types of magnifying metamaterials-based superlenses that can be integrated into a conventional far-field optical microscope were reported.[490,491] Liu et al. demonstrated a magnifying optical hyperlens consisting of a curved periodic stack of Ag (35 nm) and Al_2O_3 (35 nm) deposited on a half-cylindrical cavity in quartz.[491] This setup was able to image a pair of 35 nm lines spaced 150 nm apart. In a later report, Smolyaninov et al. demonstrated a superlens design based on a multilayer photonic metamaterial consisting of alternating layers of positive and negative refractive index.[490] With this design a resolution of 70 nm was reported. These are advances that serve to illustrate the inspirational opportunities for progress coming from work in this field.

6. Acknowledgments

We gratefully acknowledge the support of aspects of our work by the National Science Foundation (CHE 04-02420) and the Department of Energy (DEFG02-91ER45439). S.K.G. was supported by the Office of Basic Energy Sciences, Division of Chemical Sciences, Geosciences, and Biosciences, U.S. Department of Energy (DE-AC02-06CH11357).

7. References

(1) Atwater, H. A. *Sci. Am.* **2007**, *296*, 56.
(2) Ozbay, E. *Science* **2006**, *311*, 189.
(3) Maier, S. A.; Atwater, H. A. *Appl. Phys. Lett.* **2005**, *98*, 011101/1.
(4) Hu, M.; Chen, J.; Li, Z.-Y.; Au, L.; Hartland, G. V.; Li, X.; Marquez, M.; Xia, Y. *Chem. Soc. Rev.* **2006**, *35*, 1084.
(5) Nath, N.; Chilkoti, A. *Anal. Chem.* **2002**, *74*, 504.
(6) Bozhevolnyi, S. I.; Volkov, V. S.; Devaux, E.; Laluet, J.-Y.; Ebbesen, T. W. *Nature* **2006**, *440*, 508.
(7) Haes, A. J.; Van Duyne, R. P. *J. Am. Chem. Soc.* **2002**, *124*, 10596.
(8) Malyarchuk, V.; Hua, F.; Mack, N. H.; Velasquez, V. T.; White, J. O.; Nuzzo, R. G.; Rogers, J. A. *Opt. Express* **2005**, *13*, 5669.
(9) Rothschild, M.; Bloomstein, T. M.; Efremow, N., Jr.; Fedynyshyn, T. H.; Fritze, M.; Pottebaum, I.; Switkes, M. *MRS Bull.* **2005**, *30*, 942.
(10) Stewart, M. E.; Motala, M. J.; Yao, J. T., L. B.; Nuzzo, R. G. *Proc. ImechE, Part N: J. Nanoeng. Nanosyst.* **2007**, *220*, 81.
(11) Tseng, A. A. *Small* **2005**, *1*, 594.
(12) Watt, F.; Bettiol, A. A.; Van Kan, J. A.; Teo, E. J.; Breese, M. B. H. *Int. J. Nanosci.* **2005**, *4*, 269.
(13) Daniel, M.-C.; Astruc, D. *Chem. Rev.* **2004**, *104*, 293.
(14) Brolo, A. G.; Gordon, R.; Leathem, B.; Kavanagh, K. L. *Langmuir* **2004**, *20*, 4813.
(15) Huang, C.-J.; Chiu, P.-H.; Wang, Y.-H.; Yang, C.-F. *J. Colloid Interface Sci.* **2006**, *303*, 430.
(16) Murphy, C. J.; Sau, T. K.; Gole, A. M.; Orendorff, C. J.; Gao, J.; Gou, L.; Hunyadi, S. E.; Li, T. *J. Phys. Chem. B* **2005**, *109*, 13857.
(17) Wiley, B.; Sun, Y.; Mayers, B.; Xia, Y. *Chem. Eur. J.* **2005**, *11*, 454.
(18) Bartlett, P. N.; Baumberg, J. J.; Coyle, S.; Abdelsalam, M. E. *Faraday Discuss.* **2004**, *125*, 117.
(19) Gates, B. D.; Xu, Q.; Stewart, M.; Ryan, D.; Willson, C. G.; Whitesides, G. M. *Chem. Rev.* **2005**, *105*, 1171.
(20) Genevieve, M.; Vieu, C.; Carles, R.; Zwick, A.; Briere, G.; Salome, L.; Trevisiol, E. *Microelectron. Eng.* **2007**, *84*, 1710.
(21) Wang, C.; Ma, Z.; Wang, T.; Su, Z. *Adv. Funct. Mater.* **2006**, *16*, 1673.
(22) Kneipp, K.; Kneipp, H.; Bohr, H. G. *Top. Appl. Phys.* **2006**, *103*, 261.
(23) Raether, H. 1988.
(24) Wark, A. W.; Lee, H. J.; Corn, R. M. *Anal. Chem.* **2005**, *77*, 3904.
(25) Lee, K.-S.; El-Sayed, M. A. *J. Phys. Chem. B* **2006**, *110*, 19220.
(26) Ghosh, S. K.; Nath, S.; Kundu, S.; Esumi, K.; Pal, T. *J. Phys. Chem. B* **2004**, *108*, 13963.
(27) Hutter, E.; Fendler, J. H. *Adv. Mater.* **2004**, *16*, 1685.
(28) Ly, N.; Foley, K.; Tao, N. *Anal. Chem.* **2007**, *79*, 2546.
(29) Chau, L.-K.; Lin, Y.-F.; Cheng, S.-F.; Lin, T.-J. *Sens. Actuators B* **2006**, *113*, 100.
(30) Zhao, J.; Zhang, X.; Yonzon, C. R.; Haes, A. J.; Van Duyne, R. P. *Nanomedicine* **2006**, *1*, 219.
(31) Zhang, X.; Shah, N. C.; Van Duyne, R. P. *Vib. Spectrosc.* **2006**, *42*, 2.
(32) Bohren, C. F.; Huffman, D. R. *Absorption and Scattering of Light by Small Particles*; John Wiley and Sons: New York, 1983; p 530.
(33) Kreibig, U.; Vollmer, M. *Optical Properties of Metal Clusters*; Springer: Berlin, 1995; Vol. 25, p 532.
(34) Willets, K. A.; Van Duyne, R. P. *Ann. Rev. Phys. Chem.* **2006**, *58*, 267.
(35) Kelly, K. L.; Coronado, E.; Zhao, L. L.; Schatz, G. C. *J. Phys. Chem. B* **2003**, *107*, 668.
(36) Underwood, S.; Mulvaney, P. *Langmuir* **1994**, *10*, 3427.
(37) Mulvaney, P. *Langmuir* **1996**, *12*, 788.
(38) Mie, G. *Ann. Phys.* **1908**, *25*, 377.
(39) Calander, N.; Willander, M. *J. Appl. Phys.* **2002**, *92*, 4878.
(40) Asano, S.; Yamamoto, G. *Appl. Opt.* **1975**, *14*, 29.
(41) Voshchinnikov, N. V.; Farafonov, V. G. *Astrophys. Space Sci.* **1993**, *204*, 19.
(42) Sun, Y. G.; Xia, Y. N. *Proc. SPIE* **2003**, *5221*, 164.
(43) Link, S.; El-Sayed, M. A. *Ann. Rev. Phys. Chem.* **2003**, *54*, 331.
(44) Perez-Juste, J.; Pastoriza-Santos, I.; Liz-Marzan, L. M.; Mulvaney, P. *Coord. Chem. Rev.* **2005**, *249*, 1870.
(45) Perez-Juste, J.; Liz-Marzan, L. M.; Carnie, S.; Chan, D. Y. C.; Mulvaney, P. *Adv. Funct. Mater.* **2004**, *14*, 571.
(46) Kou, X.; Zhang, S.; Tsung, C.-K.; Yang, Z.; Yeung, M. H.; Stucky, G. D.; Sun, L.; Wang, J.; Yan, C. *Chem. Eur. J.* **2007**, *13*, 2929.
(47) Hu, M.; Wang, X.; Hartland, G. V.; Mulvaney, P.; Perez-Juste, J.; Sader, J. E. *J. Am. Chem. Soc.* **2003**, *125*, 14925.
(48) Link, S.; Mohamed, M. B.; El-Sayed, M. A. *J. Phys. Chem. B* **1999**, *103*, 3073.
(49) Yu, Y.-Y.; Chang, S.-S.; Lee, C.-L.; Wang, C. R. C. *J. Phys. Chem. B* **1997**, *101*, 6661.
(50) Lee, K.-S.; El-Sayed, M. A. *J. Phys. Chem. B* **2005**, *109*, 20331.
(51) El-Sayed, M. A. *Acc. Chem. Res.* **2001**, *34*, 257.
(52) Kottmann, J.; Martin, O.; Smith, D.; Schultz, S. *Opt. Express* **2000**, *6*, 213.
(53) Hao, E.; Bailey, R. C.; Schatz, G. C.; Hupp, J. T.; Li, S. *Nano Lett.* **2004**, *4*, 327.
(54) Kuwata, H.; Tamaru, H.; Esumi, K.; Miyano, K. *Appl. Phys. Lett.* **2003**, *83*, 4625.
(55) Barber, P. W.; Hill, S. C. *Light Scattering by Particles: Computational Methods*; World Scientific Publishing: Singapore, 1990; Vol. 2.
(56) Yang, W.-H.; Schatz, G. C.; Van Duyne, R. P. *J. Chem. Phys.* **1995**, *103*, 869.
(57) Sosa, I. O.; Noguez, C.; Barrera, R. G. *J. Phys. Chem. B* **2003**, *107*, 6269.
(58) Shlager, K. L.; Schneider, J. B. *IEEE Antenn. Propag. Mag.* **1995**, *37*, 39.
(59) Gray, S. K.; Kupta, T. *Phys. Rev. B* **2003**, *68*, 045415.
(60) Meier, M.; Wokaun, A. *Opt. Lett.* **1983**, *8*, 581.
(61) Wokaun, A.; Gordon, J. P.; Liao, P. F. *Phys. Rev. Lett.* **1982**, *48*, 957.
(62) Maier, S. A.; Brongersma, M. L.; Kik, P. G.; Atwater, H. A. *Phys. Rev. B* **2002**, *65*, 193408/1.
(63) Maier, S. A.; Kik, P. G.; Atwater, H. A. *Appl. Phys. Lett.* **2002**, *81*, 1714.
(64) Maier, S. A.; Kik, P. G.; Atwater, H. A.; Meltzer, S.; Harel, E.; Koel, B. E.; Requicha, A. A. G. *Nat. Mater.* **2003**, *2*, 229.
(65) Gunnarsson, L.; Rindzevicius, T.; Prikulis, J.; Kasemo, B.; Kall, M.; Zou, S.; Schatz, G. C. *J. Phys. Chem. B* **2005**, *109*, 1079.
(66) Su, K.-H.; Wei, Q.-H.; Zhang, X.; Mock, J. J.; Smith, D. R.; Schultz, S. *Nano Lett.* **2003**, *3*, 1087.
(67) Rechberger, W.; Hohenau, A.; Leitner, A.; Krenn, J. R.; Lamprecht, B.; Aussenegg, F. R. *Opt. Commun.* **2003**, *220*, 137.
(68) Krenn, J. R.; Dereux, A.; Weeber, J. C.; Bourillot, E.; Lacroute, Y.; Goudonnet, J. P.; Schider, G.; Gotschy, W.; Leitner, A.; Aussenegg, F. R.; Girard, C. *Phys. Rev. Lett.* **1999**, *82*, 2590.
(69) Lamprecht, B.; Schider, G.; Lechner, R. T.; Ditlbacher, H.; Krenn, J. R.; Leitner, A.; Aussenegg, F. R. *Phys. Rev. Lett.* **2000**, *84*, 4721.
(70) Mirkin, C. A. L.; Robert, L.; Mucic, R. C.; Storhoff, J. J. *Nature* **1996**, *382*, 607.
(71) Born, M.; Wolf, E. 1999.

(72) Prikulis, J.; Hanarp, P.; Olofsson, L.; Sutherland, D.; Kaell, M. *Nano Lett.* **2004**, *4*, 1003.
(73) Wannemacher, R. *Opt. Commun.* **2001**, *195*, 107.
(74) Yin, L.; Vlasko-Vlasov, V. K.; Rydh, A.; Pearson, J.; Welp, U.; Chang, S.-H.; Gray, S. K.; Brown, D. B.; Kimball, C. W. *Appl. Phys. Lett.* **2004**, *85*, 467.
(75) Ebbesen, T. W.; Lezec, H. J.; Ghaemi, H. F.; Thio, T.; Wolff, P. A. *Nature* **1998**, *391*, 667.
(76) Chang, S.-H.; Gray, S. K.; Schatz, G. C. *Opt. Express* **2005**, *13*, 3150.
(77) Stewart, M. E.; Mack, N. H.; Malyarchuk, V.; Soares, J. A. N. T.; Lee, T.-W.; Gray, S. K.; Nuzzo, R. G.; Rogers, J. A. *PNAS* **2006**, *103*, 17143.
(78) Yin, L.; Vlasko-Vlasov, V. K.; Pearson, J.; Hiller, J. M.; Hua, J.; Welp, U.; Brown, D. E.; Kimball, C. W. *Nano Lett.* **2005**, *5*, 1399.
(79) Dionne, J. A.; Lezec, H. J.; Atwater, H. A. *Nano Lett.* **2006**, *6*, 1928.
(80) Satuby, Y.; Orenstein, M. *Opt. Express* **2007**, *15*, 4247.
(81) Weeber, J. C.; Gonzalez, M. U.; Baudrion, A.-L.; Dereux, A. *Appl. Phys. Lett.* **2005**, *87*, 221101/1.
(82) Bozhevolnyi, S. I.; Volkov, V. S.; Devaux, E.; Ebbesen, T. W. *Phys. Rev. Lett.* **2005**, *95*, 046802.
(83) Ko, S. H.; Park, I.; Pan, H.; Grigoropoulos, C. P.; Pisano, A. P.; Luscombe, C. K.; Frechet, J. M. J. *Nano Lett.* **2007**, ACS ASAP.
(84) Herderick, E. D.; Tresback, J. S.; Vasiliev, A. L.; Padture, N. P. *Nanotechnology* **2007**, *18*, 155204/1.
(85) Bluemel, A.; Klug, A.; Eder, S.; Scherf, U.; Moderegger, E.; List, E. J. W. *Org. Electron.* **2007**, *8*, 389.
(86) Ko, S. H.; Pan, H.; Grigoropoulos, C. P.; Luscombe, C. K.; Frechet, J. M. J.; Poulikakos, D. *Appl. Phys. Lett.* **2007**, *90*, 141103/1.
(87) Liu, J.; Lu, Y. *Angew. Chem., Int. Ed.* **2006**, *45*, 90.
(88) Lee, J.-S.; Han, M. S.; Mirkin, C. A. *Angew. Chem., Int. Ed.* **2007**, *46*, 4093.
(89) Storhoff, J. J.; Elghanian, R.; Mucic, R. C.; Mirkin, C. A.; Letsinger, R. L. *J. Am. Chem. Soc.* **1998**, *120*, 1959.
(90) Gao, D.; Chen, W.; Mulchandani, A.; Schultz, J. S. *Appl. Phys. Lett.* **2007**, *90*, 073901/1.
(91) Haes, A. J.; Haynes, C. L.; McFarland, A. D.; Schatz, G. C.; Van Duyne, R. P.; Zou, S. *MRS Bull.* **2005**, *30*, 368.
(92) Haes, A. J.; Chang, L.; Klein, W. L.; Van Duyne, R. P. *J. Am. Chem. Soc.* **2005**, *127*, 2264.
(93) Chen, J.; Wang, D.; Xi, J.; Au, L.; Siekkinen, A.; Warsen, A.; Li, Z.-Y.; Zhang, H.; Xia, Y.; Li, X. *Nano Lett.* **2007**, *7*, 1318.
(94) Loo, C.; Lowery, A.; Halas, N.; West, J.; Drezek, R. *Nano Lett.* **2005**, *5*, 709.
(95) Loo, C.; Lin, A.; Hirsch, L.; Lee, M.-H.; Barton, J.; Halas, N.; West, J.; Drezek, R. *Technol. Cancer Res. Treat.* **2004**, *3*, 33.
(96) Huang, X.; El-Sayed, I. H.; Qian, W.; El-Sayed, M. A. *J. Am. Chem. Soc.* **2006**, *128*, 2115.
(97) Durr, N. J.; Larson, T.; Smith, D. K.; Korgel, B. A.; Sokolov, K.; Ben-Yakar, A. *Nano Lett.* **2007**, *7*, 941.
(98) Chen, H. M.; Hsin, C. F.; Liu, R.-S.; Lee, J.-F.; Jang, L.-Y. *J. Phys. Chem. C* **2007**, *111*, 5909.
(99) Lu, L.; Kobayashi, A.; Tawa, K.; Ozaki, Y. *Chem. Mater.* **2006**, *18*, 4894.
(100) Murphy, C. J.; Sau, T. K.; Gole, A.; Orendorff, C. J. *MRS Bull.* **2005**, *30*, 349.
(101) Wiley, B.; Im, S. H.; Li, Z.-Y.; McLellan, J.; Siekkinen, A.; Xia, Y. *J. Phys. Chem. B* **2006**, *110*, 15666.
(102) Xiong, Y.; Cai, H.; Wiley, B. J.; Wang, J.; Kim, M. J.; Xia, Y. *J. Am. Chem. Soc.* **2007**, *129*, 3665.
(103) Nehl, C. L.; Liao, H.; Hafner, J. H. *Nano Lett.* **2006**, *6*, 683.
(104) Evanoff, D. D.; Chumanov, G. *J. Phys. Chem. B* **2004**, *108*, 13948.
(105) Grand, J.; Adam, P.-M.; Grimault, A.-S.; Vial, A.; de la Chapelle, M. L.; Bijeon, J.-L.; Kostcheev, S.; Royer, P. *Plasmonics* **2006**, *1*, 135.
(106) Whitesides, G. M.; Love, C. J. *Sci. Am.* **2001**, *285*, 38.
(107) Hanarp, P.; Sutherland, D. S.; Gold, J.; Kasemo, B. *Colloids Surf., A* **2003**, *214*, 23.
(108) Aizpurua, J.; Hanarp, P.; Sutherland, D. S.; Kall, M.; Bryant, G. W.; Garcia de Abajo, F. J. *Phys. Rev. Lett.* **2003**, *90*, 057401.
(109) Haynes, C. L.; Van Duyne, R. P. *J. Phys. Chem. B* **2001**, *105*, 5599.
(110) Hicks, E. M.; Lyandres, O.; Hall, W. P.; Zou, S.; Glucksberg, M. R.; Van Duyne, R. P. *J. Phys. Chem. B* **2007**, *111*, 4116.
(111) Haes, A. J.; Zhao, J.; Zou, S.; Own, C. S.; Marks, L. D.; Schatz, G. C.; Van Duyne, R. P. *J. Phys. Chem. B* **2005**, *109*, 11158.
(112) Hostetler, M. J.; Wingate, J. E.; Zhong, C.-J.; Harris, J. E.; Vachet, R. W.; Clark, M. R.; Londono, J. D.; Green, S. J.; Stokes, J. J.; Wignall, G. D.; Glish, G. L.; Porter, M. D.; Evans, N. D.; Murray, R. W. *Langmuir* **1998**, *14*, 17.
(113) Frens, G. *Nat.: Phys. Sci.* **1973**, *241*, 20.
(114) Pillai, Z. S.; Kamat, P. V. *J. Phys. Chem. B* **2004**, *108*, 945.
(115) Jacob, J. A.; Kapoor, S.; Biswas, N.; Mukherjee, T. *Colloids Surf., A* **2007**, *301*, 329.
(116) He, P.; Zhu, X. *Mater. Res. Bull.* **2007**, *42*, 1310.
(117) Sun, Y.; Zhang, L.; Zhou, H.; Zhu, Y.; Sutter, E.; Ji, Y.; Rafailovich, M. H.; Sokolov, J. C. *Chem. Mater.* **2007**, *19*, 2065.
(118) Liz-Marzan, L. M. *Langmuir* **2006**, *22*, 32.
(119) Mallin, M. P.; Murphy, C. J. *Nano Lett.* **2002**, *2*, 1235.
(120) Steinbruck, A.; Csaki, A.; Festag, G.; Fritzsche, W. *Plasmonics* **2006**, *1*, 79.
(121) Lu, X.; Tuan, H.-Y.; Chen, J.; Li, Z.-Y.; Korgel, B. A.; Xia, Y. *J. Am. Chem. Soc.* **2007**, *129*, 1733.
(122) Selvakannan, P. R.; Sastry, M. *Chem. Commun.* **2005**, *1684*.
(123) Roucoux, A.; Schulz, J.; Patin, H. *Chem. Rev.* **2002**, *102*, 3757.
(124) Khomutov, G. B.; Koksharov, Y. A. *Adv. Colloid Interface Sci.* **2006**, *122*, 119.
(125) Ott, L. S.; Finke, R. G. *Inorg. Chem.* **2006**, *45*, 8382.
(126) Anad, M.; Bell, P. W.; Fan, X.; Enick, R. M.; Roberts, C. B. *J. Phys. Chem. B* **2006**, *110*, 14693.
(127) Hunter, R. J. *Foundations of Colloid Science*; Oxford University Press: Oxford, 2001.
(128) Starowicz, M.; Stypula, B.; Banas, J. *Electrochem. Commun.* **2006**, *8*, 227.
(129) Plieth, W.; Dietz, H.; Anders, A.; Sandmann, G.; Meixner, A.; Weber, M.; Kneppe, H. *Surf. Sci.* **2005**, *597*, 119.
(130) Vosgroene, T.; Meixner, A. J.; Anders, A.; Dietz, H.; Sandmann, G.; Plieth, W. *Surf. Sci.* **2005**, *597*, 102.
(131) Lee, W.; Scholz, R.; Nielsch, K.; Goesele, U. *Angew. Chem., Int. Ed.* **2005**, *44*, 6050.
(132) Huang, C.-J.; Chiu, P.-H.; Wang, Y.-H.; Yang, C.-F.; Feng, S.-W. *J. Colloid Interface Sci.* **2007**, *306*, 56.
(133) Kim, F.; Song, J. H.; Yang, P. *J. Am. Chem. Soc.* **2002**, *124*, 14316.
(134) Zhu, J.; Shen, Y.; Xie, A.; Qiu, L.; Zhang, Q.; Zhang, S. *J. Phys. Chem. C* **2007**, *111*, 7629.
(135) Sakamoto, M.; Tachikawa, T.; Fujitsuka, M.; Majima, T. *Adv. Funct. Mater.* **2007**, *17*, 857.
(136) McGilvray, K. L.; Decan, M. R.; Wang, D.; Scaiano, J. C. *J. Am. Chem. Soc.* **2006**, *128*, 15980.
(137) Park, J.-E.; Atobe, M.; Fuchigami, T. *Ultrason. Sonochem.* **2006**, *13*, 237.
(138) Su, C.-H.; Wu, P.-L.; Yeh, C.-S. *J. Phys. Chem. B* **2003**, *107*, 14240.
(139) Jiang, L.-P.; Wang, A.-N.; Zhao, Y.; Zhang, J.-R.; Zhu, J.-J. *Inorg. Chem. Commun.* **2004**, *7*, 506.
(140) Rodriguez-Gonzalez, B.; Mulvaney, P.; Liz-Marzan, L. M. *Z. Phys. Chem.* **2007**, *221*, 415.
(141) Pal, A.; Shah, S.; Devi, S. *Colloids Surf., A* **2007**, *302*, 483.
(142) Kariuki, N. N.; Luo, J.; Maye, M. M.; Hassan, S. A.; Menard, T.; Naslund, H. R.; Lin, Y.; Wang, C.; Engelhard, M. H.; Zhong, C.-J. *Langmuir* **2004**, *20*, 11240.
(143) Toshima, N.; Yonezawa, T. *New J. Chem.* **1998**, *22*, 1179.
(144) Wiley, B.; Herricks, T.; Sun, Y.; Xia, Y. *Nano Lett.* **2004**, *4*, 1733.
(145) Yuan, H.; Ma, W.; Chen, C.; Zhao, J.; Liu, J.; Zhu, H.; Gao, X. *Chem. Mater.* **2007**, *19*, 1592.
(146) Srnova-Sloufova, I.; Vlckova, B.; Bastl, Z.; Hasslett, T. L. *Langmuir* **2004**, *20*, 3407.
(147) Youk, J. H.; Park, M.-K.; Locklin, J.; Advincula, R.; Yang, J.; Mays, J. *Langmuir* **2002**, *18*, 2455.
(148) Shi, X.; Ganser, T. R.; Sun, K.; Balogh, L. P.; Baker, J., Jr. *Nanotechnology* **2006**, *17*, 1072.
(149) Shahverdi, A. R.; Minaeian, S.; Shahverdi, H. R.; Jamalifar, H.; Nohi, A.-A. *Process Biochem.* **2007**, *42*, 919.
(150) Rangnekar, A.; Sarma, T. K.; Singh, A. K.; Deka, J.; Ramesh, A.; Chattopadhyay, A. *Langmuir* **2007**, *23*, 5700.
(151) Willner, I.; Baron, R.; Willner, B. *Adv. Mater.* **2005**, *18*, 1109.
(152) Gericke, M.; Pinches, A. *Gold Bull.* **2006**, *39*, 22.
(153) Klaus, T.; Joerger, R.; Olsson, E.; Granqvist, C.-G. *PNAS* **1999**, *96*, 13611.
(154) Raveendran, P.; Fu, J.; Wallen, S. L. *J. Am. Chem. Soc.* **2003**, *125*, 13940.
(155) McLeod, C. M.; Gale, W. F.; Roberts, C. B. *Langmuir* **2004**, *20*, 7078.
(156) Dahl, J. A.; Maddux, B. L. S.; Hutchison, J. E. *Chem. Rev.* **2007**, *107*, 2228.
(157) Turkevitch, J.; Stevenson, P. C.; Hillier, J. *Discuss. Faraday Soc.* **1951**, *11*, 55.
(158) Hayat, M. A. *Colloidal Gold: Principles, Methods and Applications*; Academic Press: San Diego, 1989.
(159) Brust, M.; Walker, M.; Bethell, D.; Schiffrin, D. J.; Whyman, R. *J. Chem. Soc., Chem. Commun.* **1994**, *801*.
(160) Donkers, R. L.; Lee, D.; Murray, R. W. *Langmuir* **2004**, *20*, 1945.
(161) Jimenez, V. L.; Georganopoulou, D. G.; White, R. J.; Harper, A. S.; Mills, A. J.; Lee, D.; Murray, R. W. *Langmuir* **2004**, *20*, 6864.
(162) Nerambourg, N.; Werts, M. H. V.; Charlot, M.; Blanchard-Desce, M. *Langmuir* **2007**, *23*, 5563.
(163) Tracy, J. B.; Kalyuzhny, G.; Crowe, M. C.; Balasubramanian, R.; Choi, J.-P.; Murray, R. W. *J. Am. Chem. Soc.* **2007**, *129*, 6706.

(164) Ackersonn, C. J.; Sykes, M. T.; Kornberg, R. D. *PNAS* **2005**, *102*, 13383.
(165) Becker, C. F. W.; Marsac, Y.; Hazarika, P.; Moser, J.; Goody, R. S.; Niemeyer, C. M. *Chembiochem* **2007**, *8*, 32.
(166) Hostetler, M. J.; Templeton, A. C.; Murray, R. W. *Langmuir* **1999**, *15*, 3782.
(167) Kassam, A.; Bremner, G.; Clark, B.; Ulibarri, G.; Lennox, R. B. *J. Am. Chem. Soc.* **2006**, *128*, 3476.
(168) Shaffer, A. W.; Worden, J. G.; Huo, Q. *Langmuir* **2004**, *20*, 8343.
(169) Montalti, M.; Prodi, L.; Zaccheroni, N.; Baxter, R.; Teobaldi, G.; Zerbetto, F. *Langmuir* **2003**, *19*, 5172.
(170) Jana, N. R.; Peng, X. *J. Am. Chem. Soc.* **2003**, *125*, 14280.
(171) Leff, D. V.; Brandt, L.; Heath, J. R. *Langmuir* **1996**, *12*, 4723.
(172) Gomez, S.; Philippot, K.; Colliere, V.; Chaudret, B.; Senocq, F.; Lecante, P. *Chem. Commun.* **2000**, *19*45.
(173) Weare, W. W.; Reed, S. M.; Warner, M. G.; Hutchison, J. E. *J. Am. Chem. Soc.* **2000**, *122*, 12890.
(174) Yamamoto, M.; Nakamoto, M. *Chem. Lett.* **2003**, *32*, 452.
(175) Templeton, A. C.; Chen, S.; Gross, S. M.; Murray, R. W. *Langmuir* **1999**, *15*, 66.
(176) Chen, S.; Kimura, K. *Langmuir* **1999**, *15*, 1075.
(177) Rowe, M. P.; Plass, K. E.; Kim, K.; Kurdak, C.; Zellers, E. T.; Matzger, A. J. *Chem. Mater.* **2004**, *16*, 3513.
(178) Jana, N. R.; Gearheart, L.; Murphy, C. J. *Adv. Mater.* **2001**, *13*, 1389.
(179) Iqbal, M.; Chung, Y.-I.; Tae, G. *J. Mater. Chem.* **2007**, *17*, 335.
(180) Brown, K. R.; Walter, D. G.; Natan, M. J. *Chem. Mater.* **2000**, *12*, 306.
(181) Brown, K. R.; Natan, M. J. *Langmuir* **1998**, *14*, 726.
(182) Zou, X.; Ying, E.; Dong, S. *Nanotechnology* **2006**, *17*, 4758.
(183) Gu, G. H.; Kim, J.; Kim, L.; Suh, J. S. *J. Phys. Chem. C* **2007**, *111*, 7906.
(184) Wang, H.-W.; Shieh, C.-F.; Chen, H.-Y.; Shiu, W.-C.; Russo, B.; Cao, G. *Nanotechnology* **2006**, *17*, 2689.
(185) Wang, Z. L.; Mohamed, M. B.; Link, S.; El-Sayed, M. A. *Surf. Sci.* **1999**, *440*, L809.
(186) Niidome, Y.; Nishioka, K.; Kawasaki, H.; Yamada, S. *Colloids Surf., A* **2005**, *257*−258, 161.
(187) Jana, N. R.; Gearheart, L.; Murphy, C. J. *Chem. Commun.* **2001**, *617*.
(188) Gole, A.; Murphy, C. J. *Chem. Mater.* **2004**, *16*, 3633.
(189) Sau, T. K.; Murphy, C. J. *Langmuir* **2004**, *20*, 6414.
(190) Nikoobakht, B.; El-Sayed, M. A. *Chem. Mater.* **2003**, *15*, 1957.
(191) Ha, T. H.; Koo, H.-J.; Chung, B. H. *J. Phys. Chem. C* **2007**, *111*, 1123.
(192) Mieszawska, A. J.; Jalilian, R.; Sumanasekera, G. U.; Zamborini, F. P. *J. Am. Chem. Soc.* **2005**, *127*, 10822.
(193) Mieszawska, A. J.; Slawinski, G. W.; Zamborini, F. P. *J. Am. Chem. Soc.* **2006**, *128*, 5622.
(194) Mieszawska, A. J.; Zamborini, F. P. *Chem. Mater.* **2005**, *17*, 3415.
(195) Lee, K.-H.; Huang, K.-M.; Tseng, W.-L.; Chiu, T.-C.; Lin, Y.-W.; Chang, H.-T. *Langmuir* **2007**, *23*, 1435.
(196) Neeves, A. E.; Birnboim, M. H. *J. Opt. Soc. Am. B* **1989**, *6*, 787.
(197) Oldenburg, S. J.; Averitt, R. D.; Westcott, S. L.; Halas, N. J. *Chem. Phys. Lett.* **1998**, *288*, 243.
(198) Halas, N. *MRS Bull.* **2005**, *30*, 362.
(199) Wang, H.; Brandl, D. W.; Le, F.; Nordlander, P.; Halas, N. J. *Nano Lett.* **2006**, *6*, 827.
(200) Wiley, B.; Sun, Y.; Chen, J.; Cang, H.; Li, Z.-Y.; Li, X.; Xia, Y. *MRS Bull.* **2005**, *30*, 356.
(201) Sun, Y.; Mayers, B.; Xia, Y. *Nano Lett.* **2003**, *3*, 675.
(202) Sun, Y.; Mayers, B.; Xia, Y. *Adv. Mater.* **2003**, *15*, 641.
(203) Chen, J.; Wiley, B.; Li, Z.-Y.; Campbell, D.; Saeki, F.; Cang, H.; Au, L.; Lee, J.; Li, X.; Xia, Y. *Adv. Mater.* **2005**, *17*, 2255.
(204) Pileni, M.-P. *Nat. Mater.* **2003**, *2*, 145.
(205) Landfester, K. *Annu. Rev. Mater. Res.* **2006**, *36*, 231.
(206) Salzemann, C.; Urban, J.; Lisiecki, I.; Pileni, M.-P. *Adv. Funct. Mater.* **2005**, *15*, 1277.
(207) Maillard, M.; Giorgio, S.; Pileni, M.-P. *J. Phys. Chem. B* **2003**, *107*, 2466.
(208) Hou, G.; Zhu, L.; Chen, D.; Jiang, M. *Macromolecules* **2007**, *40*, 2134.
(209) Chaudhari, V. R.; Haram, S. K.; Kulshreshtha, S. K.; Bellare, J. R.; Hassan, P. A. *Colloids Surf., A* **2007**, *301*, 475.
(210) Cushing, B. L.; Kolesnichenko, V. L.; O'Connor, C. J. *Chem. Rev.* **2004**, *104*, 3893.
(211) Ohno, T.; Bain, J. A.; Schlesinger, T. E. *J. Appl. Phys.* **2007**, *101*, 083107/1.
(212) Wang, S.; Pile, D. F. P.; Sun, C.; Zhang, X. *Nano Lett.* **2007**, *7*, 1076.
(213) Billot, L.; Lamy de la Chapelle, M.; Grimault, A. S.; Vial, A.; Barchiesi, D.; Bijeon, J. L.; Adam, P. M.; Royer, P. *Chem. Phys. Lett.* **2006**, *422*, 303.
(214) De Jesus, M. A.; Giesfeldt, K. S.; Oran, J. M.; Abu-Hatab, N. A.; Lavrik, N. V.; Sepaniak, M. J. *Appl. Spectrosc.* **2005**, *59*, 1501.
(215) Corrigan, T. D.; Guo, S.; Phaneuf, R. J.; Szmacinski, H. *J. Fluoresc.* **2005**, *15*, 777.
(216) Yamazaki, K.; Namatsu, H. *Jpn. J. Appl. Phys.* **2004**, *43*, 3767.
(217) Word, M. J.; Adesida, I.; Berg, P. R. *J. Vac. Sci. Technol. B* **2003**, *21*, L12.
(218) Isaacson, M.; Murray, A. *J. Vac. Sci. Technol.* **1981**, *19*, 1117.
(219) Hinsberg, W.; Houle, F.; Sanchez, M.; Hoffnagle, J.; Wallraff, G.; Medeiros, D.; Gallatin, G.; Cobbc, J. *Proc. SPIE* **2003**, *5039*, 1.
(220) Fu, Y.; Ngoi, B. K. A.; Zhou, W.; Loh, T. F. *Int. J. Nanosci.* **2006**, *5*, 529.
(221) Chang, C.-K.; Lin, D.-Z.; Yeh, C.-S.; Lee, C.-K.; Chang, Y.-C.; Lin, M.-W.; Yeh, J.-T.; Liu, J.-M. *Appl. Phys. Lett.* **2007**, *90*, 061113/1.
(222) Cabrini, S.; Carpentiero, A.; Kumar, R.; Businaro, L.; Candeloro, P.; Prasciolu, M.; Gosparini, A.; Andreani, C.; De Vittorio, M.; Stomeo, T.; Di Fabrizio, E. *Microelectron. Eng.* **2005**, *78*−79, 11.
(223) Taniguchi, J.; Ohno, N.; Takeda, S.; Miyamoto, I.; Komuro, M. *J. Vac. Sci. Technol. B* **1998**, *16*, 2506.
(224) Reyntjens, S.; Puers, R. *J. Micromech. Microeng.* **2000**, *10*, 181.
(225) Ishida, M.; Fujita, J.; Ichihashi, T.; Ochiai, Y.; Kaito, T.; Matsui, S. *J. Vac. Sci. Technol. B* **2003**, *21*, 2728.
(226) Kubena, R. L.; Ward, J. W.; Stratton, F. P.; Joyce, R. L.; Atkinson, G. M. *J. Vac. Sci. Technol. B* **1991**, *9*, 3079.
(227) Gierak, J.; Vieu, C.; Schneider, M.; Launois, H.; Ben Assayag, G.; Septier, A. *J. Vac. Sci. Technol. B* **1997**, *15*, 2373.
(228) Przybilla, F.; Genet, C.; Ebbesen, T. W. *Appl. Phys. Lett.* **2006**, *89*, 121115/1.
(229) Dintinger, J.; Klein, S.; Ebbesen, T. W. *Adv. Mater.* **2006**, *18*, 1267.
(230) Gonzalez, M. U.; Weeber, J.-C.; Baudrion, A.-L.; Dereux, A.; Stepanov, A. L.; Krenn, J. R.; Devaux, E.; Ebbesen, T. W. *Phys. Rev. B* **2006**, *73*, 155416/1.
(231) Lopez-Tejeira, F.; Rodrigo, S. G.; Martin-Moreno, L.; Garcia-Vidal, F. J.; Devaux, E.; Ebbesen, T. W.; Krenn, J. R.; Radko, I. P.; Bozhevolnyi, S. I.; Gonzalez, M. U.; Weeber, J. C.; Dereux, A. *Nat. Phys.* **2007**, *3*, 324.
(232) Volkov, V. S.; Bozhevolnyi, S. I.; Devaux, E.; Laluet, J.-Y.; Ebbesen, T. W. *Nano Lett.* **2007**, *7*, 880.
(233) Malinsky, M. D.; Kelly, K. L.; Schatz, G. C.; Van Duyne, R. P. *J. Phys. Chem. B* **2001**, *105*, 2343.
(234) Fischer, U. C.; Zingsheim, H. P. *J. Vac. Sci. Technol.* **1981**, *19*, 881.
(235) Deckman, H. W.; Dunsmuir, J. H. *Appl. Phys. Lett.* **1982**, *41*, 377.
(236) Hulteen, J. C.; Treichel, D. A.; Smith, M. T.; Duval, M. L.; Jensen, T. R.; Van Duyne, R. P. *J. Phys. Chem. B* **1999**, *103*, 3854.
(237) Hulteen, J. C.; Van Duyne, R. P. *J. Vac. Sci. Technol. A* **1995**, *13*, 1553.
(238) Whitney, A. V.; Myers, B. D.; Van Duyne, R. P. *Nano Lett.* **2004**, *4*, 1507.
(239) Freunscht, P.; Van Duyne, R. P.; Schneider, S. *Chem. Phys. Lett.* **1997**, *281*, 372.
(240) Hulteen, J. C.; Young, M. A.; Van Duyne, R. P. *Langmuir* **2006**, *22*, 10354.
(241) Stuart, D. A.; Yuen, J. M.; Shah, N.; Lyandres, O.; Yonzon, C. R.; Glucksberg, M. R.; Walsh, J. T.; Van Duyne, R. P. *Anal. Chem.* **2006**, *78*, 7211.
(242) Zhang, X.; Zhao, J.; Whitney, A. V.; Elam, J. W.; Van Duyne, R. P. *J. Am. Chem. Soc.* **2006**, *128*, 10304.
(243) Riboh, J. C.; Haes, A. J.; McFarland, A. D.; Yonzon, C. R.; Van Duyne, R. P. *J. Phys. Chem. B* **2003**, *107*, 1772.
(244) Schmidt, J. P.; Cross, S. E.; Buratto, S. K. *J. Chem. Phys.* **2004**, *121*, 10657.
(245) Haynes, C. L.; Van Duyne, R. P. *J. Phys. Chem. B* **2003**, *107*, 7426.
(246) Haes, A. J.; Hall, W. P.; Chang, L.; Klein, W. L.; Van Duyne, R. P. *Nano Lett.* **2004**, *4*, 1029.
(247) Kelf, T. A.; Sugawara, Y.; Cole, R. M.; Baumberg, J. J.; Abdelsalam, M. E.; Cintra, S.; Mahajan, S.; Russell, A. E.; Bartlett, P. N. *Phys. Rev. B* **2006**, *74*, 245415/1.
(248) Kelf, T. A.; Sugawara, Y.; Baumberg, J. J.; Abdelsalam, M.; Bartlett, P. N. *Phys. Rev. Lett.* **2005**, *95*, 116802.
(249) Baumberg, J. J.; Kelf, T. A.; Sugawara, Y.; Cintra, S.; Abdelsalam, M. E.; Bartlett, P. N.; Russell, A. E. *Nano Lett.* **2005**, *5*, 2262.
(250) Cintra, S.; Abdelsalam, M. E.; Bartlett, P. N.; Baumberg, J. J.; Kelf, T. A.; Sugawara, Y.; Russell, A. E. *Faraday Discuss.* **2006**, *132*, 191.
(251) Mahajan, S.; Abdelsalam, M.; Sugawara, Y.; Cintra, S.; Russell, A.; Baumberg, J.; Bartlett, P. *Phys. Chem. Chem. Phys.* **2007**, *9*, 104.
(252) Abdelsalam, M. E.; Bartlett, P. N.; Baumberg, J. J.; Cintra, S.; Kelf, T. A.; Russell, A. E. *Electrochem. Commun.* **2005**, *7*, 740.
(253) Hicks, E. M.; Zhang, X.; Zou, S.; Lyandres, O.; Spears, K. G.; Schatz, G. C.; Van Duyne, R. P. *J. Phys. Chem. B* **2005**, *109*, 22351.
(254) Kosiorek, A.; Kandulski, W.; Chudzinski, P.; Kempa, K.; Giersig, M. *Nano Lett.* **2004**, *4*, 1359.

(255) Kosiorek, A.; Kandulski, W.; Glaczynska, H.; Giersig, M. *Small* **2005**, *1*, 439.
(256) Haynes, C. L.; McFarland, A. D.; Hulteen, J. C.; Van Duyne, R. P. *J. Phys. Chem. B* **2002**, *106*, 1898.
(257) Jensen, T. R.; Malinsky, M. D.; Haynes, C. L.; Van Duyne, R. P. *J. Phys. Chem. B* **2000**, *104*, 10549.
(258) Zhang, X.; Hicks, E. M.; Zhao, J.; Schatz, G. C.; Van Duyne, R. P. *Nano Lett.* **2005**, *5*, 1503.
(259) Rindzevicius, T.; Alaverdyan, Y.; Dahlin, A.; Hoeoek, F.; Sutherland, D. S.; Kaell, M. *Nano Lett.* **2005**, *5*, 2335.
(260) Hanarp, P.; Kaell, M.; Sutherland, D. S. *J. Phys. Chem. B* **2003**, *107*, 5768.
(261) Langhammer, C.; Yuan, Z.; Zoric, I.; Kasemo, B. *Nano Lett.* **2006**, *6*, 833.
(262) Weibel, D. B.; DiLuzio, W. R.; Whitesides, G. M. *Nat. Rev. Microbiol.* **2007**, *5*, 209.
(263) Rogers, J. A.; Nuzzo, R. G. *Mater. Today* **2005**, *8*, 50.
(264) Xia, Y.; Whitesides, G. M. *Ann. Rev. Mater. Sci.* **1998**, *28*, 153.
(265) Delamarche, E.; Schmid, H.; Michel, B.; Biebuyck, H. *Adv. Mater.* **1997**, *9*, 741.
(266) Odom, T. W.; Love, J. C.; Wolfe, D. B.; Paul, K. E.; Whitesides, G. M. *Langmuir* **2002**, *18*, 5314.
(267) Hua, F.; Sun, Y.; Gaur, A.; Meitl, M. A.; Bilhaut, L.; Rotkina, L.; Wang, J.; Geil, P.; Shim, M.; Rogers, J. A. *Nano Lett.* **2004**, *4*, 2467.
(268) Schmid, H.; Michel, B. *Macromolecules* **2000**, *33*, 3042.
(269) Choi, K. M.; Rogers, J. A. *J. Am. Chem. Soc.* **2003**, *125*, 4060.
(270) Kwak, E.-S.; Henzie, J.; Chang, S.-H.; Gray, S. K.; Schatz, G. C.; Odom, T. W. *Nano Lett.* **2005**, *5*, 1963.
(271) Henzie, J.; Barton, J. E.; Stender, C. L.; Odom, T. W. *Acc. Chem. Res.* **2006**, *39*, 249.
(272) Odom, T. W.; Thalladi, V. R.; Love, J. C.; Whitesides, G. M. *J. Am. Chem. Soc.* **2002**, *124*, 12112.
(273) Gao, H.; Henzie, J.; Odom, T. W. *Nano Lett.* **2006**, *6*, 2104.
(274) Henzie, J.; Kwak, E.-S.; Odom, T. W. *Nano Lett.* **2005**, *5*, 1199.
(275) Henzie, J.; Shuford, K. L.; Kwak, E.-S.; Schatz, G. C.; Odom, T. W. *J. Phys. Chem. B* **2006**, *110*, 14028.
(276) Truskett, V. N.; Watts, M. P. C. *Trends Biotechnol.* **2006**, *24*, 312.
(277) Chou, S. Y.; Krauss, P. R.; Zhang, W.; Guo, L.; Zhuang, L. *J. Vac. Sci. Technol. B* **1997**, *15*, 2897.
(278) Stewart, M. D.; Johnson, S. C.; Sreenivasan, S. V.; Resnick, D. J.; Willson, G. C. *J. Microlith., Microfab., Microsyst.* **2005**, *4*, 011002/1.
(279) Malyarchuk, V.; Stewart, M.; Nuzzo, R. G.; Rogers, J. A. *Appl. Phys. Lett.* **2007**, *90*, 203113/1.
(280) Alvarez-Puebla, R. A.; Cui, B.; Bravo-Vasquez, J.-P.; Veres, T.; Fenniri, H. *J. Phys. Chem. C* **2007**, *111*, 6720.
(281) Rosi, N. L.; Mirkin, C. A. *Chem. Rev.* **2005**, *105*, 1547.
(282) Nakashima, H.; Furukawa, K.; Kashimura, Y.; Torimitsu, K. *Chem. Commun.* **2007**, *1080*.
(283) Reynolds, R. A.; Mirkin, C. A.; Letsinger, R. L. *J. Am. Chem. Soc.* **2000**, *122*, 3795.
(284) Schofield, C. L.; Haines, A. H.; Field, R. A.; Russell, D. A. *Langmuir* **2006**, *22*, 6707.
(285) McFarland, A. D.; VanDuyne, R. P. *Nano Lett.* **2003**, *3*, 1057.
(286) Yu, C.; Irudayaraj, J. *Anal. Chem.* **2007**, *79*, 572.
(287) Han, M. S.; Lytton-Jean, A. K. R.; Mirkin, C. A. *J. Am. Chem. Soc.* **2006**, *128*, 4954.
(288) Han, M. S.; Lytton-Jean, A. K. R.; Oh, B.-K.; Heo, J.; Mirkin, C. A. *Angew. Chem., Int. Ed.* **2006**, *45*, 1807.
(289) Kanaras, A. G.; Wang, Z.; Brust, M.; Cosstick, R.; Bates, A. D. *Small* **2007**, *3*, 590.
(290) Chakrabarti, R.; Klibanov, A. M. *J. Am. Chem. Soc.* **2003**, *125*, 12531.
(291) Ellington, A. D. S., J. W. *Nature* **1990**, *346*, 818.
(292) Huang, C. C.; Huang, Y. F.; Cao, Z.; Tan, W.; Chang, H. T. *Anal. Chem.* **2005**, *77*, 5735.
(293) Tuerk, C. G., L. *Science* **1990**, *249*, 505.
(294) Baron, R.; Zayats, M.; Willner, I. *Anal. Chem.* **2005**, *77*, 1566.
(295) Dykman, L. A.; Bogatyrev, V. A.; Khlebtsov, B. N.; Khlebtsov, N. G. *Anal. Biochem.* **2005**, *341*, 16.
(296) Kuong, C.-L.; Chen, W.-Y.; Chen, Y.-C. *Anal. Bioanal. Chem.* **2007**, *387*, 2091.
(297) Lin, S.-Y.; Wu, S.-H.; Chen, C.-h. *Angew. Chem., Int. Ed.* **2006**, *45*, 4948.
(298) Lu, C.; Zu, Y.; Yam, V. W. W. *Anal. Chem.* **2007**, *79*, 666.
(299) Schofield, C. L.; Field, R. A.; Russell, D. A. *Anal. Chem.* **2007**, *79*, 1356.
(300) Suzuki, D.; Kawaguchi, H. *Langmuir* **2006**, *22*, 3818.
(301) Wang, Z.; Levy, R.; Fernig, D. G.; Brust, M. *J. Am. Chem. Soc.* **2006**, *128*, 2214.
(302) Watanabe, S.; Seguchi, H.; Yoshida, K.; Kifune, K.; Tadaki, T.; Shiozaki, H. *Tetrahedron Lett.* **2005**, *46*, 8827.
(303) Wu, Z.-S.; Zhang, S.-B.; Guo, M.-M.; Chen, C.-R.; Shen, G.-L.; Yu, R.-Q. *Anal. Chim. Acta* **2007**, *584*, 122.
(304) Liu, J.; Lu, Y. *J. Am. Chem. Soc.* **2004**, *126*, 12298.
(305) Liu, J.; Lu, Y. *J. Am. Chem. Soc.* **2003**, *125*, 6642.
(306) Lin, S. Y.; Chen, C. h.; Lin, M. C.; Hsu, H. F. *Anal. Chem.* **2005**, *77*, 4821.
(307) Homola, J. *Anal. Bioanal. Chem.* **2003**, *377*, 528.
(308) Homola, J.; Yee, S. S.; Gauglitz, G. *Sens. Actuators B* **1999**, *54*, 3.
(309) Fu, E.; Ramsey, S. A.; Chen, J.; Chinowsky, T. M.; Wiley, B.; Xia, Y.; Yager, P. *Sens. Actuators B* **2007**, B123, 606.
(310) Liu, X.; Song, D.; Zhang, Q.; Tian, Y.; Liu, Z.; Zhang, H. *Sens. Actuators B* **2006**, B117, 188.
(311) Liu, X.; Song, D.; Zhang, Q.; Tian, Y.; Ding, L.; Zhang, H. *TrAC* **2005**, *24*, 887.
(312) Lee, H. J.; Li, Y.; Wark, A. W.; Corn, R. M. *Anal. Chem.* **2005**, *77*, 5096.
(313) Li, Y.; Lee, H. J.; Corn, R. M. *Anal. Chem.* **2007**, *79*, 1082.
(314) Lyon, L. A.; Musick, M. D.; Natan, M. J. *Anal. Chem.* **1998**, *70*, 5177.
(315) Hutter, E.; Cha, S.; Liu, J.-F.; Park, J.; Yi, J.; Fendler, J. H.; Roy, D. *J. Phys. Chem. B* **2001**, *105*, 8.
(316) Li, Y.; Wark, A. W.; Lee, H. J.; Corn, R. M. *Anal. Chem.* **2006**, *78*, 3158.
(317) Mitchell, J. S.; Wu, Y.; Cook, C. J.; Main, L. *Anal. Biochem.* **2005**, *343*, 125.
(318) Matsui, J.; Akamatsu, K.; Hara, N.; Miyoshi, D.; Nawafune, H.; Tamaki, K.; Sugimoto, N. *Anal. Chem.* **2005**, *77*, 4282.
(319) He, L.; Musick, M. D.; Nicewarner, S. R.; Salinas, F. G.; Benkovic, S. J.; Natan, M. J.; Keating, C. D. *J. Am. Chem. Soc.* **2000**, *122*, 9071.
(320) Teramura, Y.; Iwata, H. *Anal. Biochem.* **2007**, *365*, 201.
(321) Gobi, K. V.; Matsumoto, K.; Toko, K.; Ikezaki, H.; Miura, N. *Anal. Bioanal. Chem.* **2007**, *387*, 2727.
(322) Aizawa, H.; Tozuka, M.; Kurosawa, S.; Kobayashi, K.; Reddy, S. M.; Higuchi, M. *Anal. Chim. Acta* **2007**, *591*, 191.
(323) Shankaran, D. R.; Gobi, K. V.; Miura, N. *Sens. Actuators B* **2007**, *121*, 158.
(324) Goodrich, T. T.; Lee, H. J.; Corn, R. M. *J. Am. Chem. Soc.* **2004**, *126*, 4086.
(325) Goodrich, T. T.; Lee, H. J.; Corn, R. M. *Anal. Chem.* **2004**, *76*, 6173.
(326) Teramura, Y.; Arima, Y.; Iwata, H. *Anal. Biochem.* **2006**, *357*, 208.
(327) He, L.; Smith, E. A.; Natan, M. J.; Keating, C. D. *J. Phys. Chem. B* **2004**, *108*, 10973.
(328) Hutter, E.; Fendler, J. H.; Roy, D. *J. Phys. Chem. B* **2001**, *105*, 11159.
(329) Lyon, A. L.; Pena, D. J.; Natan, M. J. *J. Phys. Chem. B* **1999**, *103*, 5826.
(330) Lee, W.; Oh, B.-K.; Kim, Y.-W.; Choi, J.-W. *J. Nanosci. Nanotechnol.* **2006**, *6*, 3521.
(331) Hayashida, M.; Yamaguchi, A.; Misawa, H. *Jpn. J. Appl. Phys.* **2005**, *44*, L1544.
(332) Kang, T.; Hong, S.; Choi, I.; Sung, J. J.; Kim, Y.; Hahn, J. S.; Yi, J. *J. Am. Chem. Soc.* **2006**, *128*, 12870.
(333) Fang, S.; Lee, H. J.; Wark, A. W.; Corn, R. M. *J. Am. Chem. Soc.* **2006**, *128*, 14044.
(334) Tokareva, I.; Minko, S.; Fendler, J. H.; Hutter, E. *J. Am. Chem. Soc.* **2004**, *126*, 15950.
(335) Tokareva, I.; Tokarev, I.; Minko, S.; Hutter, E.; Fendler, J. H. *Chem. Commun.* **2006**, *3343*.
(336) Hutter, E.; Pileni, M. P. *J. Phys. Chem. B* **2003**, *107*, 6497.
(337) Stuart, D. A.; Haes, A. J.; Yonzon, C. R.; Hicks, E. M.; Van Duyne, R. P. *IEE Proc.-Nanobiotechnol.* **2005**, *152*, 13.
(338) Aslan, K.; Lakowicz, J. R.; Geddes, C. D. *Curr. Opin. Chem. Biol.* **2005**, *9*, 538.
(339) Yguerabide, J.; Yguerabide, E. E. *Anal. Biochem.* **1998**, *262*, 137.
(340) Yguerabide, J.; Yguerabide, E. E. *Anal. Biochem.* **1998**, *262*, 157.
(341) Reinhard, B. M.; Sheikholeslami, S.; Mastroianni, A.; Alivisatos, A. P.; Liphardt, J. *PNAS* **2007**, *104*, 2667.
(342) Sherry, L. J.; Chang, S.-H.; Schatz, G. C.; Van Duyne, R. P.; Wiley, B. J.; Younan, X. *Nano Lett.* **2005**, *5*, 2034.
(343) Raschke, G.; Kowarik, S.; Franzl, T.; Sonnichsen, C.; Klar, T. A.; Feldmann, J.; Nichtl, A.; Kurzinger, K. *Nano Lett.* **2003**, *3*, 935.
(344) Du, B.-A.; Li, Z.-P.; Liu, C.-H. *Angew. Chem., Int. Ed.* **2006**, *45*, 8022.
(345) Bally, M.; Halter, M.; Voros, J.; Grandin, H. M. *Surf. Interface Anal.* **2006**, *38*, 1442.
(346) Taton, A. T.; Mirkin, C. A.; Letsinger, R. L. *Science* **2000**, *289*, 1757.
(347) Storhoff, J. J.; Marla, S. S.; Bao, P.; Hagenow, S.; Mehta, H.; Lucas, A.; Garimella, V.; Patno, T.; Buckingham, W.; Cork, W.; Muller, U. R. *Biosens. Bioelectron.* **2004**, *19*, 875.
(348) Bao, P. Y.; Huber, M.; Wei, T.-F.; Marla, S. S.; Storhoff, J. J.; Muller, U. R. *Nucleic Acids Res.* **2005**, *33*, e15.
(349) Alivisatos, P. *Nat. Biotechnol.* **2004**, *22*, 47.
(350) Liu, G. L.; Yin, Y.; Kunchakarra, S.; Mukherjee, B.; Gerion, D.; Jett, S. D.; Bear, D. G.; Gray, J. W.; Alivisatos, A. P.; Lee, L. P.; Chen, F. F. *Nat. Nanotechnol.* **2006**, *1*, 47.

(351) Reinhard, B. M.; Siu, M.; Agarwal, H.; Alivisatos, A. P.; Liphardt, J. *Nano Lett.* **2005**, *5*, 2246.
(352) Storhoff, J. J.; Lucas, A. D.; Garimella, V.; Bao, Y. P.; Muller, U. R. *Nat. Biotechnol.* **2004**, *22*, 883.
(353) Aslan, K.; Lacowicz, J. R.; Geddes, C. D. *Anal. Chem.* **2005**, *77*, 2007.
(354) Roll, D.; Malicka, J.; Gryczynski, I.; Gryczynski, Z.; Lakowicz, J. R. *Anal. Chem.* **2003**, *75*, 3440.
(355) Aslan, K.; Holley, P.; Davies, L.; Lakowicz, J. R.; Geddes, C. D. *J. Am. Chem. Soc.* **2005**, *127*, 12115.
(356) Aslan, K.; Lakowicz, J. R.; Geddes, C. D. *Appl. Phys. Lett.* **2005**, *87*, 234108/1.
(357) http://www.nanosphere.us/, 2007.
(358) Pokorski, J. K.; Nam, J.-M.; Vega, R. A.; Mirkin, C. A.; Appella, D. H. *Chem. Commun.* **2005**, *210*1.
(359) Nam, J.-M.; Stoeva, S. I.; Mirkin, C. A. *J. Am. Chem. Soc.* **2004**, *126*, 5932.
(360) Katz, E.; Willner, I. *Angew. Chem., Int. Ed.* **2004**, *43*, 6042.
(361) Lin, A. W. H.; Lewinski, N. A.; West, J. L.; Halas, N. J.; Drezek, R. A. *J. Biomed. Opt.* **2005**, *10*, 064035/1.
(362) Sokolov, K.; Follen, M.; Aaron, J.; Pavlova, I.; Malpica, A.; Lotan, R.; Richards-Kortum, R. *Cancer Res.* **2003**, *63*, 1999.
(363) Tkaczyk, T. S.; Rahman, M.; Mack, V.; Sokolov, K.; Rogers, J. D.; Richards-Kortum, R.; Descour, M. R. *Opt. Express* **2004**, *12*, 3745.
(364) El-Sayed, I.; Huang, X.; El-Sayed, M. A. *Nano Lett.* **2005**, *5*, 829.
(365) Aaron, J. S.; Oh, J.; Larson, T. A.; Kumar, S.; Milner, T. E.; Sokolov, K. V. *Opt. Express* **2006**, *14*, 12930.
(366) Kumar, S.; Harrison, N.; Richards-Kortum, R.; Sokolov, K. *Nano Lett.* **2007**, *7*, 1338.
(367) Wadia, J. S.; Stan, R. V.; Dowdy, S. F. *Nat. Med.* **2004**, *309*, 121.
(368) Pissuwan, D.; Valenzuela, S. M.; Cortie, M. B. *Trends Biotechnol.* **2006**, *24*, 62.
(369) El-Sayed, I. H.; Huang, X.; El-Sayed, M. A. *Cancer Lett.* **2006**, *239*, 129.
(370) Pattnaik, P. *Appl. Biochem. Biotechnol.* **2005**, *126*, 79.
(371) Myszka, D. G. *Curr. Opin. Biotechnol.* **1997**, *8*, 50.
(372) Brockman, J. M.; Nelson, B. P.; Corn, R. M. *Annu. Rev. Phys. Chem.* **2000**, *51*, 41.
(373) Piliarik, M.; Vaisocherova, H.; Homola, J. *Sens. Actuators B* **2007**, B121, 187.
(374) Schuck, P. *Ann. Rev. Biophys. Biomol. Struct.* **1997**, *26*, 541.
(375) Hahnefeld, C.; Drewianka, S.; Herberg, F. W. *Methods Mol. Med.* **2004**, *94*, 299.
(376) Nath, N.; Chilkoti, A. *Anal. Chem.* **2004**, *76*, 5370.
(377) De Leebeeck, A.; Kumar, L. K. S.; de Lange, V.; Sinton, D.; Gordon, R.; Brolo, A. G. *Anal. Chem.* **2007**, *79*, 4094.
(378) Tetz, K. A.; Pang, L.; Fainman, Y. *Opt. Lett.* **2006**, *31*, 1528.
(379) Kalyuzhny, G.; Vaskevich, A.; Schneeweiss, M. A.; Rubinstein, I. *Chem. Eur. J.* **2002**, *8*, 3850.
(380) Doron-Mor, I.; Cohen, H.; Barkay, Z.; Shanzer, A.; Vaskevich, A.; Rubinstein, I. *Chem. Eur. J.* **2005**, *11*, 5555.
(381) Ruach-Nir, I.; Bendikov, T. A.; Doron-Mor, I.; Barkay, Z.; Vaskevich, A.; Rubinstein, I. *J. Am. Chem. Soc.* **2007**, *129*, 84.
(382) Yonzon, C. R.; Jeoung, E.; Zou, S.; Schatz, G. C.; Mrksich, M.; Van Duyne, R. P. *J. Am. Chem. Soc.* **2004**, *126*, 12669.
(383) Larsson, E. M.; Alegret, J.; Kaell, M.; Sutherland, D. S. *Nano Lett.* **2007**, *7*, 1256.
(384) Nath, N.; Chilkoti, A. *J. Fluoresc.* **2004**, *14*, 377.
(385) Frederix, F.; Friedt, J.-M.; Choi, K.-H.; Laureyn, W.; Campitelli, A.; Mondelaers, D.; Maes, G.; Borghs, G. *Anal. Chem.* **2003**, *75*, 6894.
(386) Thio, T.; Ghaemi, H. F.; Lezec, H. J.; Wolff, P. A. *J. Opt. Soc. Am. B* **1999**, *16*, 1743.
(387) Ekgasit, S.; Thammacharoen, C.; Yu, F.; Knoll, W. *Appl. Spectrosc.* **2005**, *25*, 661.
(388) Mitsui, K.; Handa, Y.; Kajikawa, K. *Appl. Phys. Lett.* **2004**, *85*, 4231.
(389) Weikel, A. L.; Conklin, S. D.; Richardson, J. N. *Sens. Actuators B* **2005**, B110, 112.
(390) Taue, S.; Nishida, K.; Sakaue, H.; Takahagi, T. *e-J. Surf. Sci. Nanotechnol.* **2007**, *5*, 74.
(391) Malynych, S.; Chumanov, G. *J. Opt. A: Pure Appl. Opt.* **2006**, *8*, S144.
(392) Fujiwara, K.; Watarai, H.; Itoh, H.; Nakahama, E.; Ogawa, N. *Anal. Bioanal. Chem.* **2006**, *386*, 639.
(393) Lin, H.-Y.; Chen, C.-T.; Chen, Y.-C. *Anal. Chem.* **2006**, *78*, 6873.
(394) Marinakos, S. M.; Chen, S.; Chilkoti, A. *Anal. Chem.* **2007**, ASAP Article.
(395) Cheng, S.-F.; Chau, L.-K. *Anal. Chem.* **2003**, *75*, 16.
(396) Tam, F.; Moran, C.; Halas, N. *J. Phys. Chem. B* **2004**, *108*, 17290.
(397) Jensen, T. R.; Duval, M. L.; Kelly, K. L.; Lazarides, A. A.; Schatz, G. C.; Van Duyne, R. P. *J. Phys. Chem. B* **1999**, *103*, 9846.
(398) Dahlin, A. B.; Tegenfeldt, J. O.; Hook, F. *Anal. Chem.* **2006**, *78*, 4416.
(399) Dahlin, A.; Zaech, M.; Rindzevicius, T.; Kaell, M.; Sutherland, D. S.; Hoeoek, F. *J. Am. Chem. Soc.* **2005**, *127*, 5043.
(400) Lahav, M.; Vaskevich, A.; Rubinstein, I. *Langmuir* **2004**, *20*, 7365.
(401) Kalyuzhny, G.; Schneeweiss, M. A.; Shanzer, A.; Vaskevich, A.; Rubinstein, I. *J. Am. Chem. Soc.* **2001**, *123*, 3177.
(402) Haes, A. J.; Zou, S.; Schatz, G. C.; Van Duyne, R. P. *J. Phys. Chem. B* **2004**, *108*, 6961.
(403) Haes, A. J.; Zou, S.; Schatz, G. C.; Van Duyne, R. P. *J. Phys. Chem. B* **2004**, *108*, 109.
(404) Whitney, A. V.; Elam, J. W.; Zou, S.; Zinovev, A. V.; Stair, P. C.; Schatz, G. C.; Van Duyne, R. P. *J. Phys. Chem. B* **2005**, *109*, 20522.
(405) Jung, L. S.; Campbell, C. T.; Chinowsky, T. M.; Mar, M. N.; Yee, S. S. *Langmuir* **1998**, *14*, 5636.
(406) Zhao, J.; Das, A.; Zhang, X.; Schatz, G. C.; Sligar, S. G.; Van Duyne, R. P. *J. Am. Chem. Soc.* **2006**, *128*, 11004.
(407) Haes, A. J.; Zou, S.; Zhao, J.; Schatz, G. C.; Van Duyne, R. P. *J. Am. Chem. Soc.* **2006**, *128*, 10905.
(408) Mock, J. J.; Smith, D. R.; Schultz, S. *Nano Lett.* **2003**, *3*, 485.
(409) Sherry, L. J.; Jin, R.; Mirkin, C. A.; Schatz, G. C.; Van Duyne, R. P. *Nano Lett.* **2006**, *6*, 2060.
(410) Sonnichsen, C.; Geier, S.; Hecker, N. E.; von Plessen, G.; Feldmann, J.; Ditlbacher, H.; Lamprecht, B.; Krenn, J. R.; Aussenegg, F. R.; Chan, V. Z.-H.; Spatz, J. P.; Moller, M. *Appl. Phys. Lett.* **2000**, *77*, 2949.
(411) Mock, J. J.; Barbic, M.; Smith, D. R.; Schultz, D. A.; Schultz, S. *J. Chem. Phys.* **2002**, *116*, 6755.
(412) Novo, C.; Gomez, D.; Perez-Juste, J.; Zhang, Z.; Petrova, H.; Reismann, M.; Mulvaney, P.; Hartland, G. V. *Phys. Chem. Chem. Phys.* **2006**, *8*, 3540.
(413) Kalyuzhny, G.; Vaskevich, A.; Ashkenasy, G.; Shanzer, A.; Rubinstein, I. *J. Phys. Chem. B* **2000**, *104*, 8238.
(414) Cao, Q.; Lalanne, P. *Phys. Rev. Lett.* **2002**, *88*, 057403.
(415) Lezec, H.; Thio, T. *Opt. Express* **2004**, *12*, 3629.
(416) Sarrazin, M.; Vigneron, J.-P. *Phys. Rev. B* **2005**, *71*, 075404/1.
(417) Ghaemi, H. F.; Thio, T.; Grupp, D. E.; Ebbesen, T. W.; Lezec, H. J. *Phys. Rev. B* **1998**, *58*, 6779.
(418) Dintinger, J.; Degiron, A.; Ebbesen, T. W. *MRS Bull.* **2005**, *30*, 381.
(419) Sarrazin, M.; Vigneron, J.-P.; Vigoureux, J.-M. *Phys. Rev. B* **2003**, *67*, 085415/1.
(420) Genet, C.; van Exter, M. P.; Woerdman, J. P. *Opt. Commun.* **2003**, *225*, 331.
(421) Benabbas, A.; Halte, V.; Bigot, J.-Y. *Opt. Express* **2005**, *13*, 8730.
(422) Kim, T. J.; Thio, T.; Ebbesen, T. W.; Grupp, D. E.; Lezec, H. J. *Opt. Lett.* **1999**, *24*, 256.
(423) Stark, P. R. H.; Halleck, A. E.; Larson, D. N. *Methods* **2005**, *37*, 37.
(424) Muller, R.; Malyarchuk, V.; Lienau, C. *Phys. Rev. B* **2003**, *68*, 205415/1.
(425) Huang, T. T.; Sturgis, J.; Gomez, R.; Geng, T.; Bashir, R.; Bhunia, A. K.; Robinson, P. J.; Ladisch, M. R. *Biotechnol. Bioeng.* **2003**, *81*, 618.
(426) Brewer, S. H.; Glomm, W. R.; Johnson, M. C.; Knag, M. K.; Franzen, S. *Langmuir* **2005**, *21*, 9303.
(427) Haussling, L.; Ringsdorf, H.; Schmitt, F.-J.; Knoll, W. *Langmuir* **1991**, *7*, 1837.
(428) Kim, D. S.; Hohng, S. C.; Malyarchuk, V.; Yoon, Y. C.; Ahn, Y. H.; Yee, K. J.; Park, J. W.; Kim, J.; Park, Q. H.; Lienau, C. *Phys. Rev. Lett.* **2003**, *91*, 143901.
(429) Snopok, B. A.; Kostyukevych, K. V.; Rengevych, O. V.; Shirshov, Y. M.; Venger, E. F.; Kolesnikova, I. N.; Lugovskoi, E. V. *Semicond. Phys. Quantum Elect. Optoelect.* **1998**, *1*, 121.
(430) Donahue, J. P.; Patel, H.; Anderson, W. F.; Hawiger, J. *PNAS* **1994**, *91*, 12178.
(431) Svedhem, S.; Pfeiffer, I.; Larsson, C.; Wingren, C.; Borrebaeck, C.; Hook, F. *ChemBioChem* **2003**, *4*, 339.
(432) Reviakine, I.; Brisson, A. *Langmuir* **2000**, *16*, 1806.
(433) Dieringer, J. A.; McFarland, A. D.; Shah, N. C.; Straurt, D. A.; Whitney, A. V.; Yonzon, C. R.; Young, M. A.; Zhang, X.; Van Duyne, R. P. *Faraday Discuss.* **2006**, *132*, 9.
(434) Kneipp, K.; Kneipp, H. *Appl. Spectrosc.* **2006**, *60*, 322A.
(435) Jeanmarie, D. L.; Van Duyne, R. P. *J. Electroanal. Chem.* **1977**, *84*, 1.
(436) Albrecht, M. G.; Creighton, J. A. *J. Am. Chem. Soc.* **1977**, *99*, 5215.
(437) Stockman, M. I. *Top. Appl. Phys.* **2006**, *103*, 47.
(438) Schatz, G. C.; Young, M. A.; Van Duyne, R. P. *Top. Appl. Phys.* **2006**, *103*, 19.
(439) Moskovits, M. *Top. Appl. Phys.* **2006**, *103*, 1.
(440) Otto, A. *J. Raman Spectrosc.* **2006**, *37*, 937.
(441) Anderson, D. J.; Moskovits, M. *J. Phys. Chem. B* **2006**, *110*, 13722.
(442) Kuncicky, D. M.; Prevo, B. G.; Velev, O. D. *J. Mater. Chem.* **2006**, *16*, 1207.
(443) Li, Z.; Tong, W. M.; Stickle, W. F.; Neiman, D. L.; Williams, R. S. *Langmuir* **2007**, *23*, 5135.

(444) Brolo, A. G.; Arctander, E.; Gordon, R.; Leathem, B.; Kavanagh, K. L. *Nano Lett.* **2004**, *4*, 2015.
(445) Zhang, X.; Young, M. A.; Lyandres, O.; Van Duyne, R. P. *J. Am. Chem. Soc.* **2005**, *127*, 4484.
(446) Lim, J. K.; Kim, I.; Kim, K.; Shin, K. S.; Kang, W.; Choo, J.; Joo, S. *Chem. Phys.* **2006**, *330*, 245.
(447) Bell, S. E. J.; Sirimuthu, N. M. S. *J. Am. Chem. Soc.* **2006**, *128*, 15580.
(448) Chowdhury, M. H.; Campbell, C. J.; Theofanidou, E.; Lee, S. J.; Baldwin, A.; Sing, G.; Yeh, A. T.; Crain, J.; Ghazal, P.; Coté, G. L. *Proc. SPIE* **2006**, *6099*, 609905.
(449) Tang, H.; Yang, X. B.; Kirkham, J.; Smith, D. A. *Anal. Chem.* **2007**, *79*, 3646.
(450) Zhang, J.; Gao, Y.; Alvarez-puebla, R. A.; Buriak, J. M.; Fenniri, H. *Adv. Mater.* **2006**, *18*, 3233.
(451) Orendorff, C. J.; Gearheart, L.; Jana, N. R.; Murphy, C. J. *Phys. Chem. Chem. Phys.* **2006**, *8*, 165.
(452) Wang, T.; Hu, X.; Dong, S. *J. Phys. Chem. B* **2006**, *110*, 16930.
(453) Dick, L. A.; McFarland, A. D.; Haynes, C. L.; Van Duyne, R. P. *J. Phys. Chem. B* **2002**, *106*, 853.
(454) Ruan, C.; Eres, G.; Wang, W.; Zhang, Z.; Gu, B. *Langmuir* **2007**, *23*, 5757.
(455) Shanmukh, S.; Jones, L.; Driskell, J.; Zhao, Y.; Dluhy, R.; Tripp, R. A. *Nano Lett.* **2006**, *6*, 2630.
(456) White, D. J.; Mazzolini, A. P.; Stoddart, P. R. *J. Raman Spectrosc.* **2007**, *38*, 377.
(457) Willis, R. C. *Anal. Chem.* **2007**, *79*, 1785.
(458) Cornish, P. V.; Ha, T. *ACS Chem. Biol.* **2007**, *2*, 53.
(459) Delfino, I.; Bizzarri, A. R.; Cannistrato, S. *Chem. Phys.* **2006**, *326*, 356.
(460) Kim, J.; Song, K.-B. *Micron* **2007**, *38*, 409.
(461) Frey, H. G.; Bolwein, C.; Brandenburg, A.; Ros, R.; Anselmetti, D. *Nanotechnology* **2006**, *17*, 3105.
(462) Pettinger, B. *Top. Appl. Phys.* **2006**, *103*, 217.
(463) Zhang, W.; Cui, X.; Yeo, B.-S.; Schmid, T.; Hafner, C.; Zenobi, R. *Nano Lett.* **2007**, *7*, 1401.
(464) Becker, M.; Sivakov, V.; Andrä, G.; Geiger, R.; Schreiber, J.; Hoffman, S.; Michler, J.; Milenin, A. P.; Werner, P.; Christiansen, S. H. *Nano Lett.* **2007**, *7*, 75.
(465) Matsui, R.; Verma, P.; Ichimura, T.; Inouye, Y.; Kawata, S. *Appl. Phys. Lett.* **2007**, *90*, 061906.
(466) Huebsch, N. D.; Mooney, D. J. *Biomaterials* **2007**, *28*, 2424.
(467) Wei, D.; Wang, Y.; Luo, Q.; Bi-Feng, L. *Anal. Bioanal. Chem.* **2006**, *386*, 444.
(468) Brolo, A. G.; Kwok, S. C.; Moffitt, M. G.; Gordon, R.; Riordon, J.; Kavanagh, K. L. *J. Am. Chem. Soc.* **2005**, *127*, 14936.
(469) Hseih, B.; Chang, Y.-F.; Ng, M.-Y.; Liu, W.-C.; Lin, C.-H.; Wu, H.-T.; Chou, C. *Anal. Chem.* **2007**, *79*, 3487.
(470) Lacowicz, J. R. *Plasmonics* **2006**, *1*, 5.
(471) Lakowicz, J. R.; Geddes, C. D.; Gryczynski, I.; Malicka, J.; Gryczynski, Z.; Aslan, K.; Lukomska, J.; Matveeva, E.; Zhang, J.; Badugu, R.; Huang, J. *J. Fluoresc.* **2004**, *14*, 425441.
(472) Garrett, S. H.; Smith, L. H.; Barnes, W. L. *J. Mod. Opt.* **2005**, *52*, 1105.
(473) Huang, C. C.; Chang, H. T. *Anal. Chem.* **2006**, *78*, 8332.
(474) Nagamura, T.; Yamamoto, M.; Terasawa, M.; Shiratori, K. *Appl. Phys. Lett.* **2003**, *83*, 803.
(475) He, X.; Liu, H.; Li, Y.; Wang, S.; Li, Y.; Wang, N.; Xiao, J.; Xu, X.; Zhu, D. *Adv. Mater.* **2005**, *17*, 2811.
(476) Brolo, A. G.; Kwok, S. C.; Cooper, M. D.; Moffitt, M. G.; Wang, C.-W.; Gordon, R.; Riordon, J.; Kavanagh, K. L. *J. Phys. Chem. B* **2006**, *110*, 8307.
(477) Shelby, R. A.; Smith, D. R.; Schultz, S. *Science* **2001**, *292*, 77.
(478) Lezec, H. J.; Dionne, J. A.; Atwater, H. A. *Science* **2007**, *316*, 430.
(479) Soukoulis, C. M.; Kafesaki, M.; Economou, E. N. *Adv. Mater.* **2006**, *18*, 1941.
(480) Shalaev, V. M. *Nat. Photonics* **2007**, *1*, 41.
(481) Pendry, J. B. *Phys. Rev. Lett.* **2000**, *85*, 3966.
(482) Hohng, S. C.; C., Y. Y.; Kim, D. S.; Malyarchuk, V.; Muller, R.; Lienau, C. H.; Park, J. W.; Yoo, K. H.; Kim, J.; Ryu, H. Y.; Park, Q. H. *Appl. Phys. Lett.* **2002**, *81*, 3239.
(483) Luo, X.; Ishihara, T. *Appl. Phys. Lett.* **2004**, *84*, 4780.
(484) Dragnea, B.; Szarko, J. M.; Kowarik, S.; Weimann, T.; Feldmann, J.; Leone, S. R. *Nano Lett.* **2003**, *3*, 3.
(485) Srituravanich, W.; Fang, N.; Sun, C.; Luo, Q.; Zhang, X. *Nano Lett.* **2004**, *4*, 1085.
(486) Liu, Z.-W.; Wei, Q.-H.; Zhang, X. *Nano Lett.* **2005**, *5*, 957.
(487) Smolyaninov, I. I.; Elliot, J.; Zayats, A. V.; Davis, C. C. *Phys. Rev. Lett.* **2005**, *94*, 057401.
(488) Garini, Y.; Kutchoukov, V. G.; Bossche, A.; Alkemade, P. F. A.; Docter, M.; Verbeek, P. W.; van Vliet, L. J.; Young, I. T. *Proc. SPIE* **2004**, *5327*, 115.
(489) Docter, M. W.; Young, I. T.; Kutchoukov, V. G.; Bossche, A.; Alkemade, P. F. A.; Garini, Y. *Proc. SPIE* **2005**, *5703*, 118.
(490) Smolyaninov, I. I.; Hung, Y.-J.; Davis, C. C. *Science* **2007**, *315*, 1699.
(491) Liu, Z.-w.; Lee, H.; Xiong, Y.; Sun, C.; Zhang, X. *Science* **2007**, *315*, 1686.

CR068126N